Accelerated Insulation Aging Due to Thermal and Electrical Stresses in Future Power Grids

Accelerated Insulation Aging Due to Thermal and Electrical Stresses in Future Power Grids

Proefschrift

ter verkrijging van de graad van doctor
aan de Technische Universiteit Delft
op gezag van de Rector Magnificus Prof. Ir. K.C.A.M Luyben,
voorzitter van het College voor Promoties,
in het openbaar te verdedigen,
op maandag 3 februari 2014 om 10:00 uur
door

Tomasz Lech KOLTUNOWICZ

Master of Electrical and Electronic Engineering,
The University of Nottingham (UK)
geboren te Warschau (Polen)

Dit proefschrift is goedgekeurd door de promotor:

Prof. dr. J. J. Smit

Copromotor:
Dr. Ir. D. Djairam

Samenstelling promotiecommissie:

Rector Magnificus	voorzitter
Prof. dr. J. J. Smit	Technische Universiteit Delft, promotor
Dr. ir. D. Djairam	Technische Universiteit Delft, copromotor
Prof. dr. S. J. Picken	Technische Universiteit Delft
Prof. Dipl. –Ing.	
Dr. h.c. M. Muhr	Technische Universität Graz, Austria
Dr. A. Cavallini	Università di Bologna, Italy
Prof. dr. S. Gubanski	Chalmers Tekniska Högskola, Sweden
Prof. dr. ir. E.F. Steennis	Technische Universiteit Eindhoven
Prof. dr. M. Zeman	Technische Universiteit Delft, reservelid

The investigations in this thesis have been performed within the framework of the research project “Synergie van Intelligentie en Energie in elektriciteitsnetten van de toekomst” (SINERGIE), which is financially supported as part of the research program “Energie Onderzoek Subsidie – Lange Termijn” (EOS-LT04034) of AgentschapNL, an agency of the Dutch Ministry of Economic Affairs.

ISBN 978-90-8891-819-3
Key words: Repetitive Transients, Paper-oil Electrical Insulation, Life Consumption, Aging model.

Copyright © 2014 by T.L. Koltunowicz
All rights reserved. No part of this work may be reproduced in any form without the permission in writing of the publisher

Printed by: Proefschriftmaken.nl ||Uitgeverij BOXPress

Summary

The electric grid is in a period of substantial changing. Alternative transmission techniques such as HVDC are increasing and sustainable solutions are replacing coal and nuclear plants. Though these technologies have been studied in the past, it is relatively unknown what the impact on the current electric grid will be. One of the main worries is the effect of repetitive transients on the insulation lifetime and dielectric capabilities.

Repetitive transients are created when DC to AC conversion takes place due to the fast switching operations in the range of 1-10 kHz of MOSFETs in power electronic inverters and converters. This technique is already widely implemented in AC motors and offers the best economic advantage thanks to the relative low cost of electronics. Such converters are already in place at HVDC substations and wind farms. With power generation moving towards local-generation, such converters are expected to be installed closer to homes.

Little was known about influence of fast repeating switching pulses on insulating materials. Most of the knowledge available to date involves the aging of insulation of electric motor exposed to the operation of adjustable speed drives generating fast transients. The goal of this thesis was therefore to demonstrate substantial evidence that repetitive transients can degrade other type of insulation, such as paper-oil insulation, and to propose an aging hypothesis together with an aging model based on the repetition frequency of transients and estimated time to breakdown of the insulation.

A “divide and conquer” method was applied in this thesis to investigate the effect of repetitive transients on paper-oil insulation samples. The influence of the individual parameter of the repetitive transients was investigated: rise time, repetition frequency and magnitude. To do so, different voltage waveforms that simulated field conditions were applied: a square wave, single pulses and AC waveform with superimposed repetitive transients. At last a temperature effect was added to investigate whether the aging influence of repetitive transients is amplified at elevated operating temperature.

A square wave was applied to paper-oil samples and two values were measured at the combination of various rise times and repetition frequencies: breakdown voltage and partial discharge inception voltage. The investigated range was 300 ns

to 1000 ns for the rise time and 1 kHz to 10 kHz for the repetition frequency. The acquired data indicated that shortening the rise time and increasing the repetition frequency cause the breakdown voltage and PDIV to decrease. Single voltage pulses were also applied to the identical type of insulation material yielding similar results in terms of breakdown voltage at shorter rise times.

To simulate the field conditions in the lab, a device capable of generating repetitive transients of different repetition frequencies and magnitudes superimposed on a sinusoidal waveform of variable magnitude was designed. In this particular test configuration, the time to breakdown was observed at room temperature and on selected samples; the tan (δ) was measured after 24 hours electrical aging in a wide range of measuring frequencies of transients. The data collected indicated that the time to breakdown decreased 3 times when the repetition frequency was increased from 1 kHz to 10 kHz on an AC waveform of 48.5 kV/mm. Tan (δ) measurements indicated a probable stronger degradation of the molecular bonds within the paper when higher repetitive transient frequencies in combination with higher magnitudes of AC waveforms were applied.

When temperatures of 40 °C, 60 °C and 80 °C were applied to the insulation samples, similar aging results were observed. During the short-term application of the transients (22 h) it was noticed that the tan (δ) values increase.

A Lifetime consumption model was created based on the Weibull analysis of the data. It was shown that increasing the repetition frequency of transients, whilst keeping the carrier waveform constant, the expected lifetime of the insulation substantially shortened.

Aging of the insulation by repetitive transients can become an influential factor in the reliability of operation of the future electric grid. As the grid's task will evolve into more complicated ones and additional loading of the HV components will take place it is expected that the lifetime of the present components could be shortened. In order to avoid this, studying the phenomenon of repetitive transients is the first important step.

Table of Contents

Summary iv

Table of Contents vi

Chapter 1

Introduction 1

1.1 Future Trends in Power Transmission and Distribution 1

1.2 Transients from Power Electronics 5

1.3. Goals of the Research 6

1.4. Layout of the thesis 7

Chapter 2

The Future Grid and Related Insulation Problems 9

2.1 The smart grid 9

2.2 Repetitive Transients 11

2.2.1 Origin and characteristics 11

2.2.2 Effect of repetitive transients on electrical insulation 13

2.2.3 Reaction of paper-oil insulation to heat fluctuations 17

2.3 Aging of Transformers 19

2.3.1 Failure rate 19

2.3.2 Aging factors 21

2.3.3 Currently available aging models 23

2.3.3.1 Graphical models 24

2.3.3.2 Equation models 25

2.4 Conclusion 26

Chapter 3

Dielectric Evaluation of Paper-Oil Test Samples 29

3.1. Paper-oil Insulation 29

3.2 Preparation of the Samples and Test Electrodes Selection 33

3.2.1 Test samples 33
3.2.2 Sample impregnation and electrode selection 34
3.3 AC Dielectric Strength Tests 38
3.3.1 Data representation 38
3.3.2 AC dielectric breakdown test 38
3.3.3 Life time estimation based on time to breakdown and applied voltage 39
3.4 Tangent Delta Measurement Results 42
3.5 Conclusion 44
Chapter 4
Electrical Aging by Repetitive Transients 47
4.1. Conversion between DC and AC Voltage Waveforms 48
4.2. Square Wave Dielectric Strength of Paper-oil Insulation 49
4.2.1. Test set-up and procedure 50
4.2.2. Test results 51
4.2.3. Discussion 58
4.3. Impulse Dielectric Strength of Paper-oil Insulation 60
4.3.1. Test set-up and procedure 60
4.3.2. Test results 62
4.3.3. Discussion 64
4.4. Aging by Repetitive Transients 64
4.4.1. Test set-up 65
4.4.2. Test procedure 70
4.4.3. Test results 72
4.4.4. Discussion 75
4.4.5. Influence of the number of repetitive pulses on AC dielectric strength 76
4.5. Tangent Delta 78

4.5.1. Test set-up and procedure 78
4.5.2. Test results 78
4.5.3. Discussion and Hypothesis 80
4.7. Conclusions .....
Chapter 5
Effect of Repetitive Transients on Paper-oil Insulation
at Elevated Temperatures 83
5.1. Heat Fluctuations in Transformer 83
5.2. AC Dielectric Strength at Elevated Temperature 85
5.2.1. Test set-up and procedure 85
5.2.2. Test results 87
5.2.3. Discussion 88
5.3. Aging by Repetitive Transient in Elevated Temperature 89
5.3.1 Test set-up and procedure 89
5.3.2. Tan (δ) measurements results 91
5.3.3 Discussion 96
5.4. Conclusion 98
Chapter 6
The Aging Model for Paper-oil Insulation Considering Repetitive Transients 101
6.1.1. Dependency of Time to Breakdown on AC Voltage
and Repetition Frequency of Transients 101
6.1.2. The Fluctuation Model 104
6.1.3. Weibull Unreliability Plots 108
6.1.4. Discussion 115
6.2. Selecting the Appropriate Model 116
6.2.1. Probability Lifetime Models 117
6.2.2. Results 119
6.2.3. The Transient Aging Model 123

6.2.4. Discussion 127
6.3. Conclusion 127
Chapter 7 129
Conclusions and Recommendations 129
7.1. Conclusions 129
7.2. Recommendations for Future Work 131
Appendix A – Weibull Statistics 133
Appendix B – Dielectric Spectroscopy 135
The test set-up 135
Appendix C - Weibull Analysis 137
Appendix – D - Data Comparison 143
List of Figures and Tables 147
Bibliography 155
Samenvatting 161
Publications 165
Acknowledgments 167
Curriculum Vitae 169

Chapter 1
Introduction

"*We will make electricity so cheap, that only the rich will burn candles*" – Thomas Edison making a statement during the first demonstration of the incandescent light bulb in 1879. So far he has been almost right, except the fact that we burn candles out of necessity and fun.

Mankind's adventure with natural sources of energy has almost been as old as his struggle to control it. The first hydroelectric power plant was installed in 1870 in a country house in northern England named Cragside [1]. This installation used a Siemens dynamo to power the house fitted with an electric installation, also considered to be the first proper installation in the world. Since then, the electric grid has evolved and it can be found in almost all places on Earth where mankind is present.

Nowadays, the electric power system is a huge network that deals with generation, transmission and distribution of electricity between the supplier and the user. This process is complex and well organised in order to avoid overloading the grid components [2]. Such scenario could lead to their failures and therefore cause power outages for the users. New challenges are presenting themselves for the power grid as modernisation is taking effect.

New generation and transmission techniques are being implemented causing additional stresses on high voltage (HV) devices, especially on their electrical insulation. Repetitive transients at inverter stations might cause such stresses, introduced in chapter 1.2 [3, 4]. These new stresses are diminishing the insulation withstand voltage levels and consequently affecting its reliability. The interest in understanding this behaviour and predicting aging scenarios for HV devices, in particular power transformers, have inspired this thesis.

1.1 Future Trends in Power Transmission and Distribution

Economic growth goes hand in hand with higher demand for electric power. This trend is not only attributed to single household, but also to the industry. Simply

increasing power production is not the solution and also not that straight forward. Most of the electricity production in the EU is coming from burning fossil and from nuclear fission; both methods are not popular within the community. Energy generation from coal is polluting and with the current policies of reducing CO_2 emissions it makes this energy source rather unacceptable. Nuclear energy on the other hand is considered very dangerous for the environment and the population living in the vicinity. The most suitable solution seems to be switching to renewable sources such as wind, biomass, water and the sun.

Substantial changes, modernizations and extensions in the transmission system have been implemented in the 1960's and 1970's, years of industrial boom in Europe. This means that most of the installed HV devices have reached the end of their designed life. However, some of them have not been operated at 100 % power load, for which aging of the insulation has to be determined and re-evaluated. This theoretically could give some extra years of lifetime. Unfortunately, energy demand is expected to increase worldwide [5]. This makes it harder to re-estimate the remaining lifetime [6].

The grid is set to experience many changes in the coming 25 years. The decentralisation of distributed generation and increased storage capabilities are the main driving factors. Most of the changes regard smart metering and the application of smart control systems in order to optimise the operation of the grid [7]. It is predicted that these tasks will be performed by measuring and controlling current flows and voltages in an intelligent way so that they can be implemented in the smart grid of the future. Even though these trends seem likely to take place, the core function of the grid remains to reliable transporting and distributing energy [2, 8, 9].

We can already observe a continuous shift towards a wider use of renewable sources of energy.

Most of the energy generated today in the industrialised countries is coming from non-renewable energy sources, such as coal, oil, gas and nuclear [2], which accounts for 82 % (Fig. 1.1). A mere 17 % is generated from a renewable source, with hydro power plants holding the biggest share.

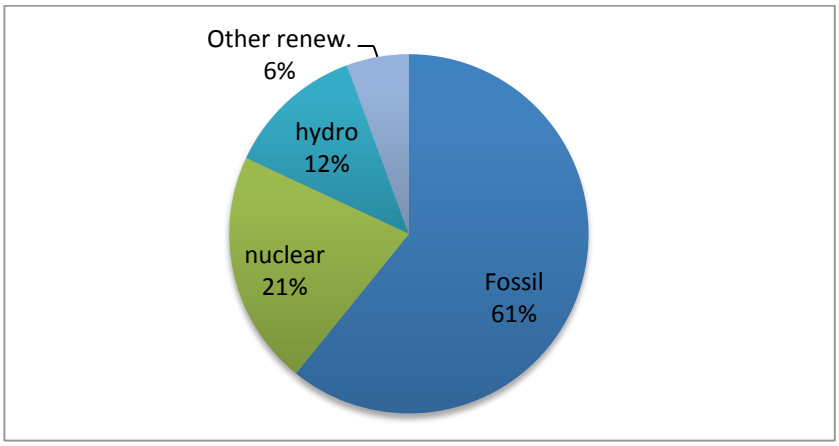


Fig. 1.1 – Energy generation sources in the industrialised nations in 2010 [5]. Fossil includes oil, gas and coal

Wind, solar and hydro generation are the fastest growing sectors with a significant impact on the generation process at the moment in Europe, followed by tidal, geothermal and biomass [2, 5]. Several scenarios are predicted to take place in the development of renewable energies. Some of them predict that:

- Wind; the output power reached 95 GW in 2012 in Europe. This value is predicted to triple by 2035;
- Solar; the total worldwide amount of power production was at 30 GW in 2011. By 2035, the EU is expected to produce 5% of its electricity from photovoltaic plants by producing 146 GW;
- Hydro; with a current capacity of 180 GW in the EU. Hydropower is still set to rise as it is predicted that many countries are capable of producing enough electricity to satisfy the internal demand by purely converting to 100 % hydro, as it is the case of Norway.

Even though installing renewables brings up many advantages, their main disadvantage is that they are not available in the same quantities in all locations. When focusing on Europe, wind is more prevalent in coastal areas and in the north, such as the North Sea, sun is abundant in the south, in such countries as Spain or Italy and hydro power generation is available in mountainous areas such as the Alps. In order to efficiently distribute electricity, long overhead transmission lines from these sites need to be built. Over short distances of a few hundred kilometres, HVAC lines are used. However, when the transmission line's length is in the thousands of kilometres, it is advisable to implement high voltage direct

current (HVDC) transmission. The advantage of HVDC is the ability to transmit large amounts of power over long distances with lower costs and with lower losses than with HVAC. In this way it's easier to connect a remote generation plant to the distribution grid, facilitate power transmission between different countries that use AC at different rated voltages and/or frequencies [2,10].

HVDC links are already present in Europe but more of them are scheduled to be constructed. DESERTEC is the name of the project in which HVDC lines are planned to be utilised. This venture has the goal to connect renewable plants in and around Europe. Fig. 1.2 shows the distribution of the planned renewable energy plants, from photovoltaic (PV) plants in southern Europe and northern Africa to large wind and hydro plants in the middle and at the coastal areas of the continent and geothermal as far as Iceland. All the main long distance interconnections are scheduled to utilise HVDC.

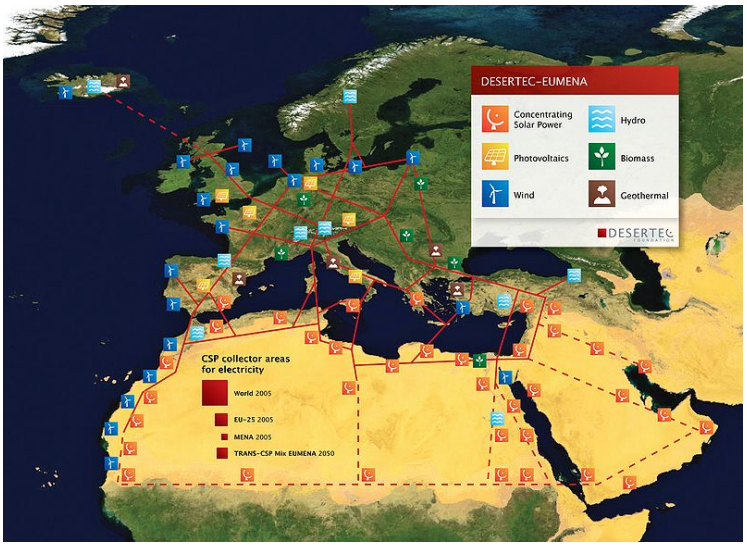


Fig. 1.2 – Planned DESERTEC spread of renewable energy plants around Europe with HVDC interconnections [www.desertec.org]

To perform the changes from DC to AC and vice-versa, voltage source converters (VSC) are necessary [3]. Additional substations would need to be built to perform these operations. However, as it will be explored in this thesis, repetitive transients are generated during this conversion process harming electrical insulation.

Diagnostics will play a part in the grid of the future. Based on the health state and the various aging factors acting on the HV device, lifetime estimation could be

determined. This process is part of a predictive health model (PHM) that needs to be developed for each HV device in the grid [7].

Determining the aging factors and their influence on the HV device's life is a complicated task. It is not always possible to estimate with accuracy the influence of the known aging factors, but also new ones are expected to appear whose influence on the aging rate is not known.

1.2 Transients from Power Electronics

Since the 1980's, electronics have been appearing in most household appliances due to their miniature size and increased reliability. The power grid is also changing and some aspects, such as DC-AC conversion, would not be possible to perform as efficiently as required without the integration of power electronics.

Wind and solar plants can generate electricity in DC, which creates incompatibility with the electric grid where electricity is transported in AC. The distant location of these plants requires the construction of HVDC links. Both cases require the installation of power electronic inverters.

Power electronic inverters utilise semiconductor switches such as transistors, in particular MOSFETS or insulated gate bipolar transistor (IGBTs), in order to convert DC to AC and vice versa. By controlling the operation of these switches, it is possible to achieve a sinusoidal waveform that can be amplified by a step-up transformer and injected into the transmission grid. However, this process is not entirely harmless for the grid's components. Several failures in wind farms in the North Sea region have experienced unknown failures within their first two years of operation. The root cause of failure was unknown at the time and the suspicions were placed on voltage transients generated by power electronics and salinity due to the sea. However no detailed reports or literature were published. An illustration of a repetitive transient is shown in Fig. 1.3.

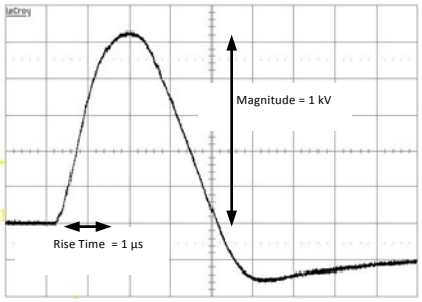


Fig. 1.3 – An illustration of a repetitive transient

Repetitive transients affect mostly the insulation of generators, electric motors and power transformers. Literature has been published outlining the degradation of motors fed by adjustable speed drives (ASD), however little was published for transformers [3]. Repetitive transients have three outlining features: fast rise times, high magnitudes and a high repetition frequency [3, 4]. All these qualities differentiate them from any other waveforms present in the power grid such as sinusoidal waveforms or switching transients.

Transformers can be found at inverter stations and, having a similar construction to motors or generators, they are susceptible to waveforms generated by power electronic inverters, which produce similar waveforms to ASDs containing transients. The insulation of transformer varies from that of motors, so it is difficult to relate many findings in the degradation process without a high uncertainty.

Aging models are important for the estimation of a transformer's lifetime in order to plan maintenance or replacement actions. For this purpose, the effect or repetitive transients on the insulation material should be quantified and represented by an aging model. Such model could be useful to utility companies to recalculate the estimated age of their assets [6, 8]

1.3. Goals of the Research

The main goals of the investigation are to attempt modelling accelerated aging phenomena and to assess the effect of accelerated aging due to repetitive voltage transients on the dielectric withstand of paper-oil transformer insulation. The parameters of the investigation that will be altered are repetition frequency rise time and magnitude of the waveform. Thermal cycle tests will also be simulated to investigate the behaviour of the insulating material at increased temperatures

whilst being stressed with transients. The temperatures simulated will be coinciding with the transformer's typical temperatures operating range till 80 °C.

Representative samples of transformer paper-oil insulation will be prepared to mimic the insulation layer of the transformer and the results gathered will be adapted to match real operating scenarios from the field.

Several diagnostic indicators will be investigated and test parameters will be changed in order to determine dielectric degradation of paper-oil insulation samples. The most important ones are:

- Electric Strength, for AC, square wave and impulse voltages;
- Tan (δ), loss tangent of the insulation samples;
- Life curve Weibull distribution parameters needed to evaluate the lifetime of a sample under specific test conditions.

The obtained test results will be used to create an aging model for the paper-oil insulation this model will calculate the remaining lifetime of paper-oil samples depending on the repetition frequency.

1.4. Layout of the thesis

The electric grid is expected to undergo changes to a "smart grid" system, which interconnects renewable power plants. New components, such as power electronic converters, will be installed creating unwanted waveforms, in the form of repetitive transients decreasing the lifetime of HV devices such as transformers. Such changes will add several problems to the grid devices working at higher and varying load at increased operating temperatures and being affected by appearing repetitive voltage transients. These problems are presented in Chapter 2 together with the described out-dated aging models for the transformer's insulation aging.

Chapter 3 focuses on the dielectric evaluation of the paper-oil insulation samples. These test results are necessary to understand the behaviour of paper-oil insulation under known conditions, so that the effects of later tests can be compared and better quantified. The sample's preparation procedure is also discussed to justify the selection of the test set up configuration and methodology of testing and data evaluation.

Aging of test samples due to repetitive transients is presented in Chapter 4. Various testing methods are applied to understand the influence of three most

important parameters of repetitive transients: magnitude, rise time and repetition rate. Square waves, single pulses and superimposed transients on a sinusoid are the main waveforms investigated. The time to breakdown and the breakdown voltages are measured together, additionally, a dielectric evaluation of the samples using tan (δ) measurements is presented. At the end of the chapter a hypothesis is given to why paper-oil insulation fails faster under transient conditions

In Chapter 5, the transients are applied to the test samples insulation being pre-conditioned at higher temperatures. Such test results are useful in understanding how the paper-oil insulation behaves in extreme high thermal conditions. The problem of heat variations is also be addressed in this Chapter. Tan (δ) results are used to evaluate the rate of degradation of the paper. A simple degradation model is presented based on the gathered results from this chapter.

Chapter 6 combines the results obtained in Chapter 4 into an aging model for the paper-oil insulation. This lifetime consumption model integrates the magnitude of a sinusoidal waveform and the repetition frequency of the transients in order to predict the time to breakdown of the samples. The output of this model can be used to predict the aging of the transformer's insulation in the future grid with higher accuracy than the already existing ones.

The conclusions from the research are presented in Chapter 7.

Chapter 2
The Future Grid and Related Insulation Problems

The electric grid is continuously evolving triggering restructuring in its operation scheme and design layout. New objectives such as connecting renewable energy plants and system intelligence will be necessary to maintain reliability as new components such as power electronic inverters will be installed throughout the electric grid.

These new components will bring new stresses to the grid such as repetitive transients caused by the transformation of DC into AC. The shape of these transients and their repetition rate is expected to influence in longer time the insulation of HV devices such as transformers but their effect is still not quantified on how dielectric properties of paper-oil will change.

Due to this unknown aging factor, the aging models required to monitor the grid devices are rendered incomplete. These models are currently based on several diagnostic parameters such as degree of polymerisation or furanic content composition generated from known basic aging factors such as AC and constant loading. They need to be updated so that repetitive transients are included together with extreme heat fluctuations caused by the variations in the demand of electric power throughout the day.

2.1 The smart grid

In the coming 30 years, the electrical grid will undergo many changes in all of its parts: generation, transmission and distribution. These changes will force to re-examine the existing management policies in such way that a reliable delivery of electric power is guaranteed. For this purpose, future trends need to be identified and analysed so that their impact can be understood on the current grid infrastructure in terms of accelerated maintenance intervals and reduction in the device´s lifetime. Some of these trends can be identified as additional aging factors, such as repetitive transients, or an increased demand for energy leading to higher operating temperatures.

The smart grid concept began to arise about 10 years ago when the threat of global warming and electronic protection started to become a daily topic. One of the main goals in reducing the carbon dioxide emission into the atmosphere is by switching from polluting energy sources, such as coal and oil into cleaner ones such as wind and solar, to mention a few. This meant that more challenges were introduced for the grid to cope with. Wind and sunshine is not available for 24h/day meaning that some power plants might be in operation while others would not. Not every country has the same amount of renewable sources; for example, Southern Europe has much more sun whilst the North has more wind. This meant that power would have to be transmitted over long distances and redirected for each country depending on the demand. A simple illustration of the future city integrated in the smart grid system can be seen in Fig. 2.1. These are some of the basic problems encountered and every country/region has different view on how the grid is supposed to operate [2]. The common view however is the fact that changes are necessary. Some of the biggest changes will come in the orientation of power flow, DC-AC conversion and increased power load.

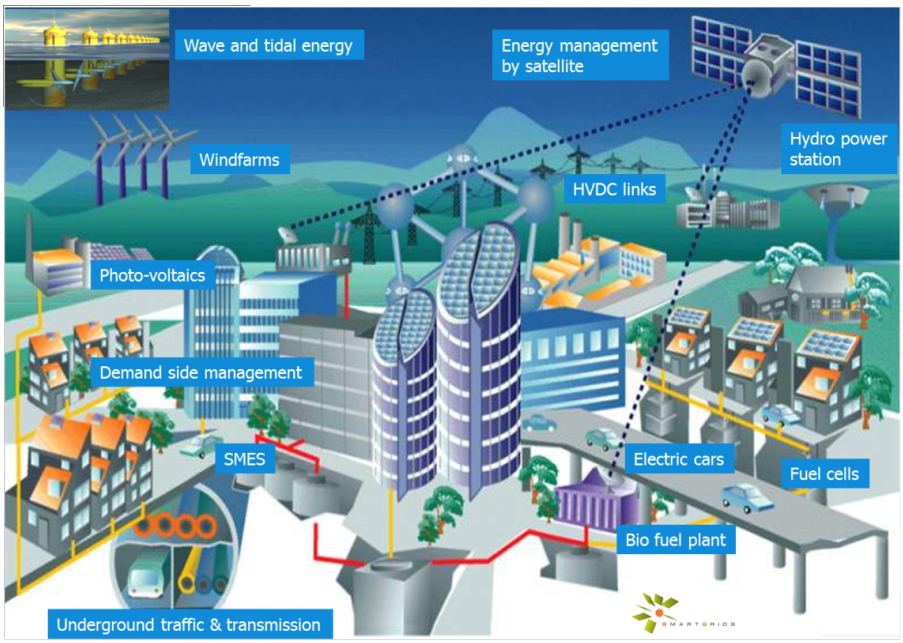


Fig. 2.1 – Concept view of the future city within the smart grid [28]

According to the EU discussion panel for smart grids [12] the definition of a smart grid is the following:

"A Smart Grid is an electricity network that can intelligently integrate the actions of all users connected to it – generators, consumers and those that do both – in order to efficiently deliver sustainable, economic and secure electricity supplies."

This goal of such system is based on the following main points, which in turn can lead to repetitive transients and increased operating temperatures:

- Provide reliable electricity to consumers by managing the power flow in case of a component failure, leading to an increase in power load;
- Manage the flow of power between the various generation plants and consumers, leading to the installation of inverters, renewable energy plants and long distance connections;
- Reduce the grid´s impact on the environment by installing more renewable energy plants;
- Manage the components in the smart grid, such as transformers and cables by the usage of up-to date aging models;
- Provide a secure infrastructure from external sources, (e.g. hacking).

Inverter stations can generate repetitive transients. These plants don't necessarily need to be located in a distant area from houses, as in the case of HVDC or wind farms, but they can be more "local" as renewable energy plants will be located more often within cities, such as PV. An increase in load will cause operating temperatures to increase thus aging faster the insulation. These two phenomena are shortly described in the following sections.

2.2 Repetitive Transients

Repetitive transients are a relatively new phenomenon in the electric grid's history. With the introduction of power electronics, repetitive transients, due to their specific shape, are considered to be a problem for HV devices such as transformers [3, 4, 11, 14, 48]. Literature research has been carried out on motor insulation, which is constituted of solid epoxy resin compositions; however, effects to paper-oil insulations are still unknown.

2.2.1 Origin and characteristics

Power electronic inverters are behind the conversion between the AC and DC waveforms. They implement IGBTs to perform the switching. Fig. 2.2 shows the input and output waveforms from such inverter.

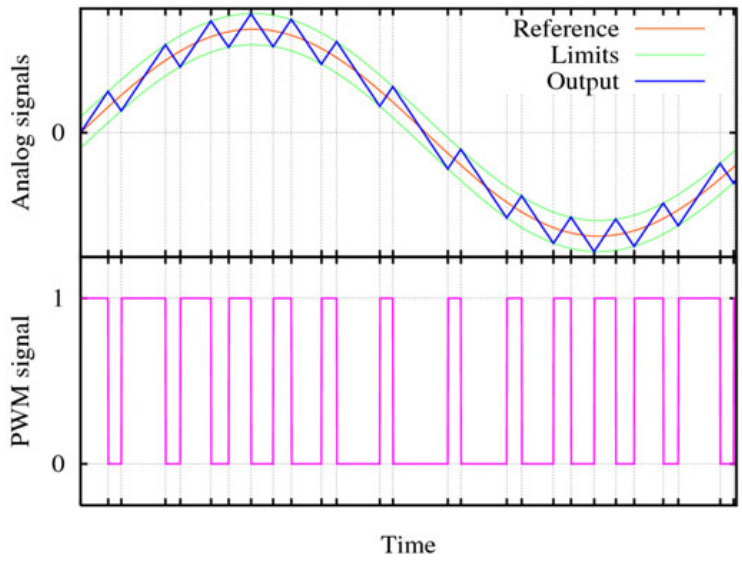


Fig. 2.2 – The input and output waveforms when converted using pulse width modulation (PWM) [13]

Repetitive transients can be characterized by magnitude, shape and repetition rate:

- Peak Voltage (V_{pk}) – the maximum voltage reached by the transient. It can be of positive or negative polarity;
- Rise Time (t_r) – the time necessary for the front of the wave to rise from 10% to 90% of its peak value;
- Fall time (t_f) – time necessary for the wave to return from peak value to its original value;
- Repetition time (t_{rep}) – time between the peak values of two consecutive transients;
- Repetition frequency (f_{tr}) – the number of transients appearing in a second. It is calculated as: $f_{tr}= 1/ t_{rep}$ (Hz).

Fig. 2.3 illustrates the terms for the parameters of a transient.

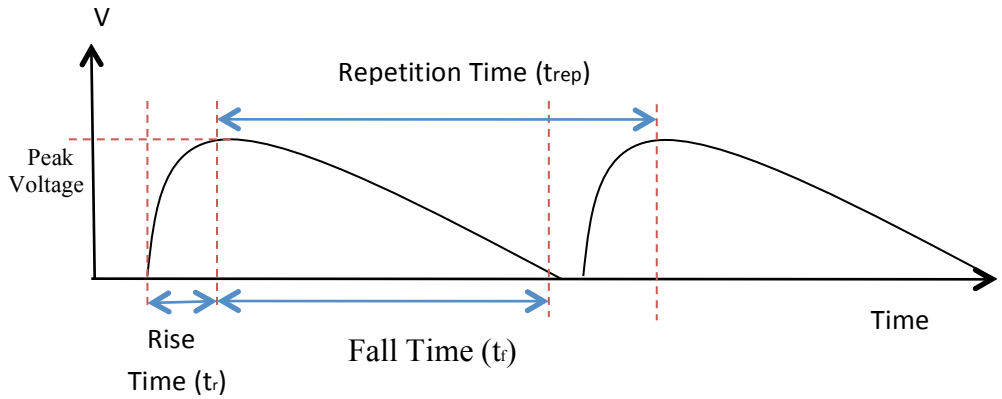


Fig 2.3 – The main terms for the parameters used in describing a repetitive transient

The influence of repetitive transients has been studied for the last 20 years, but mostly on motor winding insulation [3, 4, 13-18, 42-48]. A short overview of the effects is outlined in the following section.

2.2.2 Effect of repetitive transients on electrical insulation

Prolonged exposure to repetitive transients is expected to be hazardous for several materials. One well-documented example is the effect of transients generated by adjustable speed drives (ASD) on the motor's slot insulation constituted of epoxy resin [48]. ASDs are used to control the spinning of the motors, therefore the power, by variation of the input waveform. The input PWM waveform is characterized by frequencies between 2-20 kHz and very fast rise pulses, as illustrated in Fig. 2.4 [13].

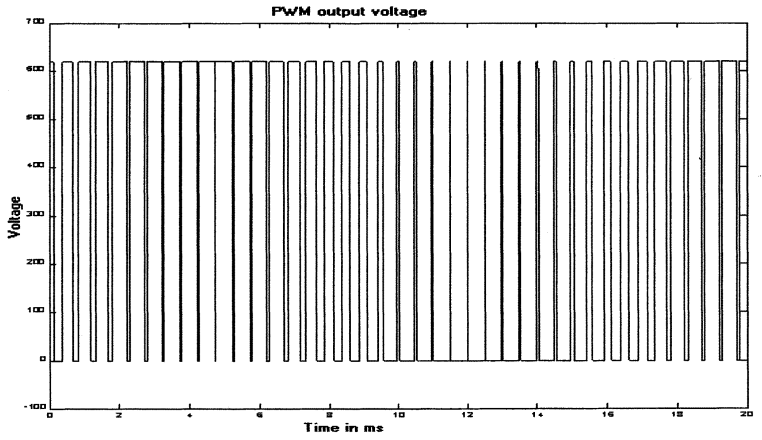


Fig.2.4 – PWM waveform generated by the power electronics in the ASD [13]

The pulses in Fig. 2.4 are generated by power electronics such as gate turn off thyristors (GTOs), bipolar junction transistors (BJTs) and IGBTs that perform the fast switching. To obtain a better quality signal, more switching pulses are required. A simple schematic of a motor controlled by power electronics is presented in Fig. 2.5.

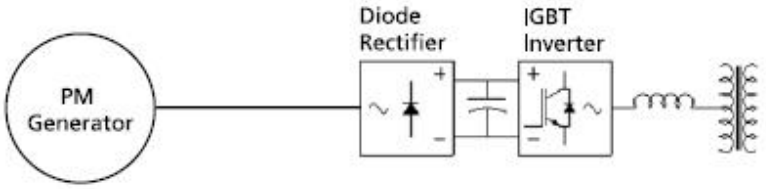


Fig.2.5 - A three-phase induction motor controlled by power electronics [13]

As illustrated, the three phases voltage passes through the diode rectifier to be switched by the IGBTs. The firing angles and the delay times (not shown) are responsible for the switching frequencies.

Information is currently available on the effect of transients on AC motors. Transient-like voltages affect the in-between winding insulation of motors by causing partial discharges (PD). Motor insulation differs from the transformer one as it is solid, usually constituted of epoxy resin.

PDs are created when a high enough electric field across a void or crack inside the insulation is applied. PDs are dangerous as prolonged exposure to them can lead to total electric breakdown within the insulation system.

In the found literature, relations have been found between partial discharge inception voltage (PDIV) and the three main parameters of repetitive transients [14, 48]. These parameters have their strong effect on the degradation of motor insulation.

High transient magnitude and repetition frequency are both inversely proportional to the time to failure of motor insulation. The higher the transient's repetition frequency is and the higher voltage magnitude, the shorter the time to failure becomes. The effect of these parameters on the time to breakdown of motor enamel wire insulation is presented in Fig. 2.6 [17, 18].

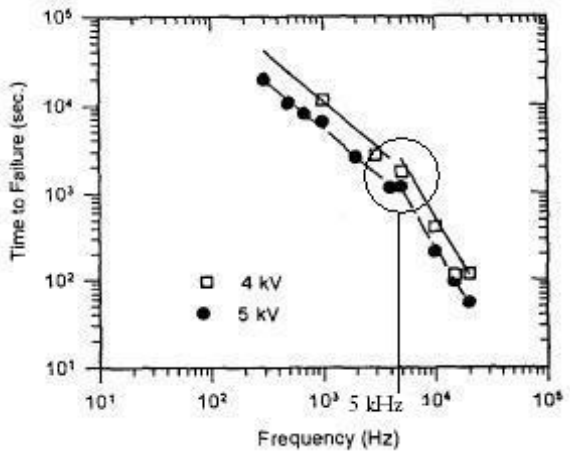


Fig. 2.6 – The time to failure of a pair of twisted wires when different magnitudes and frequencies of a square waveform are applied [17]

In Fig. 2.6, a square wave was applied to a pair of twisted wires intended to represent the insulation of a motor. The duty cycle of the square wave was 50 % and the magnitude was set to 3 $kV_{pk\text{-}pk}$. As the repetition frequency was increased, the time to failure decreased. The trend was linear but a "proportionality break" was observed at 5 kHz. The reason for this was unfortunately not explained. A similar result was obtained when the square wave's magnitude was increased to 4 kV but shorter times to failure were registered.

The effect of increasing rise time on motor insulation was also investigated and the results are shown in Fig. 2.7.

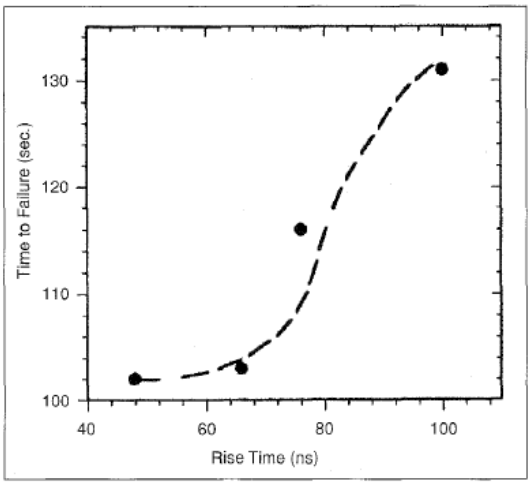


Fig 2.7 – Illustration of the effect of rise time on the life-span of insulation [18]

Fig. 2.7 was acquired by stressing a pair of twisted wires covered in epoxy resin to test their endurance to fast pulses. The applied waveform was a square wave with 50 % duty cycle, 4 kV in magnitude and a 20 kHz repetition frequency. The rise time of this wave was changed between 45 ns and 100 ns while observing the time to failure. It was noticed that as the rise time was longer, the insulation's time to failure increased. PDs were attributed to be the leading cause of failure. As the rise time was faster, the higher intensity PDs were noted leading to the failure of the insulation.

The above information was carried out for enameled wires from a motor insulation. Power transformers are similar in construction to motors, e.g. they both have insulated windings. Voltage source converters apply similar waveforms as ASD and therefore a possible reduction in lifetime due to transients can be expected even though the material used in transformers is a combination of paper-oil.

2.2.3 Reaction of paper-oil insulation to heat fluctuations

With the introduction of smart grids and an increase in power demand, the power grid's components operating temperatures are expected to rise. Temperature is one of the factors that can influence the rate of aging of an insulation system [17], e.g. paper-oil insulation in transformers. However, when applied in a short term, it can be used to improve the insulation's dielectric properties but if applied for too long time and/or at a too high temperature, chemical reactions can appear that will start to decompose the fibrous bonds found in paper [19, 20].

Temperatures up to 60°C are considered to be not harmful to the paper [19]. For this reason, this temperature is usually selected to impregnate the paper with oil before applying it on the transformer. Impregnation is necessary to remove moisture and air from insulation system in order to avoid PDs whilst in operation. As the oil's viscosity decreases with higher temperatures, the oil can impregnate the paper by filling places between the fibres that would be hard to reach otherwise.

Higher temperatures increase the chemical degradation of the paper, increasing the stiffness and brittleness of the fibres [6]. Acids are created when the paper-oil system is in contact with oxygen causing an increase in conductivity and dielectric loss [6, 19]. Gas by-products are also created by rises in temperatures. They can be found in oil or created by the decomposition of solid insulation based on cellulose. The oil becomes hygroscopic and receives more water from the atmosphere causing unwanted reactions leading to oil impairment. Oil sediments cause conductor heating whereby molecules couple into macromolecules, the oil viscosity increases, oil circulation decelerates and the cooling function decreases due to polymerization.

In general, paper is "wetter" than oil, even though dried prior to impregnation. An increase in the operating temperature of the transformer will cause moisture particles to exit the paper and enter the oil, reducing further its dielectric properties by the creation of bubbles. These bubbles are constituted of gas, they possess a different dielectric constant making them prone to the ignition of partial discharges; therefore aging the paper [19, 20]. The formation of these bubbles is related to moisture, temperature and pressure inside the tank of the transformer and is characterised by the following empirical formula [22]:

$$T = \frac{6996,7}{22,454 + 1,4495 \cdot \ln(w) - \ln(p)} - e^{0,473 \cdot w} \cdot \left(\frac{g}{30}\right)^{1,585} \quad (1)$$

Where:
T is the critical temperature in K;
w is the water content in the paper in %;
p is the total pressure in the transformer equal to the sum of the atmospheric pressure and the pressure of the oil column in Torr (1 Torr = 133.32 Pa);
g is the content of gases in the oil in %.

The effects of these parameters described in equation (1) are shown in Fig. 2.8.

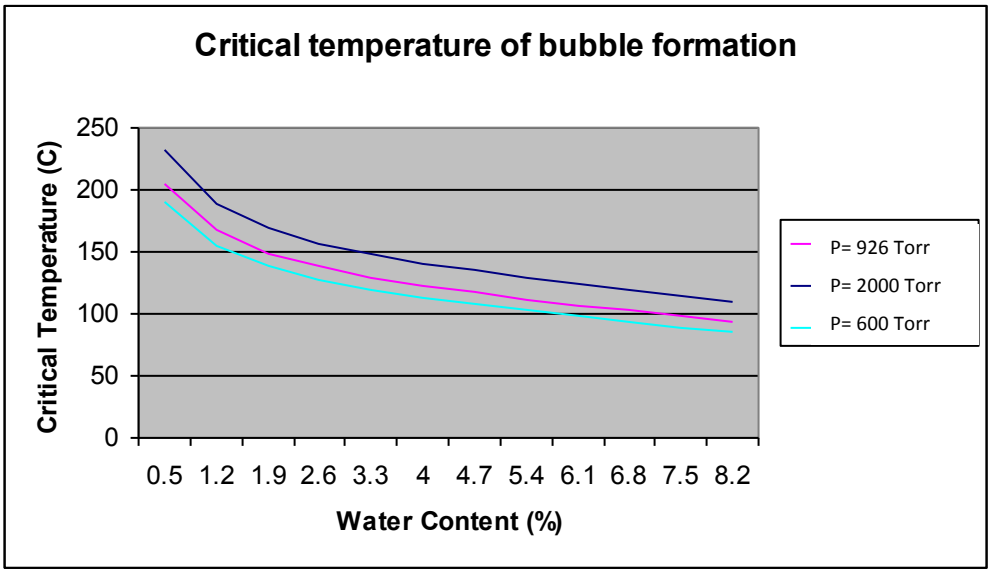


Fig 2.8 – Conditions necessary for the creation of bubbles in a transformer's insulation at different pressures

Once the operation of the transformer is returned to normal operating conditions, the temperature inside the winding is also decreased. At lower temperatures, moisture is reabsorbed by the paper. This process is repeated every time the operating temperature of the transformer varies.

As the paper ages, its absorption capabilities are diminished. This leaves some of the moisture in the oil making it wetter thus reducing its breakdown strength and increasing the loss factor (tan (δ)) [20, 22].

The temperature of the transformer is predicted to vary constantly during the day depending on the power loading. It is expected that temperatures up to 90 °C in the hottest spot can be reached [23]. This is a very high number that can be increased further by the addition of repetitive transients. For this reason, the state of the quality of paper from a dielectric point of view was carried out for 40, 60 and 80 °C and the results will be presented in Chapter 5 after the effects on paper-oil have been investigated at room temperature in Chapter 4.

2.3 Aging of Transformers

The transformer's aging rate is characterised by several parameters, referred to as aging factors. Such factors have a specific effect on a subcomponent of the transformer such as tap changer or winding, among others. Aging factors can be of several types: mechanical, thermal or electrical. For the purpose of this thesis the latter two are investigated as they fit into the theme of future trends at which this thesis focuses on.

2.3.1 Failure rate

Most of the failures in a transformer occur in the tap changer, either on load or off load ones (Fig. 2.9 [8]). This is due to the fact that the tap changer possesses moving parts that are prone to carbonisation and need to be maintained on a regular basis. The carbonisation is influenced mostly by the power at which the operations are carried out and by the waveform quality. Too high currents are most likely to cause small corona discharges and on a later stage contamination of the contacts. The insulation is the second most likely component to fail. Its failure is generated by the high power load applied and excessive moisture in the insulation system. These findings are based however on already existing stresses in the grid.

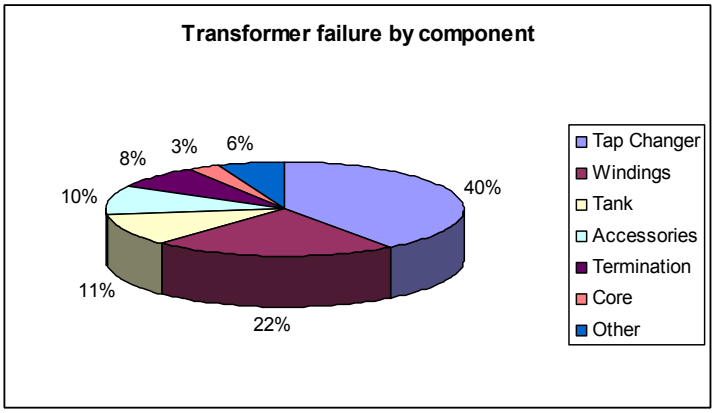


Fig. 2.9 – Failure rates in a transformer by component [8]

Many transformers are now reaching the end of their economical lifetime of approx. 40 years, as shown in Fig. 2.10.

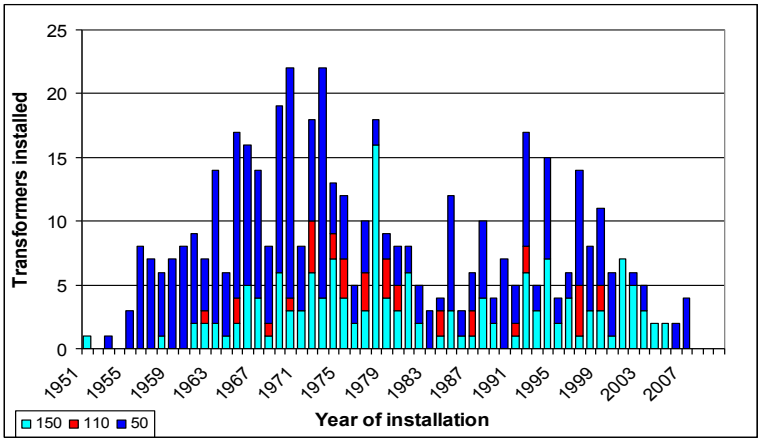


Fig. 2.10 – Number of transformers installed in the Netherlands each year [28]. The different colours indicate the voltage class.

Taking the average economical lifetime of 40 years, it can be deduced from Fig. 2.10 that several transformers may need to be replaced soon in the Netherlands. With new factors influencing the aging rate such as repetitive transients and heat variations, the rate of failure will additionally increase. For this reason it is important to quantify the aging rate together with current and future stresses.

The aging rate can be predicted by analysing all significant aging factors acting on the transformer and its subcomponents. Missing one of them can result in the

creation of an aging model that will provide non-accurate data about the remaining lifetime of the transformer.

2.3.2 Aging factors

Every component or device that is utilized in the grid has a theoretically defined lifetime. This lifetime is influenced by many factors such as operation history and working environment. Each of these aging factors has a different impact on the sub-components of the device. It is therefore important to identify all the significant aging factors and their effects in order to understand the complete aging process of the component. It has to be also noted that not each aging factor has an equal weighting on the deterioration process of the device.

The aging factors can be grouped as following:

- **Thermal** aging factors; thermal aging can be caused by both the load magnitude and by the outside environmental conditions. The temperature and its variations are mainly responsible for the degradation of the electrical insulation;
- **Electrical** aging factors; electrical aging is caused by the voltage load of the component and by the influence of the distorted voltage wave shape (e.g. with repetitive transients on it);
- **Environmental** aging factors are external causes related to weather conditions and air pollution;
- **Mechanical aging factors** are related to moving parts inside the device, such as in tap changers in a transformer.

When combined together, the aging factors can have an accelerated degrading effect on component materials such as the insulation layers of a transformer winding. For example a high power demand might be needed due to many air conditioners working on a hot day, causing a transformer to heat up well above usual operating temperatures. To determine the aging model for a component's life cycle, a relationship between its stresses and properties needs to be known. The time to failure is usually indicated by the rate of decay of a component by measuring selected quantities. Using a simplified model where we assume that the stress (S) is homogeneous throughout a certain time (t) of the component with specific properties (P). In particular, we can assume [29, 30]:

$$F(P)= K(S)t \quad (2)$$

With *K(S)* being the aging rate and F(P) the failure probability.

After a certain amount of time, the component will reach its breaking point when the material fails, P_L. Therefore, the relationship required to achieve this stage can be characterized by:

$$L = F(P_L)/K(S) \quad (3)$$

Where *L* is the breaking point in time of the component.

Unfortunately, the component will always be in a degradation cycle, as aging factors will always be acting on it leading to failures. The only parameters that might change are: the stress level and different reactions to the stresses by each different type of materials, as shown in the Fig. 2.11.

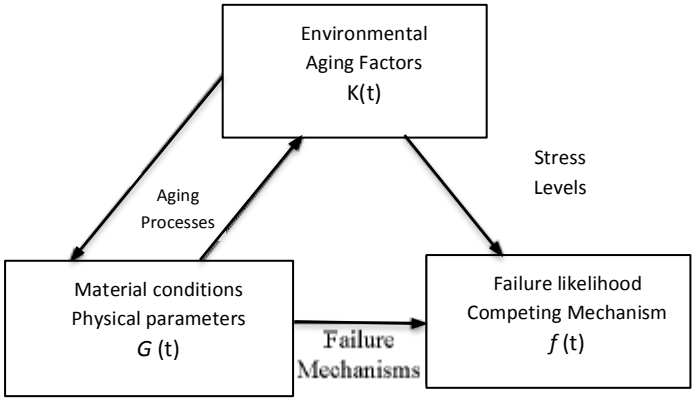


Fig. 2.11 Diagrammatic representation of the evolution of a failure in any insulation system [30]

One of the tasks of a smart grid is to assess if a component is degrading regularly. In order to do so aging models may be required. These models are usually based on a measured quantity inside the transformer like e.g. moisture content in paper and oil or gasses in oil. When such values are measured after a certain period of time since the start of service of a component, it is then compared to the value that is indicated in the model after the same amount of time.

These aging factors can be applied to any component in a grid, with some being more susceptible than others. A transformer is most prone to thermal and voltage loading as its insulation system is susceptible to all various aging factors as

temperature, moisture and electrical stresses [31] and on which we focus in this thesis. In Fig. 2.12 a diagrammatic representation of the aging factors that affect a transformer's insulation is presented.

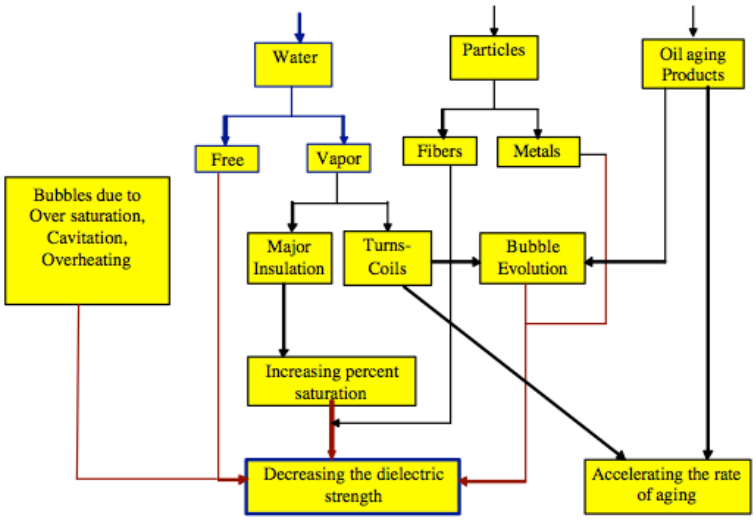


Fig. 2.12 – Several stresses on a transformer's insulation [9]

Cellulose insulation aging is a chemical phenomenon that involves the simultaneous interaction of temperature, water and oxygen, with water being the dominant aging agent [9]. An acid catalyst obtained from the oxidisation of mineral oil enhances hydrolytic decomposition of the paper. Hence keeping the insulation free from water and oxygen is still considered one of the best life prolonging actions.

2.3.3 Currently available aging models

Various transformer aging models already exist:

- **Graphical models**; based on a measured quantity such as degree of polymerization or furanic content. The measured value of one of the parameters usually corresponds to a specific point in the life of the transformer;
- **Flow chart models**; giving a "step-by-step" evolution of a fault as it develops in the solid insulation;

- **Equation models** based on different theories of insulation aging, such as Arrhenius. These theoretical models are very useful when planning maintenance.

The main purpose of the model is to determine with relatively high accuracy the time at which a device or component will fail. The main challenges of an aging model are to:

- Describe accurately the relationship between the lifetime and the stresses;
- Gather parameters needed to describe in detail the status of a component or its insulation system;
- Calculate the estimated time to failure based on a specific set of stresses.

Aging models can have many forms. They are usually presented in equation or graphical forms and for a specific transformers they are usually used for reference purposes only. Graphical models take into consideration a specific parameter and its value is compared to a time scale. Based on these values, the remaining lifetime of a component can be predicted.

2.3.3.1 Graphical models

Graphical models are based on the measurement of a specific parameter over time. The trend of change of that quantity has been recorded in the past and the limit values have been settled for a specific point in time of the material's or a component's lifetime. The most common parameters to determine the state of insulation in service are illustrated in Fig. 2.13.

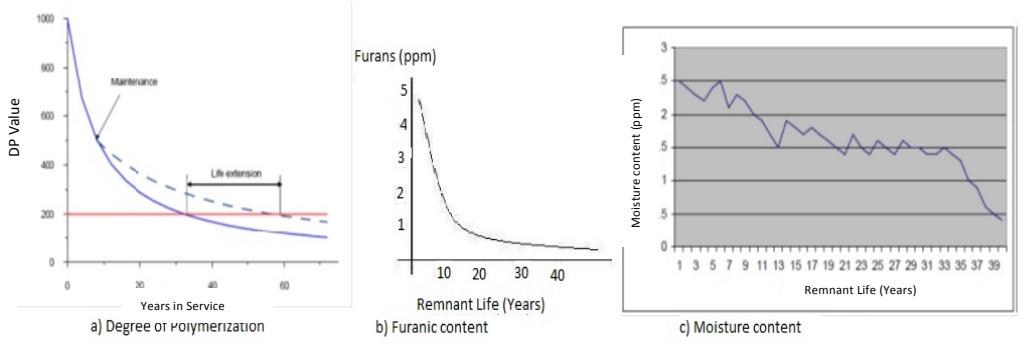


Fig. 2.13 – Graphical aging models used to determine the state of the paper-oil insulation [6, 23]

Some examples include:

- **Degree of polymerization (DP)** indicates the average number of cellulose units per molecular chain. This method is good in determining the state of the insulation degraded by dielectric and thermal stresses [6];
- **Furanic Compounds**; furans are released from the paper due to thermal and electrical aging factors. Their concentration is often a good indicator of the remaining life time [23];
- **Moisture content** is absorbed into the insulation system from the external environment and due to heat fluctuation in the paper-oil insulation system. Too high levels of moisture can lead to dielectric failure and therefore reducing the life expectancy [22].

2.3.3.2 Equation models

Equation models are theoretical models based on the insulation's material degradation phenomena. We used three equations that have been proposed to relate the thermal and electrical aging.

- Montsinger [34]

Montsinger suggested a basic equation that can be used to calculate the lifetime of a transformer insulation based on the degradation process of the oil-impregnated paper as a function of the top temperature of the oil. The equation is given as:

$$\tau=\tau_0 \bullet e^{-A\vartheta} \quad (4)$$

Where: τ is the lifetime, τ_0 is the lifetime at 0 °C, Θ is the current top temperature of the oil and A is a constant. From this model it can be deducted that an increase between 8 and 10 ° C can double the aging rate when the temperature surpasses 80 °C [6, 24, 34].

- Power law

The Power Law equation relates to electrical degradation processes due to e.g. partial discharges, however it is used more in general to characterise the lifetime of electrical equipment during operation. It relates the electric field stress (in kV/mm) to time (in hours). It is represented below as:

$$\tau=aV^{k} \quad (5)$$

Where τ is the expected life of the transformer, a and k are based on the material quality and V is the voltage.

- Arrhenius

Arrhenius formula is based on the general reaction rate of a chemical reaction. This formula is the basis of many models, one of them the Eyring model applied in Chapter 6. The general equation is shown as:

$$k = Ae^{-E_a/(RT)} \tag{6}$$

Where k is the rate of the chemical reaction, T is the temperature (K), A is the pre-factor, E_a is the activation energy (kJ/mol) and R is the universal gas constant.

The Arrhenius formula has been available for the last 30 years and is used in general to describe thermally activated electrical aging processes. The models can still be accurate in today's electrical grid environment; however, need to be adjusted and should take into account the new phenomena in the grid changing the degradation rate in insulation.

2.4 Conclusion

On a grid component level, changes will become more significant as HV devices, such as transformers, will be affected directly by grid changes. Repetitive transients and heat fluctuations will affect the lifetime of transformer insulation. Paper-oil insulation systems are the most common material type used for winding insulation and up to this date it was almost not investigated how this system reacts exposed to repetitive transients. Current aging models are based on aging factors from 20 years ago and do not quantify the new circumstances in which transients play an important role. It is therefore necessary to qualitatively test and analyse the effect of repetitive transients on paper-oil insulation.

In this thesis, the effects of the various shape parameters of repetitive transients on dielectric properties of paper-oil samples are measured and analysed in detail. In Chapter 4, various waveforms are applied to insulation samples and the results are presented in terms of time to breakdown and breakdown voltage. In Chapter 5, transients are applied in conjunction with temperatures above room temperature and the data is analysed in terms of loss factors (tan δ). A model to predict lifetime consumption due to transients is created in Chapter 6.

All paper-oil samples can vary between different transformer manufacturers. It is therefore important to identify the dielectric behaviour of the samples under standard 50 Hz AC conditions. These investigations are performed in Chapter 3 where the time to breakdown and breakdown voltages are analysed.

Chapter 3
Dielectric Evaluation of Paper-Oil Test Samples

Electrical insulation is a vital part of any HV device. Its purpose is to provide isolation of parts of the device being at different potential. In HV applications, dielectric strength is the most important functional property of the insulation system. It is the maximum electric field strength that the insulation material can withstand without breakdown.

In the previous chapter, repetitive transients were identified as a potential aging factor in the future grid, especially for transformers. Experiments are performed in this thesis to quantify the effects on paper-oil insulation by repetitive transients however, before starting this process, it is necessary to set a benchmarking point on how the paper behaves under normal 50 Hz AC conditions. Dielectric breakdown strength, time to breakdown and dielectric loss are some of the parameters that will be used and compared throughout this thesis and specifically investigated in this chapter.

Paper-oil insulation is the main material used in insulating the windings, thus a description of this material is provided. Additionally the importance of the experimental procedure is described as it is used in all the experiments throughout the investigations presented in this thesis. Electrode selection and impregnation are also discussed.

Finally, the results are presented and compared with theoretical values found in literature. These values will later be compared when the insulation samples are stressed with repetitive transients.

3.1. Paper-oil Insulation

Insulating liquids are used not only to eliminate air and other gases in order to improve the dielectric insulation but also for the component´s cooling purposes. In HV devices such as transformers, high heat dissipation abilities, due to high convection and thermal conductance, are attributed to liquids [32].

Mineral oils are derived from crude petroleum, which is distilled for several applications, dielectric insulation being one of them. The oil used for the samples tested in this thesis is Shell Diala B [33]. This oil is used in a variety of power transformers due to its good oxidation stability, dielectric strength, heat transfer characteristics and very good low temperature dielectric properties [21, 35].

Mineral oil is susceptible to various degradation factors that can influence its dielectric strength. The most significant ones are:

- Moisture; it affects the dielectric strength of the liquid and increases dielectric losses with its presence. A value of 4 % moisture level is considered risky, whereas at 7 %, failure can be imminent [22];
- Dissolved gasses; different gasses are created in the liquid due to the present conditions of temperature, pressure and moisture levels. The hazard to the liquid's dielectric properties is determined by the solubility of the gas in mineral oil;
- Oxidation; it is the chemical reaction of an oil molecule with oxygen present from ambient or trapped air. Oxidation rate increases exponentially with increasing temperature according to the Arrhenius rate rule and doubles for every 10 °C rise in temperature above 75 °C [20].

Oil is stored in a transformer tank so that moisture and air cannot contaminate it. This requires regular maintenance of the tank, usually metallic, so that no leaks can occur. Oil is also highly flammable; therefore extra caution needs to be applied so that it does not come in contact with any excessively hot materials.

The most common type of paper used for electrical insulation is cellulose based paper, constituted of pure Kraft cellulose. It is good for impregnation, and is easy to be moulded, bended and wrapped around a conductor. The paper is constituted mostly by cellulose fibres [6]. The structural chemical formula of cellulose can be seen in Fig. 3.1.

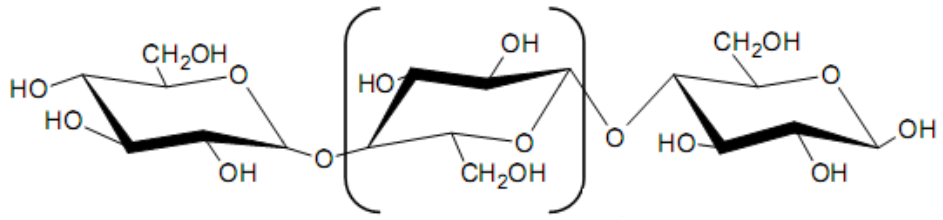


Fig 3.1 – Molecular structure of cellulose [6]

Cellulose is a linear condensation polymer consisting of anhydroglucose joined together by glycosidic bonds. The amount of glycosidic rings in a cellulose macromolecule is defined as the degree of polymerization. The value for the degree of polymerization is initially 1400, after purification procedure this value drops to 1200, which is the standard value used for defining a good quality sheet of paper.

Between 10-20 % of the paper is constituted by hemicelluloses. This non-uniform group of complex polysaccharides form the matrix in which the cellulose fibres are embedded contributing to their mechanical strength. In addition, lignin is a highly complex polymeric substance forming together with cellulose the main component of wood. It is present in small amounts, usually between 2-6 %.

The presence of contaminants influences the dielectric and hygroscopic properties of paper. Moisture, voids and foreign particles can decrease the dielectric strength of the paper and decrease the partial discharge inception voltage level leading to failure. Drying techniques are implemented to reduce the chance of contamination. The technique implemented by the author is discussed in the following Chapter.

Paper is constituted of randomly interlaced fibres. The mechanical strength of these fibres determines the dielectric characteristics of a specific sheet of paper. The more fibres are present, the higher dielectric strength can be obtained [36, 37, 38].

In “natural” paper, the fibres are aligned in a random manner (Fig. 3.2) whereas, in synthetic paper, this alignment is set to a single direction, such as Nomex® making the paper easily to tear in one direction, but very hard in the perpendicular one. The dirt seen on the photo is attributed to the build-up of oil.

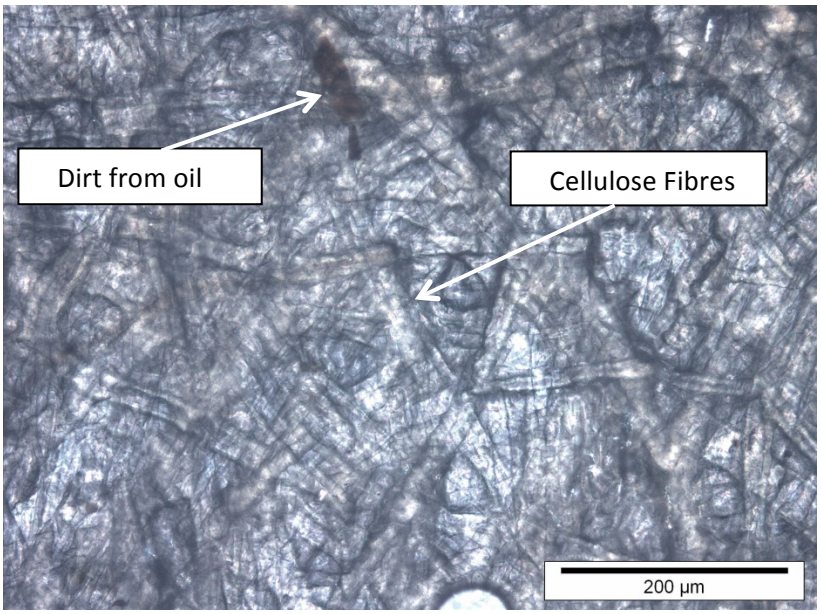


Fig. 3.2 – Fibres observed with an optical microscope in a cellulose specimen

In Chapter 2, two new insulation aging factors were introduced: repetitive transients and high temperatures. The influence of these aging factors on fibrous materials is not well understood. It is expected that the insulation's aging will vary in accordance to the magnitude, repetition frequency, rise time of repetitive transients and the applied temperature.

Before any results can be analysed, it is important to prepare the samples correctly for the investigations and to have a set of results to which the obtained experiments can be compared.

The combination of paper and mineral oil increases the dielectric properties of the insulation whilst still allowing the paper to maintain its mechanical properties. The oil, due to its low viscosity, fills any air voids between the various fibres of the paper. The utilisation of several layers of paper sheets to increase the level of applied voltage. With only few voids in the paper and between the paper sheets, PDIV level are still kept low and therefore the probability of failure is decreased.

3.2 Preparation of the Samples and Test Electrodes Selection

In the experiments we tried to eliminate all the factors, beyond the ones under experiment, which can influence the values of dielectric strength of paper-oil samples and consequently change their time to breakdown. In particular:

- The level of humidity inside the samples has to be kept at minimum possible level;
- The presence of air bubbles has to be eliminated by impregnation of the paper samples with oil according to the rigid transformer manufacturers procedure;
- The sharp edges on the electrode's curvature should be eliminated to prevent breakdown due to a local increase of the electrical field and local inception of partial discharges during the tests.

These factors of influence were therefore taken into account throughout the various stages of the research.

3.2.1 Test samples

The samples, as shown in Fig. 3.3, have been acquired from a transformer manufacturer who specialises in the production of 18 kV, transformers used in wind farms. The grade was not specified.

The samples are 0.06 mm thick, with a uniform spread of thickness (±0.005 mm). These samples were used throughout the thesis in various experiments. Only in Chapter 3.2.2 other types of paper samples were used to test the impregnation technique and the effect of a different electrode configuration.



Fig. 3.3 – Photo of a paper-oil test sample

3.2.2 Sample impregnation and electrode selection

A good impregnation of the paper sample with mineral oil is necessary to remove any moisture and air trapped inside the paper. As previously discussed, these unwanted entities can decrease the time to failure which cannot be attributed to aging or stresses induced during the test.

In a transformer factory the impregnation is performed in several stages. The paper is dried in an oven, set to 60 °C in vacuum conditions for 24 hours. The temperature selected is just enough to get rid of any excess moisture whilst not significantly aging the paper thermally and thus improving its dielectric properties.

The same procedure was applied in the laboratory on four groups of different types of paper insulation samples from other sources:

Sample A; paper of thickness 0.148 ± 0.01 mm used for cable insulation, not impregnated by the manufacturer;
Sample B; un-stretched "wrinkly" paper used for winding insulation of thickness 0.351 ± 0.03 mm. The paper is wrinkly to facilitate the winding process of a transformer's winding;
Sample C; stretched "wrinkly" paper used for transformer winding insulation (same as above) of thickness 0.2 ± 0.09 mm;
Sample D; pressboard of thickness 0.248 ± 0.012 mm.

These batches of samples were less homogeneous in the material properties and therefore only used to verify the impregnation procedure. They were later discarded and all significant tests were performed on the 0.06 mm samples shown in Fig. 3.3.

The choice of the electrode (metal and shape) needed also to be addressed at the beginning. For example, the field could be enhanced at the edges of an electrode and result in a lower breakdown voltage. Taking this into account, two types of electrodes were tested to reproduce the electric field distribution in transformer winding (Fig. 3.4):

- Stainless steel, flat contact surface, round shaped electrode of 2.5 cm diameter with curvature following a Rogowski profile and according to IEC standard 60243-1;
- Brass spherical electrode with a diameter of 3 cm.

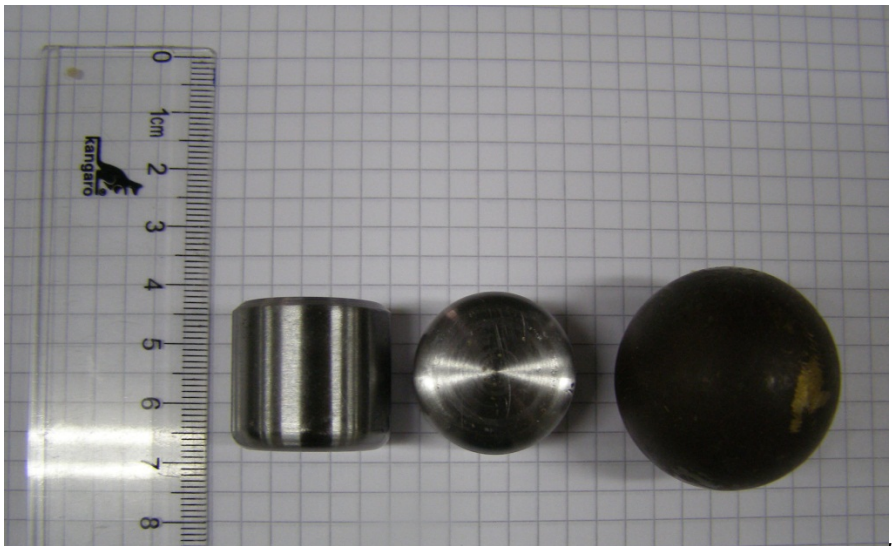


Fig. 3.4 – Photo of the two types of used electrodes

The influence of sample conditioning on AC dielectric breakdown voltage is presented in Fig 3.5. The four types of insulation samples were tested according to the IEC standard 60243-1. Conditioned samples refer to the ones that have been placed in the oven for 24 hours in vacuum at 60 °C. Twelve samples were investigated for each electrode shape and conditioning type. The average values are presented in Fig. 3.5. To limit further the influence of the previous breakdown on the next, each electrode was cleaned with sand paper to remove carbonisation spots.

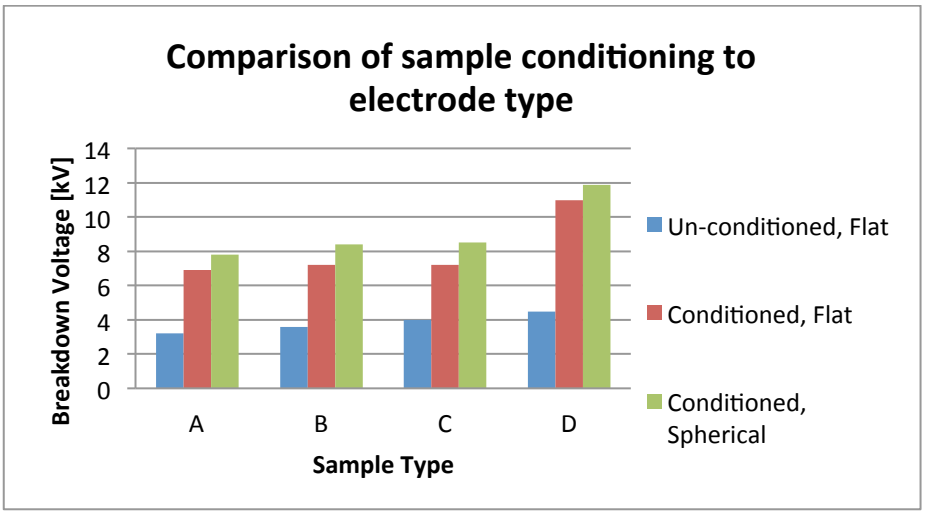


Fig. 3.5 – The effect of sample conditioning on the AC dielectric breakdown strength of four types of samples in the test set up with different electrodes

The results indicate that the breakdown voltage increases on average when the samples are conditioned. Furthermore, using a spherical shaped electrode, this value increases by approx. 12%. Conditioning the samples in an oven before testing removes most of the moisture and air trapped between the fibres of the paper. This reduces the probability of any early failures at a lower voltage level.

Using a spherical electrode to stress the paper electrically, limits the surface are stressed, thus reducing the probability of identifying any weak spots in the sample. The flat-round shaped electrode covers a larger surface area therefore stresses more of the sample at the same time. One of the drawbacks of using a flat surface electrode is the field enhancement at the edge of the stressed area. The Rogowski profile should limit these field enhancements. During the breakdown experiments, the location of the breakdown was observed. It was noticed that most of the breakdowns occurred in the central part of the electrode and less than 2% of the breakdowns occurred in the outer region of the electrode.

In conclusion, the flat electrode was chosen for the tests, as it reproduces better the shape of a transformer's winding. It was concluded that the electrode's flat shape stresses more of the paper surface thus increasing the probability of identifying more of the weak spots in the paper sample. All samples need to be conditioned to remove as much as possible the trapped moisture and air. This procedure will diminish the probability of any unwanted failures, such as infant mortality of the samples.

3.3 AC Dielectric Strength Tests

The samples described in Chapter 3.2.1 were investigated and the breakdown voltage was measured. The 50 Hz AC voltage waveform was applied to the samples. The procedure was carried out according to IEC 60243-1. This means the voltage was increased in voltage steps up to breakdown at the rate of 1 kV/s. The measured breakdown voltages are indicated in r.m.s. values.

The field strength at which breakdown occurs depends on the geometries of the dielectric sample and the electrodes with which the electric field is applied, considering a stable and repetitive rate of electric field application. Because dielectric materials usually contain minute defects, the practical dielectric strength will be a fraction of the intrinsic dielectric strength of an ideal, defect-free material.

3.3.1 Data representation

Using flat electrodes makes the Weibull analysis appropriate because of its basis as extreme value statistics for weakest links [39, 40, 41]. This method allows for an effective evaluation of the results in terms of scattering, unreliability and confidence in the results. The formula for the cumulative distribution function, derived in Appendix A, in the case of two-parameter function is:

$$F(E) = 1 - e^{(-\frac{E}{\eta})^{\beta}} \tag{3}$$

Where:

E is the electric breakdown field strength;

F is the cumulative failure probability;

η is the scale parameter characteristic for the field strength at which the failure probability is 63.2 %;

β *is the shape parameter, which is comparable to the inverse of the standard deviation.*

A three parameter Weibull function and distribution is not recommended in this case as it is only applied for long term observation of a system rather than accelerated aging tests [41].

3.3.2 AC dielectric breakdown test

The results of AC dielectric breakdown tests are represented in the Weibull unreliability plot shown in Fig. 3.6.

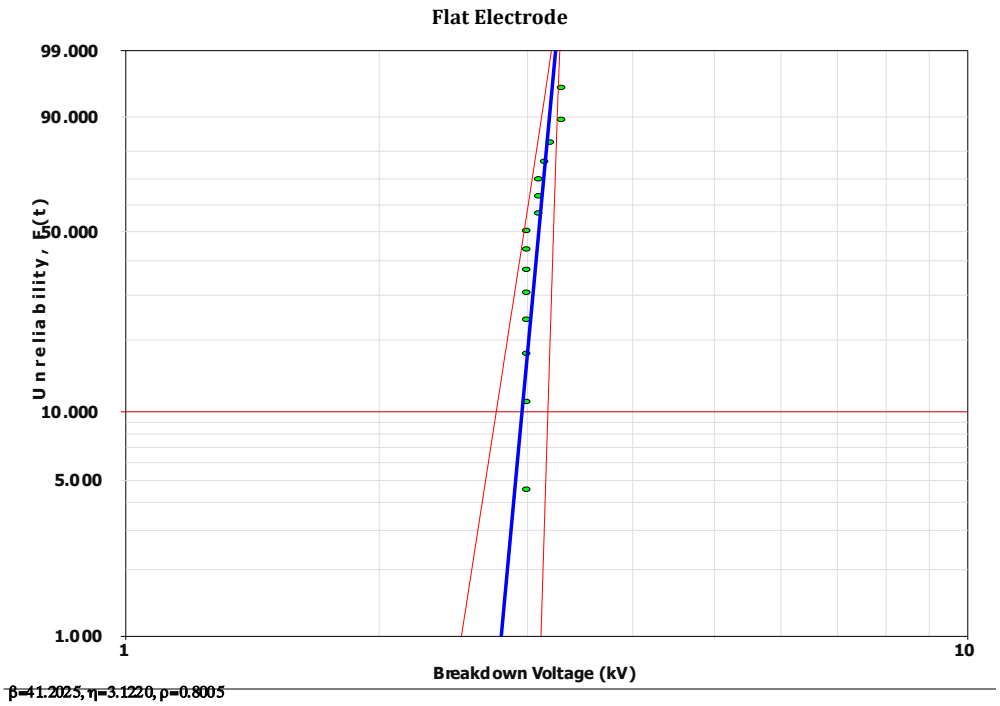


Fig. 3.6 – Weibull unreliability plot for AC step-up breakdown values of 0.06 mm thick paper samples using a flat shaped electrode. The β and η parameters are 41.2 and 3.12 kV respectively. 90 % confidence bounds are shown in red

In Fig. 3.6, a small spread of results, with a 50% average breakdown of 3.07 kV (51.2 kV/mm), ± 0.1 kV is shown. These results offer a small distribution regardless of the low homogeneity of the paper. Thinner parts will always be present, especially when the thickness of the paper is 0.06 mm, as it is in this case.

3.3.3 Life time estimation based on time to breakdown and applied voltage

The lifetime of paper samples can be related directly to the applied electric field strength, using the well-known power law model which exponent can differ depending on material quality of the sample. The work performed in this section will try to evaluate the theoretical life curve of the samples used in this research.

The test samples were aged under the effect of AC waveforms of magnitudes: 2.91 kV, 2.53 kV and 2.22 kV, so below the average breakdown voltage of 3.07 kV obtained in the tests described in Chapter 3.3.2. Twelve samples were stressed for each voltage level. The average mean lifetime was recorded which resulted in: 168

h (± 89 h), 360 h (± 148 h) and 890 (± 408 h) hours respectively to the voltage levels mentioned. The error in the brackets is the standard deviation of obtained breakdown times. The data has been further analysed and represented on the Weibull unreliability plot in Fig. 3.7 for 2.91 kV and 2.22 kV to better recognize the differences of data. The probability line is fitted according to the maximum likelihood estimation method (MLE) [39].



Fig. 3.7 – Weibull unreliability plot for paper-oil samples stressed at 2.91 kV and 2.22 kV. The Weibull parameter β is 0.84 and 2.14 for 2.22 kV and 2.91 kV respectively. The η parameter is 1491.8 h and 187.1 h for 2.22 kV and 2.91 kV respectively. 90% confidence bounds have been applied

It can be inferred from Fig. 3.6 that the life of insulation is related to the applied electric field strength value. The η parameter decreased between 3 and 20 times when considering the confidence bounds with an average value of 8 times when the field strength was lowered approx. 24 %.

It should be noted that PD measurements were performed in parallel with the AC dielectric breakdown tests. PDs are common in paper-insulated devices but are not always straightforward to detect [54]. These measurements were carried out according to conventional method (IEC 60270). The PDIV was 2.4 kV, which is above the lowest stressed voltage level and below the two higher voltage values.

The scattering of the results is higher for the voltage level of 2.22 kV. Weak points in the paper sheet are the probable reason for the high scattering of breakdown times. The weak spots are defined as thinner spots of paper, and as the thickness can vary, times to failure are dependent on the applied electric field strength [37].

Every paper manufacturer may have a different paper manufacturing process. For this reason, every type of sample needs to be electrically tested in order to understand its dielectric capabilities. Therefore, a basic theoretical lifetime was calculated based on the life estimation formula (4) [20]. This is one of the first available formulas used to calculate the lifetime of paper samples. Since then it is generally accepted that the aging of cellulose can be approximated by the power law [35].

$$g = g_s\left(1 + \frac{a}{\sqrt[4]{t}}\right) \tag{4}$$

Where:
t is the time of voltage application, in seconds;
g_s is the voltage gradient in kV/mm for an indefinite time of voltage application;
g is the voltage gradient applied in kV/mm;
a is a constant relative to the testing environment.

Two life-curves are compared in Fig. 3.8. The values of the actual applied voltage have been converted to electric field strength values based on the average sample thickness of 0.06 mm. From previously carried out research [6, 20], for cellulose paper life curve, a linear relation to the applied field strength is shown, assuming a power law approximation. Having estimated the lifetime of samples for three voltage levels, 2.91 kV, 2.53 kV and 2.22 kV, an estimated life curve was plotted according to the power law estimation model and to equation (4) by entering the corresponding times to breakdown for each voltage level.

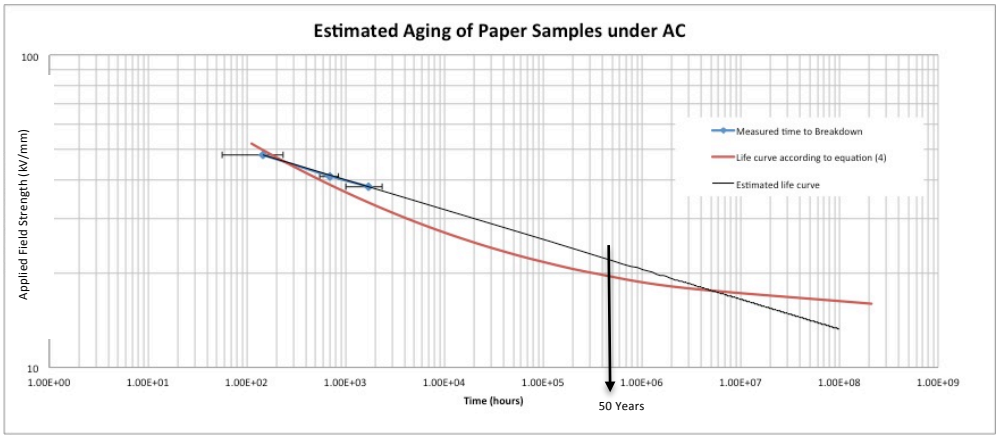


Fig. 3.8 – Life estimation curves for paper samples impregnated in oil as function of the applied field strength. Upper and lower 90% confidence bounds for characteristic 63.2% times to breakdown are shown

The power law extrapolation for the average life and the theoretical estimation of life according to eq. (4) curves are relatively close on the long run. Taking into account the measurement error limits and its extrapolation over 3 decades this is considered to be quite accidental. At lower test voltages the required time to breakdown would not be practically available within the allocated project timeframe. Furthermore variations may have arisen from error levels in the calculation of oil moisture, paper moisture and air temperature that has an effect on the "*a*" parameter in equation (4).

To achieve life spans of 50 years, the standard life expectation of a HV device, lower field strengths need to be applied, in this case 22 ± 8 kV/mm. This is equivalent to 1.32 kV ± 0.48 kV on the test samples. This voltage value is probably higher than the allowed stresses in the device. As the applied electric stresses were above PDIV, a faster degradation occurs in the paper than below PDIV. This voltage value should be treated as indicative as most of the aging tests performed in the thesis are above, or close to PDIV.

3.4 Tangent Delta Measurement Results

The degradation of the paper needed to be monitored during long-term tests. One of the ways to assess the quality of the dielectric properties of the paper is to perform tan (δ) measurements of the paper. The concept of operation is described in Appendix B.

A set of representative paper samples was measured and the results can be seen in Fig. 3.9.

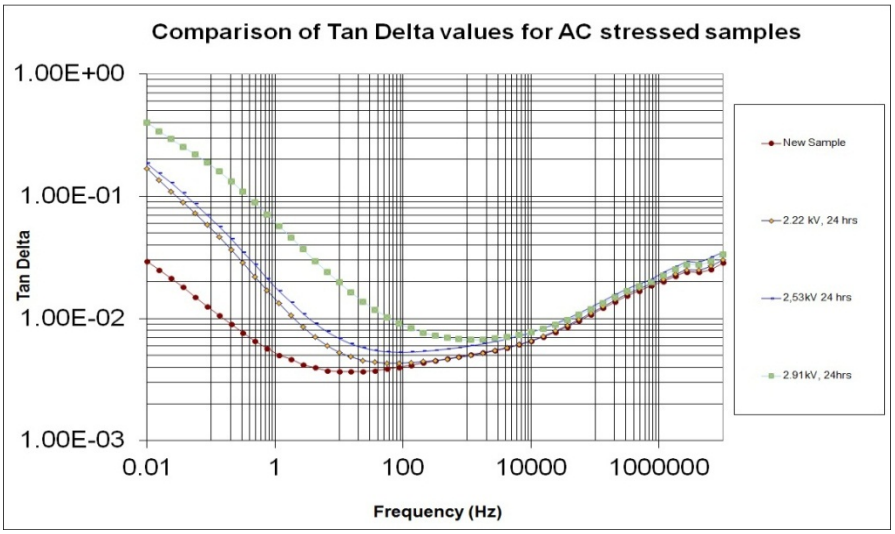


Fig. 3.9 – Results of tan (δ) measurements as a function of frequency of AC voltage after samples were electrically stressed for 24 hours prior to measurement

The results in Fig. 3.9 show tan (δ) values for the same type of paper-oil samples as discussed in Chapter 3.2.1. The paper samples have been stressed for 24 hours under different 50 Hz AC voltages of magnitude: 2.91 kV, 2.53 kV and 2.22 kV. The obtained values are compared to those of an unstressed sample. The first observation that can be deduced is that voltage magnitude has an effect on the tan (δ). The sample stressed with the highest voltage magnitude gathered much higher values in the frequency range from 0.01Hz to 300Hz. The other two voltage levels do not present such high differences between each other but present higher values than the virgin sample. The low measurement frequencies represent a DC leakage current. This is most probably caused by the PDs creating tree inside the paper leading to a low resistance path within the sample. Carbonisation has been observed on the sample when stressed for 24 hours at 2.91 kV. On the other voltage levels, the observations were not conclusive.

The second observation is that the influence of electrical aging due to 2.22 kV and 2.53 kV is much lower than 2.91 kV, which corresponds to 95% of the breakdown voltage. The high magnitude of the AC waveform will need to be taken

into consideration when aging models will be designed as it causes the most aging being well above PDIV.

3.5 Conclusion

The samples of insulation used in this research are constituted of paper-oil, the most common type of insulation used in transformer.

Kraft cellulose paper is the mostly used type of material whereas the oil is of a mineral nature usually derived from petroleum. Cellulose fibres constitute the paper and are interlaced with each other in a random manner. Although high breakdown strengths can be achieved, paper-oil insulation is very susceptible to contaminants like moisture and unwanted particles that decrease this property, so extra precautions need to be taken into consideration.

For this reason, the paper samples needed to be dried in a vacuum oven for 24 h prior to testing. This procedure decreased the scattering of breakdown voltages and breakdown times, leaving the paper homogeneousness as the main factor behind the scattering of results. Single sheets of paper were tested whose thickness were 0.06 mm. The electrodes used had a flat surface of 2.5 cm in diameter and provided good edge rounding as most of the breakdown occurred within the centre of the flat surface area.

Two types of tests were described in this chapter: short-time breakdown tests and long term aging experiments, both at AC voltage. The breakdown voltage for the samples was identified at 3.07 kV ±0,1 giving short-time breakdown strength of 51.2 kV/mm ± 1.7 kV/mm.

Average times to breakdown for 2.91 kV, 2.53 kV and 2.22 kV were investigated, the results are the following: 168 h (± 89 h), 360 h (± 148 h) and 890 (± 408 h) respectively. The most likely factor influencing the scatter of breakdown times was the lack of homogeneousness of aging in the paper samples for 2.22 kV. For the other voltage levels, PDs were the most likely cause.

The AC magnitude is also a factor to be considered as they increase the value of tan (δ). This has to be considered when the aging models are built (Chapter 6).

These results gave some information about the properties of the gathered paper samples in AC conditions. However, it is still unknown how the paper samples will react under unconventional stresses, such as repetitive transients, for which the AC measurements serve as a comparative sequence. To investigate this, the tests

performed in Chapter 4 were designed. In those tests, the influence of the magnitude, repetition frequency and rise time of repetitive transients on the dielectric strength of paper-oil insulation is investigated.

Chapter 4
Electrical Aging by Repetitive Transients

In previous chapters, repetitive transients have been identified as a potential reason influencing the lifetime of HV devices. DC and AC conversion is expected to become more popular with the integration of renewable energy plants and HVDC links into the electric grid. This conversion is performed by utilising power electronics to achieve very fast and controlled voltage switching to obtain the desired output waveform [13, 14, 42].

In this chapter a series of tests are performed to understand the influence of repetitive transients on the aging rate of electrical insulation, in particular: repetition frequency, rise time and magnitude. The tests were performed in laboratory conditions on pre-impregnated paper-oil test samples, identified in Chapter 3.

The first tests involved the application of a square wave to investigate the breakdown voltage and PDIV of paper-oil samples under different combinations of rise time and repetition frequency. This test provided the “safe” working limits of the paper under square wave conditions.

The second type of test focused on identifying the breakdown voltage of paper under short rise-time pulses, whilst eliminating the variable of repetition frequency.

In the third series of experiments, the paper-oil insulation was stressed by a specially designed voltage waveform similar to one found in the field at inverter substations. Repetitive transients were superimposed on a sinusoidal waveform and the samples were stressed until breakdown. The magnitude of the sinusoidal wave was changed to understand its aging influence on the paper-oil samples and the repetition frequency of the transients was adjusted within the most common range. The results were noted in terms of “time to breakdown”.

4.1. Conversion between DC and AC Voltage Waveforms

In the early 20th century the process of DC-AC conversion was based on vacuum and gas tubes to perform the switching functions. In the middle of the 20th century rotating converters and motor generators were introduced. As a significant reduction in costs of semiconductors in the 80's of the last century took place, today's converters are based on semiconductor devices such as IGBTs.

Pulse Width Modulation (PWM) is one of the methods used to convert from DC to AC. As explained in Chapter 2, the DC waveform is "chopped" with variable length pulse widths in order to achieve a sinusoid. The duration and amount of switching is increased to achieve sinusoidal waveforms with less harmonic distortion. Even though the output waveform is "smoother", the switching pulses can influence the aging rate of the electrical insulation system. Often, the switching pulse will appear superimposed on the carrier waveform and thus exceed the maximum voltage of the system. An example of this is illustrated in Fig. 4.1 taken from measurements at the Eagle Pass HVDC substation in the USA [14]. The repetitive transients can be seen superimposed on the sinusoidal waveform.

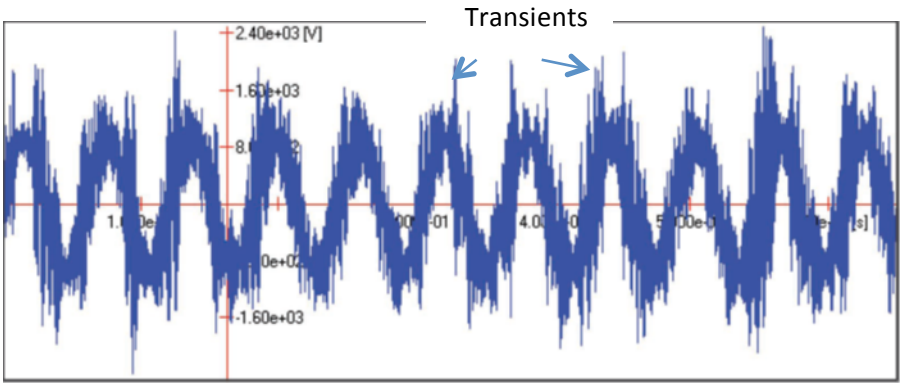


Fig. 4.1 – The output of a power electronic inverter seen by the transformer [14]

The transients are of different magnitudes and frequencies. The frequencies observed in many plants have been identified to be within 1 kHz and 10 kHz, rise times of these transients are approx. 1 µs and their magnitude can go up to two times operating voltage [44, 45, 46, 47]. These values are the representative parameters for the type of transients present in the field. The experiments described in this Chapter will be based on these parameters when attempting to recreate field conditions.

4.2. Square Wave Dielectric Strength of Paper-oil Insulation

In Fig. 2.2, a PWM technique was shown how to convert a DC waveform to AC. The initial obtained waveform is in many ways similar to a square wave with fast rise time, high frequency and high magnitude. According to [14, 16, 48], these parameters can have an accelerating aging effect on the electrical insulation.

The goal of the undertaken experiments is to investigate the breakdown voltage and PDIV of paper-oil sample when stressed with a square wave. Keeping the duty cycle at 50%, the following two parameters of the square wave were changed:

- Rise time;
- Repetition frequency.

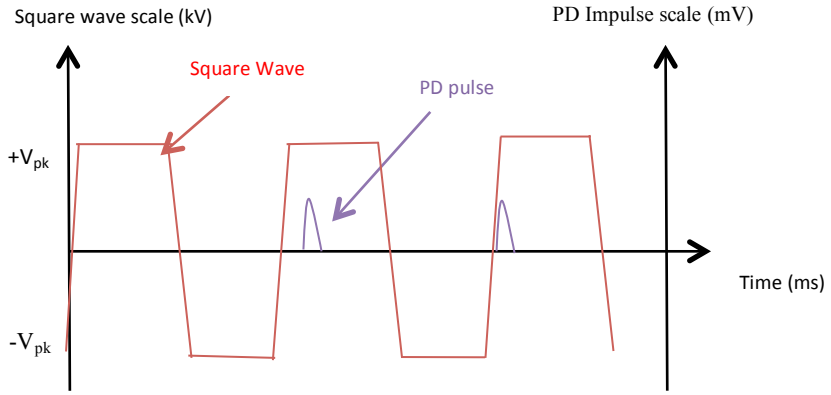


Fig. 4.2 –Example of the square wave with location of the PD pulses on the rising positive flanks

From the results from the literature survey presented in Chapter 2 and especially [16 and 48], PDs have been identified as the major cause of aging in motor insulation. Similar effects are expected for paper-oil insulation, as voids are also present in the insulation due to trapped air. The appearance of PD pulses is observed at the positive flank of the square wave. Repetition frequency is also expected to play a key role, as a higher repetition frequency should cause more PD pulses per second.

4.2.1. Test set-up and procedure

The test-set up to perform these measurements consisted of a square wave generator (TechSquare 400) [49] and a PD detector [50]. The use of both components required careful considerations as the generator needed to produce a frequency of 10 kHz and the PD detector needed to pick up only the PD signal and filter out the noise.

The PD was measured using an oscilloscope (Tektronix TDS 2014B) [51] and an antenna (PD Solver 6100) [50] pre-calibrated for the tests conditions to measure the magnitude and the inception voltage of the PD pulses. The test set-up is presented in Fig. 4.3.

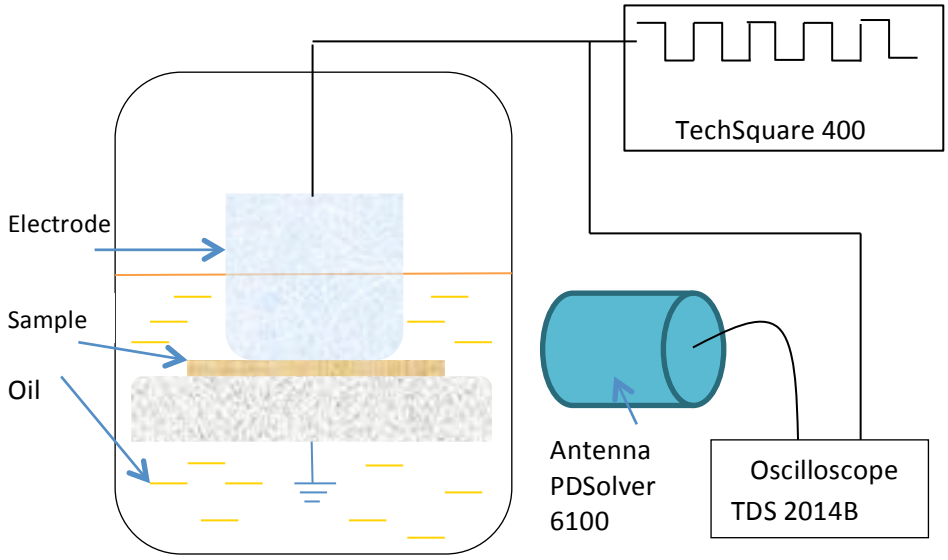


Fig. 4.3 –Test set-up where the HV square wave is applied to the electrode placed on top of the paper sample and the PD pulses are measured using an antenna connected to an oscilloscope

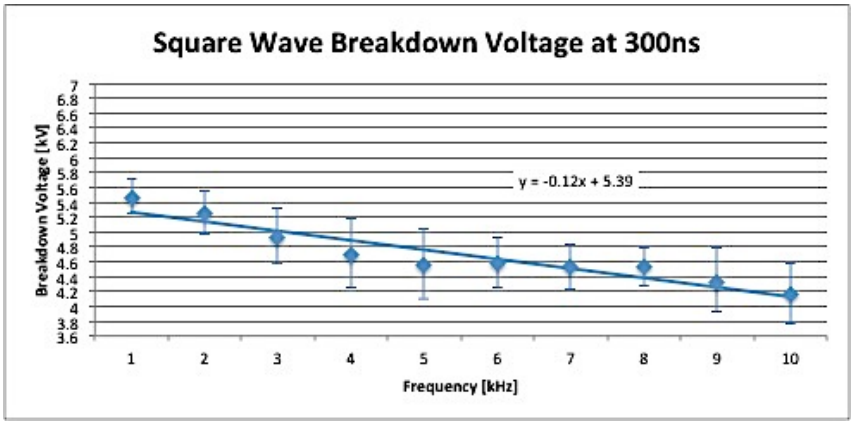
The samples were placed in a plastic container filled with mineral oil to such level that at least half of the top electrode was submerged in order to reduce the probability of external flashovers. The type of electrode and dimensions of paper-oil samples as well as the type of oil used are both described in details in Chapter 3.

The square wave generator was able to produce four different rise times: 300 ns, 500 ns, 800 ns and 1000 ns. During each test, the voltage magnitude was increased

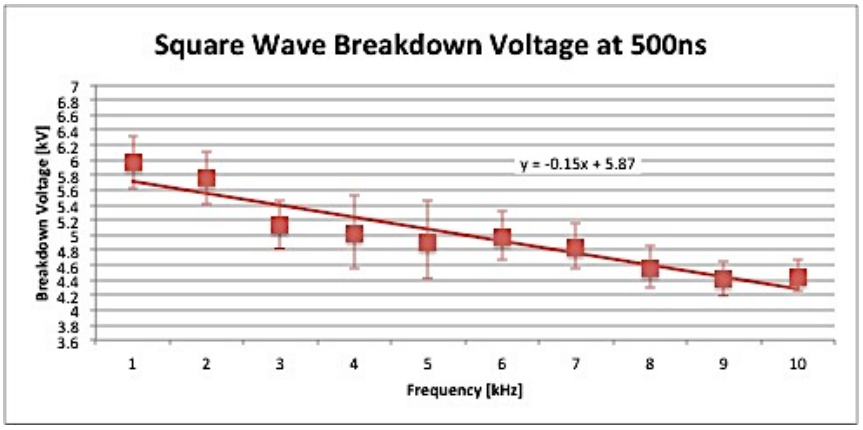
from zero up to breakdown at a rate of 1 kV per minute. Ten frequencies between 1 kHz and 10 kHz, in steps of 1 kHz, were investigated. Eight samples were investigated for each frequency and rise time combination. The top and earth electrodes were cleaned after a set of eight samples was tested.

4.2.2. Test results

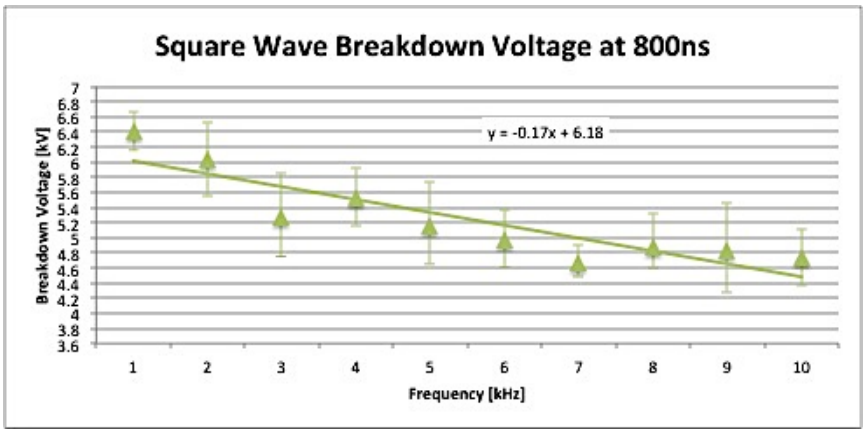
Using the test procedure described in the previous section, the results presented in Fig. 4.4 show the breakdown voltage of the sample. Each data point on the graphs is a geometric mean of the measurements performed on eight samples with 90% confidence bounds.



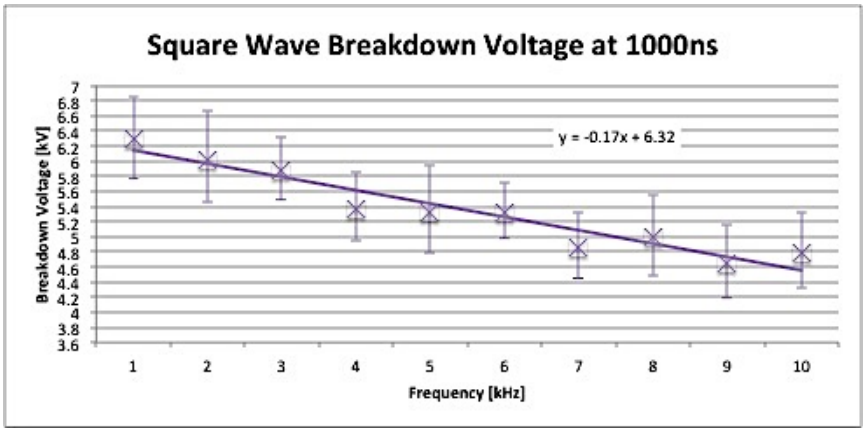
a. Risetime 300ns



b. Risetime 500ns



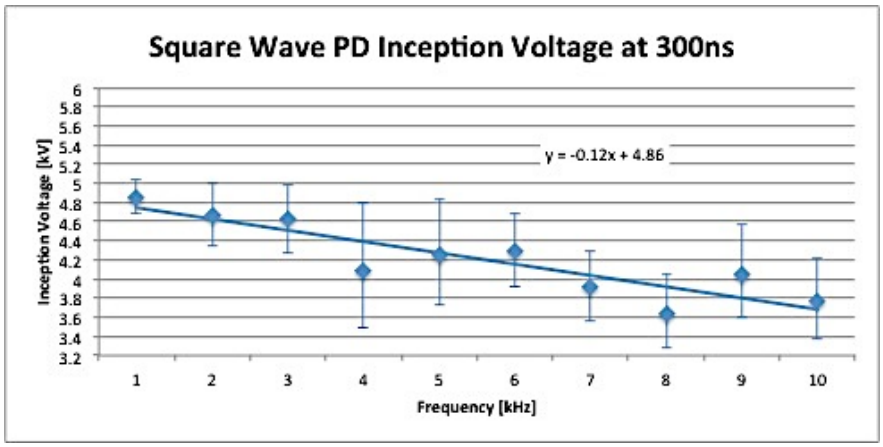
c. Risetime 800ns



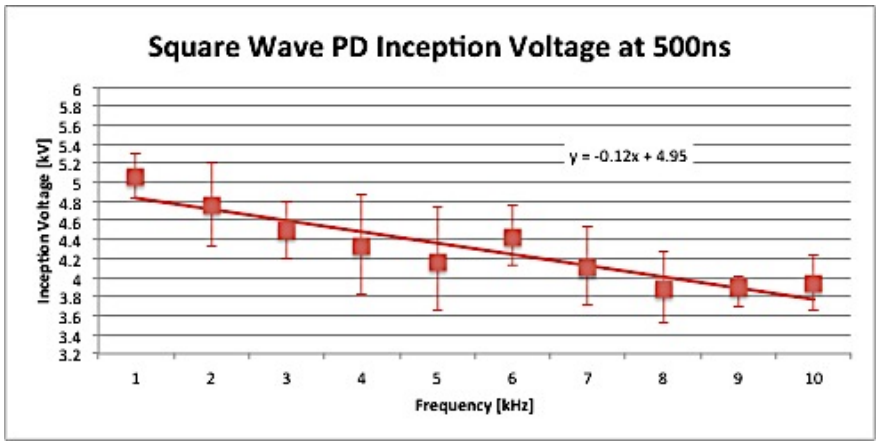
d. Risetime 1000ns

Fig. 4.4 – Mean breakdown voltages of oil paper samples as function of the frequency of the square wave for different wave rise times with 90% error bounds

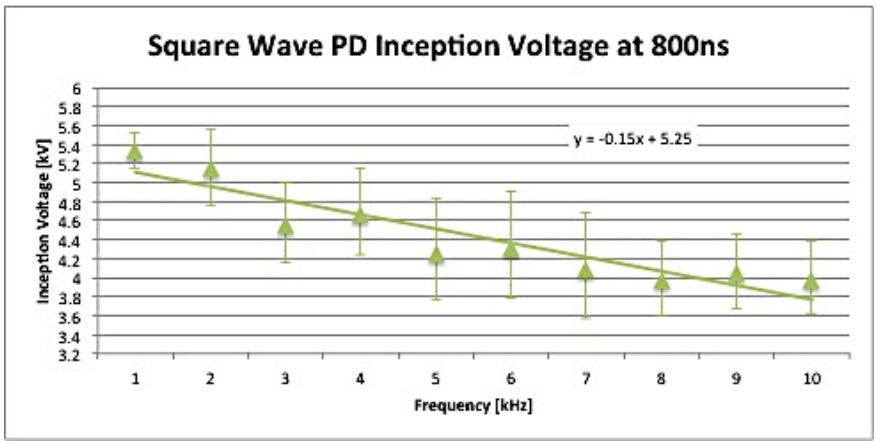
Fig. 4.5 shows the PDIV for the same samples. The value is presented as the geometric mean and the 90% confidence bounds are indicated for each result.



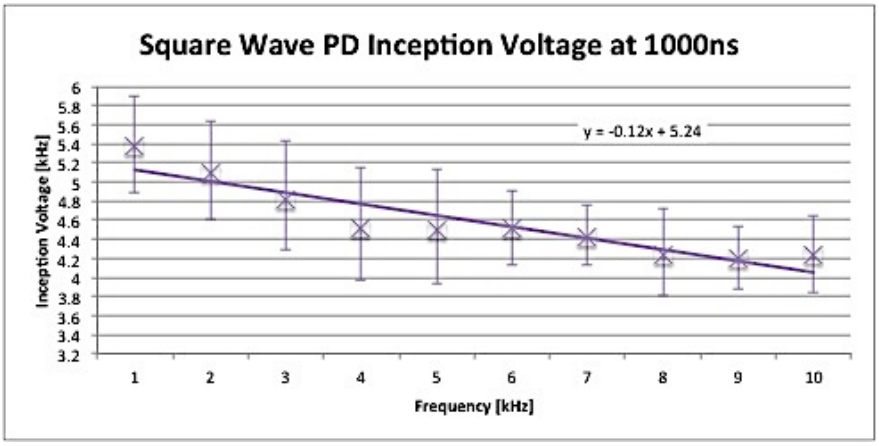
a. Risetime 300ns



b. Risetime 500ns



c. Risetime 800ns



d. Risetime 1000ns

Fig. 4.5 – Mean partial discharge inception voltage as function of the frequency of the square wave for different wave rise times with 90% error bound

A clear trend can be observed in Fig. 4.4 and 4.5. For each tested value of rise time, the breakdown voltage (VBD) and PDIV values decrease with the increase of frequency of the square wave. The linear gradient (m) and y intercept (c) of the lines y=mx+c are influenced by the rise time.

Detecting and locating the PD impulses on the oscilloscope was a non-trivial task. The sensitivity of the probe did not always allow for a clear recognition of the PD pulses and visual observation had to be performed on the oscilloscope.

A Weibull statistical analysis was carried out on the test results to distinguish any factors influencing the breakdown voltage and PDIV. The data presented from Table 4.1.1 to Table 4.1.3 is grouped according to the relative Weibull parameter and to the appropriate type of voltage measured. The procedure in calculating these parameters was described in Chapter 3.

Table 4.1.1 – β parameter of Weibull distribution for V_{BD} for different rise times and frequencies of square wave [per unit]. The 90% confidence bounds are shown in the lower table

Rise Time	Frequency									
	1 kHz	**2 kHz**	**3 kHz**	**4 kHz**	**5 kHz**	**6 kHz**	**7 kHz**	**8 kHz**	**9 kHz**	**10 kHz**
300ns	15.94	12.76	9.45	7.24	6.89	9.49	9.97	12.68	9.43	6.97
500ns	12.44	11.81	10.81	7.40	7.66	11.49	10.82	12.09	14.13	16.44
800ns	19.18	8.18	6.98	10.63	6.63	9.30	16.89	11.32	5.42	8.71
1000ns	8.22	7.66	10.27	8.30	6.29	10.47	7.89	6.29	6.50	6.78

Rise Time	Frequency									
	1 kHz	**2 kHz**	**3 kHz**	**4 kHz**	**5 kHz**	**6 kHz**	**7 kHz**	**8 kHz**	**9 kHz**	**10 kHz**
300ns	+26.3 -9.66	+20.43 -7.96	+15.05 -5.94	+11.27 -4.66	+10.69 -4.43	+15.19 -5.93	+16.57 -5.99	+20.22 -7.94	+14.20 -6.27	+11.03 -4.41
500ns	+19.38 -7.99	+18.44 -7.57	+17.90 -6.53	+11.27 -4.86	+11.87 -4.95	+17.59 -7.50	+17.77 -6.59	+19.08 -7.67	+22.03 -9.07	+19.86 -7.99
800ns	+30.22 -12.17	+13.73 -4.87	+10.61 -4.60	+16.22 -6.97	+10.58 -4.16	+14.61 -5.92	+25.61 -11.14	+17.97 -7.14	+8.85 -3.33	+13.71 -5.53
1000ns	+12.96 -5.22	+11.98 -4.90	+16.09 -6.55	+13.35 -5.16	+10.12 -3.91	+16.67 -6.58	+12.62 -4.94	+10.12 -3.92	+10.86 -3.90	+10.84 -4.24

Table 4.1.2 – η parameter of Weibull distribution for V_{BD} for different rise times and frequencies of square wave [kV]. The 90% confidence bounds are shown in the lower table

Rise Time	Frequency									
	1 kHz	**2 kHz**	**3 kHz**	**4 kHz**	**5 kHz**	**6 kHz**	**7 kHz**	**8 kHz**	**9 kHz**	**10 kHz**
300ns	5.66	5.46	5.19	5.00	4.87	4.82	4.75	4.71	4.56	4.44
500ns	6.21	6.01	5.37	5.35	5.22	5.21	5.07	4.76	4.57	4.59
800ns	6.60	6.39	5.63	5.79	5.53	5.25	4.83	5.12	5.23	4.99
1000ns	6.67	6.41	6.18	5.69	5.72	5.59	5.17	5.36	4.98	5.13

Rise Time	Frequency									
	1 kHz	**2 kHz**	**3 kHz**	**4 kHz**	**5 kHz**	**6 kHz**	**7 kHz**	**8 kHz**	**9 kHz**	**10 kHz**
300ns	+5.88 -5.44	+5.73 -5.21	+5.55 -4.87	+5.17 -4.50	+5.12 -4.41	+5.10 -4.33	+4.98 -4.45	+4.92 -4.43	+4.92 -4.12	+4.74 -3.96
500ns	+6.51 -5.82	+6.46 -5.72	+5.72 -5.04	+5.77 -4.80	+5.65 -4.69	+5.57 -4.86	+5.35 -4.75	+5.05 -4.5	+4.85 -4.39	+4.86 -4.45
800ns	+6.85 -6.36	+6.73 -5.75	+6.05 -4.95	+6.10 -5.35	+5.93 -4.85	+5.56 -4.81	+5.11 -4.68	+5.51 -4.79	+5.67 -4.47	+5.32 -4.56
1000ns	+7.05 -5.97	+6.87 -5.65	+6.51 -5.69	+6.06 -5.14	+6.14 -4.98	+5.91 -5.18	+5.51 -4.65	+5.75 -4.68	+5.35 -4.39	+5.51 -4.52

Table 4.1.3 – ρ parameter of Weibull distribution for V_{BD} for different rise times and frequencies of square wave [per unit]

Rise Time	Frequency									
	1 kHz	**2 kHz**	**3 kHz**	**4 kHz**	**5 kHz**	**6 kHz**	**7 kHz**	**8 kHz**	**9 kHz**	**10 kHz**
300ns	0.96	0.97	0.98	0.97	0.97	0.98	0.93	0.98	0.89	0.98
500ns	0.98	0.97	0.98	0.97	0.89	0.95	0.98	0.98	0.96	0.94
800ns	0.93	0.97	0.96	0.96	0.98	0.99	0.94	0.98	0.93	0.98
1000ns	0.96	0.91	0.98	0.95	0.99	0.96	0.99	0.96	0.94	0.98

The β parameter describes the inclination of the MLE line in a Weibull probability plot. The higher the value of β, the steeper the slope of the unreliability line is and consequently the V_{BD} results are less scattered. A good example of low scatter is shown in Fig. 4.6a for a rise time of 800 ns at 1 kHz. Additionally, confidence bounds of 90% have been added. On the other hand, a high-scattered line is illustrated for 1000 ns at 8 kHz, shown in Fig. 4.6b.

The ρ (correlation) parameter describes how well the best-fit line is plotted through the data points. The higher the value of ρ is, the better-fitted line is obtained. For the amount of samples used, eight in this case, any value above 0.91 is considered good. Only one combination, 300 ns/ 9 kHz, presents a value lower than 0.91.

The η parameter indicates the voltage level at which 63.2 % of the tested samples will fail. In all combinations, this number is decreasing with the increase of frequency and faster rise times.

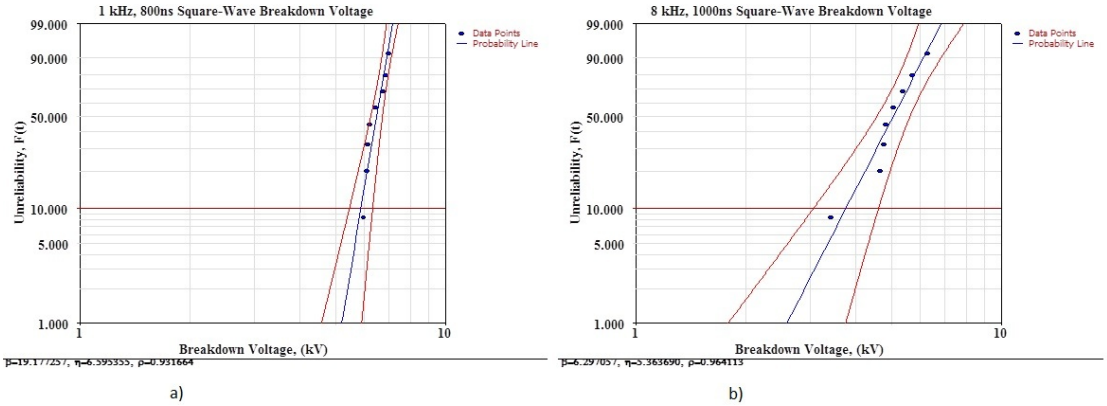


Fig 4.6 – Plots with two different types of β parameter with 90 % confidence bounds: a) high β value, small scatter b) low β value, high scatter

Overall, the Weibull shape parameter trend is very wide due to the large spread results as shown in Table 4.1.1, and any clear trends are difficult to notice. The more obvious differences can be noticed looking at the scale parameter, η. The average value of η decreases as the rise time is shortened and the repetition frequency is increased.

Weibull plot analyses were also carried out for the PDIV values. The results are presented in the following tables subdivided by the three main Weibull parameters.

Table 4.2.1 – β parameter of Weibull distribution for PDIV for different rise times and frequencies of square wave [per unit]. The 90% confidence bounds are shown in the lower table

Rise Time	Frequency									
	1 kHz	**2 kHz**	**3 kHz**	**4 kHz**	**5 kHz**	**6 kHz**	**7 kHz**	**8 kHz**	**9 kHz**	**10 kHz**
300ns	21.70	10.43	11.04	5.40	6.05	8.70	7.79	8.07	7.09	6.43
500ns	18.42	8.35	12.26	7.02	5.93	11.51	7.48	9.18	14.3	10.61
800ns	23.57	9.20	7.79	7.43	5.93	5.96	5.64	7.31	8.00	8.11
1000ns	8.30	7.26	6.53	6.52	5.46	9.59	11.5	8.10	9.26	7.82

Rise Time	Frequency									
	1 kHz	**2 kHz**	**3 kHz**	**4 kHz**	**5 kHz**	**6 kHz**	**7 kHz**	**8 kHz**	**9 kHz**	**10 kHz**
300ns	+38.72 -12.99	+17.73 -6.14	+19.64 -6.12	+8.88 -3.29	+10.46 -3.51	+15.00 -5.05	+12.92 -4.70	+15.35 -4.24	+12.89 -3.90	+10.64 -3.88
500ns	+30.57 -11.11	+13.50 -5.17	+21.18 -7.10	+12.72 -3.87	+9.55 -3.68	+15.04 -5.90	+11.98 -4.67	+16.27 -5.18	+23.50 -8.71	+16.73 -6.73
800ns	+36.81 -15.10	+15.90 -5.33	+13.17 -4.61	+12.60 -4.38	+9.60 -3.66	+10.48 -3.39	+9.91 -3.21	+12.01 -4.50	+14.01 -4.57	+14.28 -4.60
1000ns	+16.03 -5.12	+12.28 -4.29	+10.85 -3.72	+10.85 -3.72	+9.03 -3.30	+12.92 -5.01	+13.63 -5.56	+14.55 -4.52	+15.91 -5.39	+12.77 -4.79

Table 4.2.2 – η parameters of Weibull distribution for PDIV for different rise times and frequencies of square wave [kV]. The 90% confidence bounds are shown in the lower table

Rise Time	Frequency									
	1 kHz	**2 kHz**	**3 kHz**	**4 kHz**	**5 kHz**	**6 kHz**	**7 kHz**	**8 kHz**	**9 kHz**	**10 kHz**
300ns	4.98	4.89	4.83	4.44	4.58	4.53	4.16	3.87	4.33	4.05
500ns	5.21	5.04	4.68	4.61	4.49	4.63	4.38	4.10	4.03	4.13
800ns	5.46	5.43	4.85	4.98	4.60	4.65	4.43	4.24	4.30	4.22
1000ns	5.69	5.43	5.18	4.85	4.87	4.75	4.63	4.50	4.42	4.49

Rise Time	Frequency									
	1 kHz	**2 kHz**	**3 kHz**	**4 kHz**	**5 kHz**	**6 kHz**	**7 kHz**	**8 kHz**	**9 kHz**	**10 kHz**
300ns	+5.24 -4.89	+5.2 -4.54	+5.18 -4.47	+4.99 -3.69	+5.04 -3.93	+4.89 -4.12	+4.50 -3.76	+4.25 -3.48	+4.77 -3.79	+4.44 -3.57
500ns	+5.50 -5.13	+5.41 -4.53	+4.99 -4.40	+5.08 -4.12	+4.94 -3.85	+4.96 -4.33	+4.74 -3.91	+4.48 -3.72	+4.21 -3.89	+4.44 -3.85
800ns	+5.73 -5.35	+5.76 -4.96	+5.20 -4.36	+5.35 -4.44	+5.13 -3.96	+5.11 -3.98	+4.89 -3.77	+4.59 -3.79	+4.66 -3.87	+4.58 -3.82
1000ns	+6.09 -4.09	+5.83 -4.81	+5.63 -4.49	+5.35 -4.17	+5.34 -4.13	+5.11 -4.33	+4.96 -4.33	+4.92 -4.01	+4.73 -4.08	+4.85 -4.04

Table 4.2.3 – ρ parameters of Weibull distribution for PDIV for different rise times and frequencies of square wave [per unit]

Rise Time	Frequency									
	1 kHz	**2 kHz**	**3 kHz**	**4 kHz**	**5 kHz**	**6 kHz**	**7 kHz**	**8 kHz**	**9 kHz**	**10 kHz**
300ns	0.965	0.944	0.982	0.917	0.964	0.991	0.977	0.991	0.985	0.977
500ns	0.971	0.939	0.944	0.976	0.947	0.988	0.980	0.941	0.979	0.964
800ns	0.973	0.968	0.972	0.976	0.982	0.993	0.998	0.979	0.933	0.983
1000ns	0.963	0.934	0.973	0.983	0.984	0.962	0.988	0.974	0.976	0.970

No conclusions can be drawn from the shape parameter β as in the case for the breakdown voltage data. The error bounds indicate a wide spread again. The η parameter for PDIV decreases with the increase of frequency and shortening of rise time.

The *ρ* parameter is considered to be good for all the combinations, as the values are above 0.91

4.2.3. Discussion

The results have shown that, shortening the rise time values from 1000 ns to 300 ns and increasing the frequency of the square wave from 1 kHz to 10 kHz reduces the breakdown strength of the sample´s insulation between 21% and 45% when taking the error bounds into consideration. When considering only the characteristic breakdown voltage η, the reduction is 34%.

The partial discharge inception voltage is also altered by these changes. PDIV levels are considerably reduced at faster rise times and higher frequencies. By looking at one extreme to the other, data has shown a reduction between 14% and 43% when observing the error bounds. When only the characteristic breakdown voltage η is observed, the change is 30%.

In the Weibull analysis of the breakdown voltage and of the PDIV, trends in the shape parameter were not distinct in comparison to the scale parameter. This is most probably attributed to the thickness of the paper. In general, paper is prone to variations of thickness within its composition. Small variations in thickness greatly affect the field strength to which the paper is exposed during the tests. The results obtained in this chapter allowed the formation of the following " stress limits" of the investigated paper. Fig. 4.7a illustrates the boundary of the breakdown voltage, whilst Fig. 4.7b illustrates the boundary at which PD is initiated.

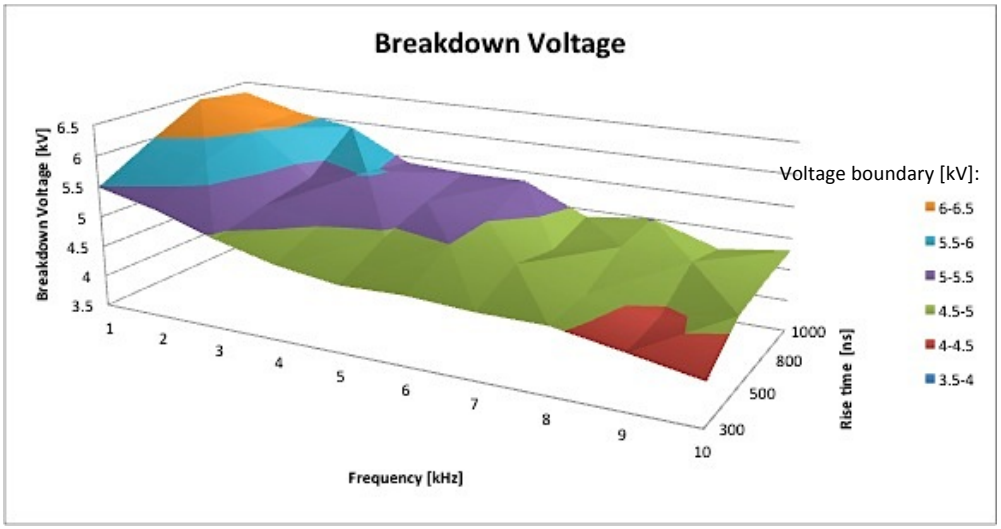


Fig. 4.7a – The characteristic breakdown voltage range of a paper sample aged with a square wave

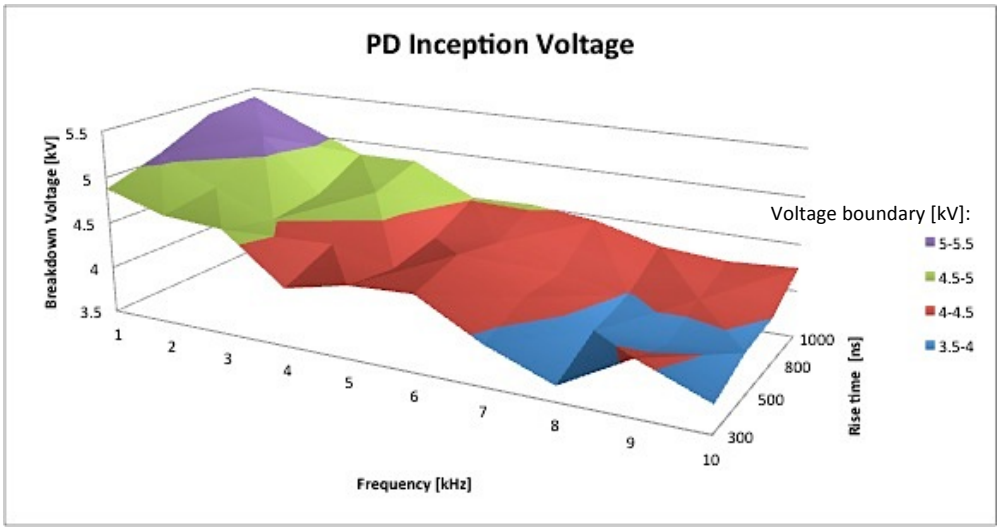


Fig. 4.7b – The characteristic partial discharge inception voltage range of a paper sample aged with a square wave

From the experiments described in this section, PD activity could be a driving factor behind the failure of paper-oil insulation systems. As the repetition frequency was increased and rise time was shortened, PDIV decreased and therefore the aging of insulation initiated earlier. A reduction in the PDIV level leads to the breakdown of the sample at lower voltage values.

4.3. Impulse Dielectric Strength of Paper-oil Insulation

Results from Chapter 4.2 showed that the duration of the rise time of the square wave has an impact on the breakdown strength of paper-oil insulation. To understand in more detail this phenomenon, the paper-oil samples were stressed with single voltage impulses of similar shape to fast transients and at a very low frequency. The goal of this experiment is to investigate the rise time and polarity effect of these fast transients on the breakdown voltage of paper-oil sample whilst eliminating the influence of fast repetition frequency.

4.3.1. Test set-up and procedure

An impulse generator was constructed for the purpose of this experiment to simulate an appropriate impulse of rise times similar to a single repetitive transient.

The impulse generator uses a spark gap, which was controlled by a DC source charged capacitor. Once a flashover appeared over the spark gap, an impulse in

the shape of a transient was released and directed on the sample. The magnitude of the transient is controlled by the size of the spark gap [52]. A basic schematic of the constructed device is shown in Fig. 4.8.

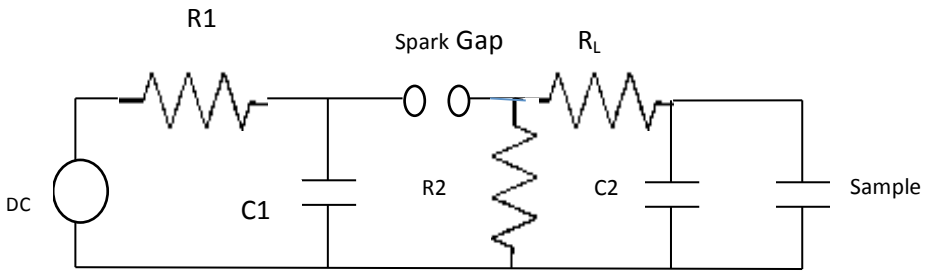


Fig. 4.8 – Schematic circuit of the impulse generator used for creating single transient-like pulses

As the rise time of a pulse is dependent on the capacitance of the sample, correct values needed to be selected for the resistors and capacitors. R1 and C1 values were chosen in order to control the speed of the repetition rate of the pulses. R_L on the other hand was chosen to control the rise time of the impulse.

The pulse produced by the spark generator can be seen in Fig. 4.9.

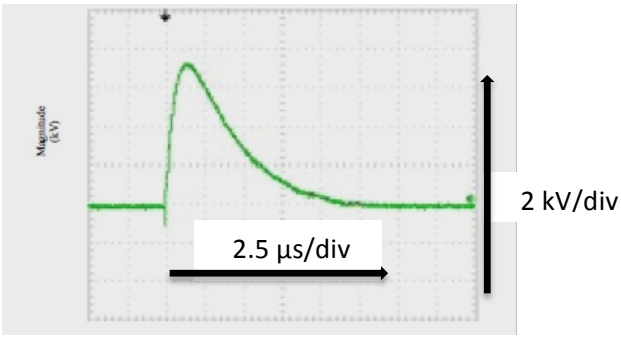


Fig. 4.9 – The pulse created by the spark generator

Tests were carried out in accordance to the IEC 60243-3 [53] standard in order to measure the breakdown voltage of the samples under impulse voltage. The requirements in the standard are:

- At least five samples should be tested to identify the breakdown voltage;
- Three pulses, at least 10 seconds apart from each other, should be applied at a specific voltage level;

- If there is no breakdown at one voltage level, the voltage is increased and another set of impulses is applied up to breakdown;
- When breakdown occurs at any of the three impulses, the voltage of the previous set of impulses is regarded as the withstand voltage.

During the preliminary tests, the impulse breakdown voltage was identified to be approx. 9 kV. For all successive tests, the first set of three impulses was applied at a magnitude of 70 % of this value, approx. 7.2 kV, and was increased by 0.4 kV until breakdown. If the sample broke down during any of the impulses in series, the voltage magnitude from the previous test sequence was assigned as the withstand voltage.

The impulse rise times selected for the tests were: 300 ns, 600 ns, 800 ns, 1000 ns, 1400 ns, 2000 ns and 2500 ns. The results are presented in the following sections.

4.3.2. Test results

Positive polarity transients were applied to paper-oil samples. The mean results are shown in Fig. 4.10 together with the standard deviation.

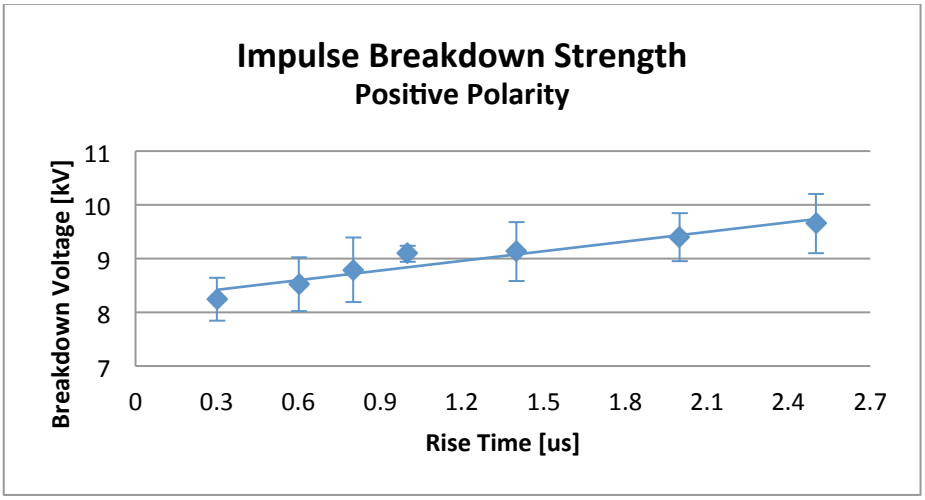


Fig. 4.10 – Positive impulse breakdown voltages of paper-oil insulation as function of impulse rise time

A trend can be indicated from the graph in Fig. 4.10, higher rise times, higher breakdown voltage value. This shows that the dielectric strength of the paper-oil insulation is dependent on the rise time of an impulse. In Fig. 4.10, the mean

values of twelve tests are shown for each rise time value. The respective standard deviation is shown for each rise time. The general trend seems to follow a linear trend and the best-fit line is plotted through the data points.

Since transients occur in the grid with both polarities, the spark generator was adapted to produce also negative impulses. The experiment was carried out according to the same IEC 60243-3 standard test procedure. The results can be seen in Fig. 4.11.

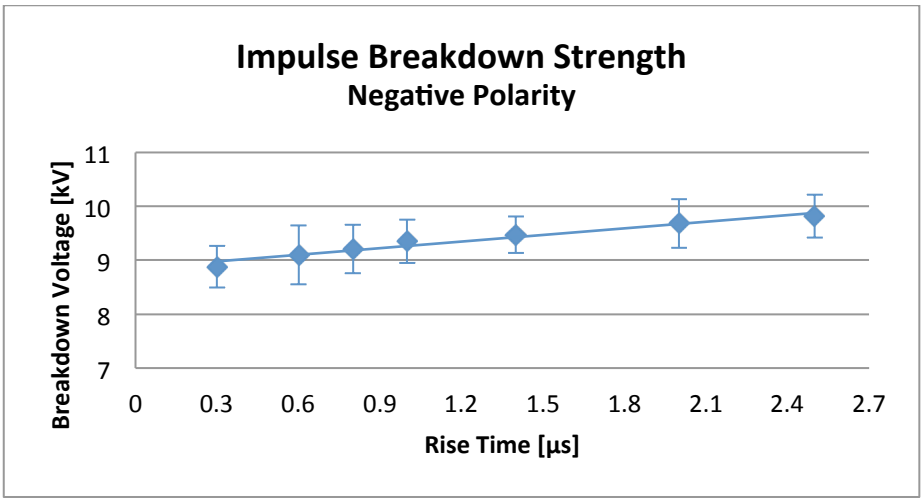


Fig. 4.11 – Negative impulse breakdown voltages of paper-oil insulation as function of impulse rise time

A similar trend like for positive impulses is observed when negative impulses are applied. As the rise time of the impulse increases, the breakdown voltage increases. The error bars indicate the standard deviation from the mean value.

When stressed with negative impulses, the paper-oil insulation system has a higher dielectric strength than at positive impulses. For example, at the lowest tested rise times of 0.3 µs, the mean breakdown voltage was 8.24 kV for positive and -8.88 kV for negative polarity. When stressed with impulse of 1 µs of rise time, the values obtained were 9.09 kV and -9.35 kV respectively. For the longest rise time of 2.5 µs, the breakdown voltages measured were 9.65 kV and -9.85 kV. These differences between the breakdown values of both polarities were of 7.2 %, 2.8 % and 2.03 % (with reference to the positive polarity impulses) for the indicated increased values of rise time.

The error in the mean indicated by the standard deviation is about 5%. This is close to the changes observed thus reducing the effects observed in the paragraphs above.

4.3.3. Discussion

The tests carried out have shown that the insulation of paper-oil breakdown voltage is dependent on the rise time of the applied single impulse. Slower rise time leads to higher breakdown voltage values. The investigated range of rise times was between 0.3 µs and 2.5 µs.

For the positive polarity impulses, the breakdown voltage increased by 14.6 %. When stressed with negative pulses in the same rise time range, this breakdown voltage increased by 9.6 %. The standard deviation in the breakdown values was of 5% for each rise time.

Positive and negative impulses have been applied to the paper-oil samples to investigate the effect of polarity reversal. The procedure consisted of stressing the samples at a specific rise time, three pulses were applied to the sample, first in a positive polarity and then three pulses were applied with a negative polarity. Breakdown values similar to the positive pulses were obtained and therefore no clear conclusions could be extrapolated from the tests.

4.4. Aging by Repetitive Transients

In the previous section, it was shown that faster impulse rise time and higher frequency of the voltage wave application have a harmful effect on the breakdown voltage of paper-oil insulation if applied close to the level of PDIV. In this Section, the aging of paper-oil samples will be investigated and the time to breakdown will be measured. The samples will be stressed using a simulated AC waveform of the actual conditions, found at the input terminals of transformers in the field, in this case with superimposed transients [13]. For this purpose, a waveform was designed in the laboratory. The advantage of this procedure was the freedom of control of all the interested parameters such as repetition frequency and rise time of the samples amongst others.

Once generated, the waveform ages the paper samples at specific AC voltage magnitude (r.m.s) with superimposed 1 kV_{pk} transients of fixed rise time of 1 kV/µs but variable frequency in the range from 1 kHz to 10 kHz, similarly to the square wave tests performed earlier in this chapter. The results are compared to the aging data of AC waveform without superimposed transients presented in Chapter 3.

4.4.1. Test set-up

From literature review presented in Chapters 1 and 2, the most common waveform observed in high power inverters (Fig. 4.1) has two components:

- AC component with adjustable magnitude;
- Superimposed transients of magnitude up to 1 kV or (0.3 U_0) but variable repetition frequency.

In particular, the transient is characterized by the following parameters that can influence the aging process:

- Transient rise time in the order of 1 kV/μs;
- Transient repetition frequency changing between 1 kHz and 10 kHz;
- Position of the transients on the positive and negative cycle of the AC component.

The frequency of the transients and the magnitude of AC waveform were selected as the main critical parameters characterising the aging process in paper-oil insulation. Equipment capable to generate transient superimposed on AC waveform was not commercially available, so it was designed, constructed and tested at the High Voltage Department in conjunction with the electronics department of the TUDelft with the participation of the author.

The simplest approach was to generate the transient with a HV switch connected to HV DC source. During the design stage, the following limitations had to be taken into account:

- The rise time of the transients depends on the capacitance of the sample;
- The rise time is slower at faster frequencies due to the limited operating conditions of the electronic equipment;
- The dielectric strength of the sample should be isolated from other unwanted effects such as moisture in the oil;
- The HV transformer should be isolated from the transient generating equipment to eliminate the danger of flashovers.

The preliminary attempt performed to create the transients involved the usage of Behlke HTS 301-03-GSM HV switch [55]. This solution was not very practical

however. The amount of power required overheated the device and a sustainable operation for a prolonged period of time couldn't be guaranteed.

The final decision, and the most straightforward, was to use a MOSFET to perform the switching at low voltage and subsequently amplify the pulse [56]. Several MOSFET types are available on the market and one with a rated voltage of 200 V was chosen to provide room for improvements in case higher voltages were to be obtained. Once the high frequency (HF) switch was connected to a logic circuit, a pulse with a very fast rise time was generated. A diode was added in order to minimise the overshoot generated by the switching (not shown). A schematic of the generator with the indication of switching operations is shown in Fig. 4.12.

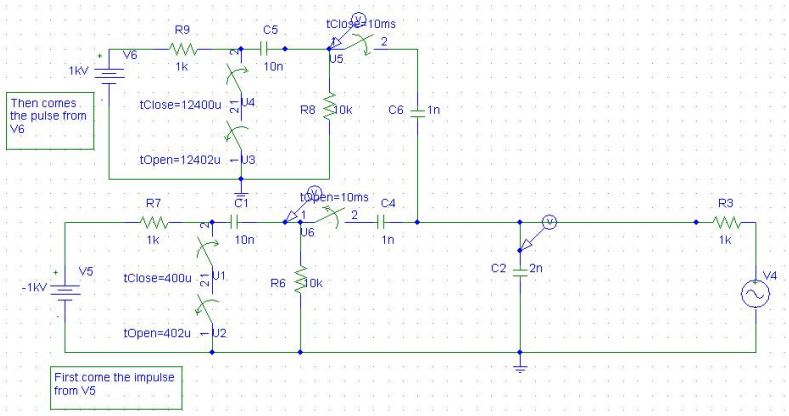


Fig. 4.12 – A schematic representation in PSpice of the circuit used to generate transients. A MOSFET switch is replaced by three switches that have been timed to open and close. The sample is represented by C2

The above schematic is programmed to perform the operation of two transients, the first 0.5 ms after the start of the positive cycle and the second 0.5 ms after the start of the negative cycle. Both transients have the same polarity of the cycle in which they are generated. A 2 nF capacitor has been added to simulate the sample and a HV source, V4 was connected in series.

In Fig. 4.13, the voltage signal simulated in the circuit presented in Fig. 4.12 is shown.

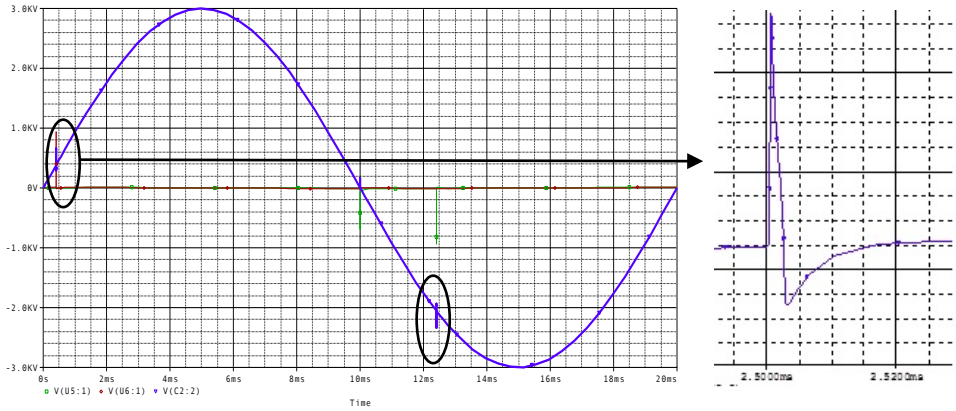


Fig. 4.13 – The results of simulation of the transients (circled) and their superposition on the AC waveform. The rise time is approx. 1 µs.

The transients are superimposed on the sinusoidal waveform and are applied directly on the sample. However, the magnitude of the fast transient is damped by the resistances in the circuit. It was noticed that when the magnitude of the transient generated by the switches is 1000 V, it drops to 400 V when reaching the sample. It was necessary to amplify signal to improve the efficiency of the circuit.

Additionally, the MOSFET were only capable of switching 200 V DC signals, thus it meant that amplification would be required to achieve 1 kV transients. For this purpose, a HF transformer, with insulation protecting from fast transients, was designed. This HF transformer was constructed using a type of magnetic core that would be capable of amplifying fast frequency pulses. This transformer is shown in Fig. 4.14.

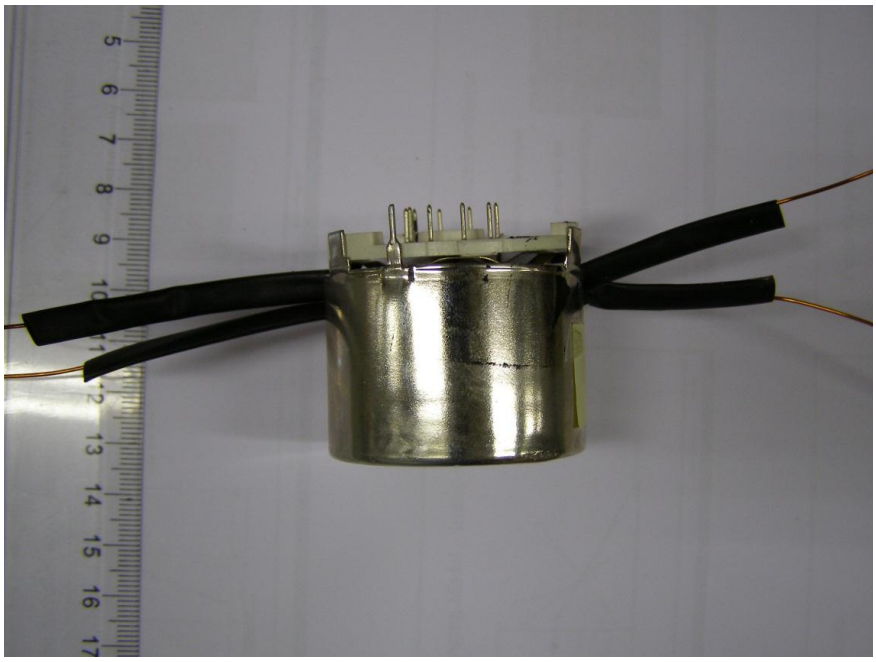


Fig. 4.14 – High Frequency transformer constructed for the purpose of amplifying high frequency impulses

The achieved efficiency of the transformer was 98 % and losses were significantly reduced in the conversion of high frequency pulses. The properties of the core in transferring the fast rise-time pulse were also acceptable, as only minor delays in the pulses width have been measured. The simplified schematic of the circuit to be used is shown in Fig. 4.15.

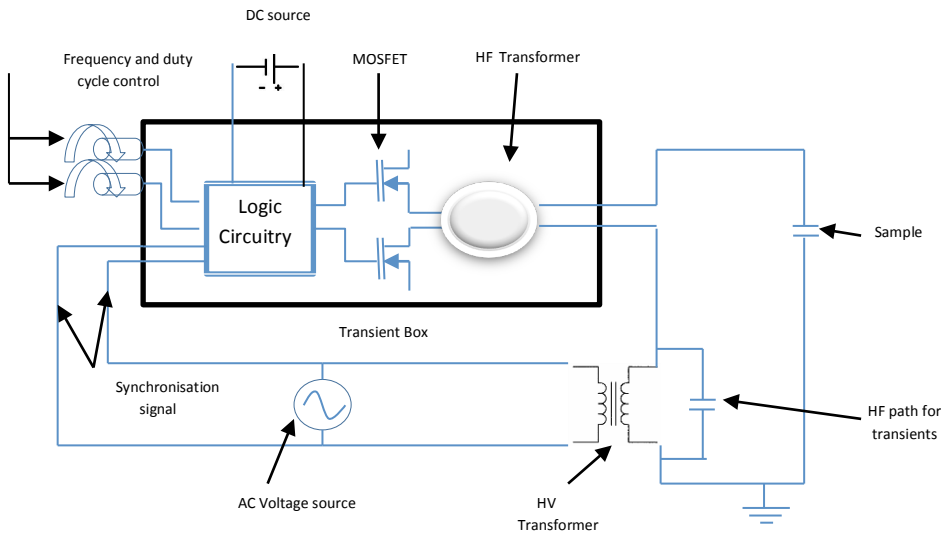


Fig. 4.15 – Schematic diagram of the set-up used to perform the ageing tests of the paper-oil samples. The "transient box" superimposes transients on sinusoidal waveform

In Fig. 4.15, three main parts of the circuit can be distinguished: the HV source, the transient generating box, and the circuit with the tested sample.

The high voltage is generated using a high voltage transformer. The input voltage at 50 Hz is regulated between 0 and 220 V and then amplified by the HV transformer whose ratio was calculated to be 1:58. The input terminals of the HV transformer are connected to the "transient box" to provide the synchronisation signal. The synchronisation signal is required to generate transients in a positive and negative polarity, as required by the imposed specifications.

The transient box generates the transients in three steps. The desired frequency and duty cycles are determined by the user and read by the logic circuit. The MOSFETs are programmed to switch the DC signal accordingly to the settings of the logic circuit to create a low voltage transient. The HF transformer amplifies the transient to reach at least a magnitude of 1 kV. The transient is injected to the circuit to which the test sample is connected by being superimposed on the sinusoidal waveform. A high frequency path was built to allow the transient to omit the HV transformer so that no damping in magnitude occurs. This was done

by placing a 1 nF capacitor across the HV transformer. The transient box construction can be seen in the photograph in Fig. 4.16.

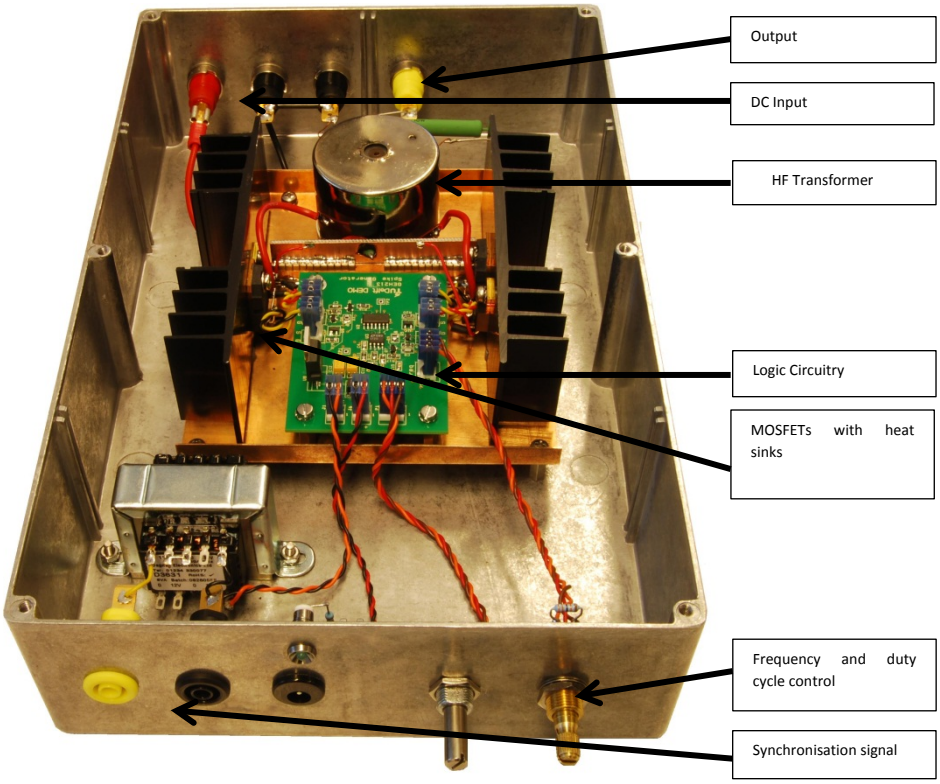


Fig. 4.16 – The transient box with the main components used to generate transients such as MOSFETs, logic circuit and HF transformer

Several additional features have been implemented to the transient box. Diodes and fuses have been added to protect the electronic components from flashovers.

This transient box has been built in collaboration with the electronics department of the TUDelft.

4.4.2. Test procedure

The test set-up equipment was tested in the laboratory using actual samples of paper-oil insulation. The samples were prepared in accordance to the procedure described in Chapter 3. A population of six samples were stressed at a time.

Two plastic tanks were used to hold the samples. The tanks were filled with Shell Diala B oil [33] and its properties such as relative humidity and water content were measured before each test using a Vaisala Humicap MM170 probe. The water

content was kept below 5 ppm and relative humidity below 5 %. In order to keep the oil “dry”, silica gels were placed on the wall of the tank to absorb any moisture that would collect when opening the tank to replace the samples. A special rubber coating was placed on the lid of the tank to prevent moisture ingress from the container.

A 1000:1 HV Tektronix P – 6015 probe was used to measure the magnitude of the output voltage. The output was observed on a screen of Tektronix TDS 2014B, of 100 MHz bandwidth and of 1 GS/s sampling rate oscilloscope. An analogue timer was used to measure the time to breakdown.

The photograph of the set-up equipment can be seen in Fig. 4.17.

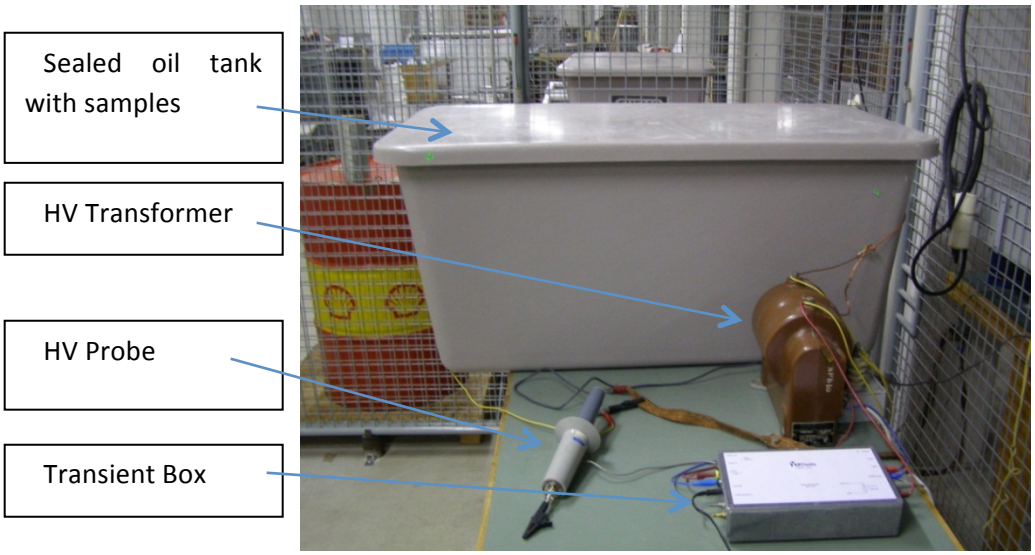


Fig 4.17 – Photograph of the equipment used

A thicker, unrelated, sample was tested to check the limitation of the test set-up equipment. The screen shots in Fig 4.18 illustrate the acquired waveforms.

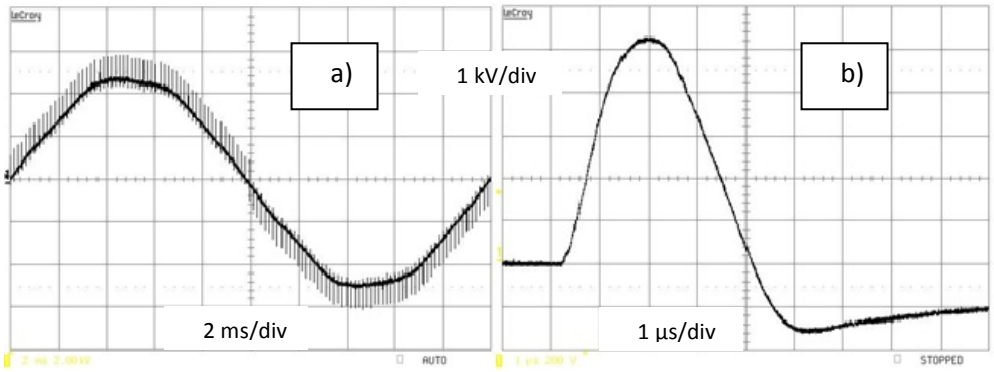


Fig 4.18 – The test waveforms at the limits of performance of the set-up:

a) The 50 Hz waveform with superimposed transients at 10 kHz and at 1 kV and b) transient of 1 kV/µs rise time.

Fig. 4.18 shows that the desired output waveform has been achieved. The repetitive transient rise times were not affected by the change in the repetition frequency of the transients or magnitude of the AC waveform. However, it was observed that the shape and rise time of the transient was affected when the number of contemporary tested samples was more than seven. At high capacitance values, the equipment had difficulties in charging the MOSFETs fast enough to obtain the desired results. For this reason, the number of samples to be stressed at one time (in parallel) was limited to six in order to guarantee the required test set-up performance.

4.4.3. Test results

The time to breakdown of paper-oil samples was analysed under different frequencies of transients and different magnitudes of AC voltage. A waveform similar to the one illustrated in Fig. 4.18 was applied. The AC voltage magnitude was initially set to 2.91 kV; the repetition frequency of the transient was altered between 1 kHz and 10 kHz in 1 kHz steps. The mean results are shown in Fig. 4.19 with the respective standard deviation.

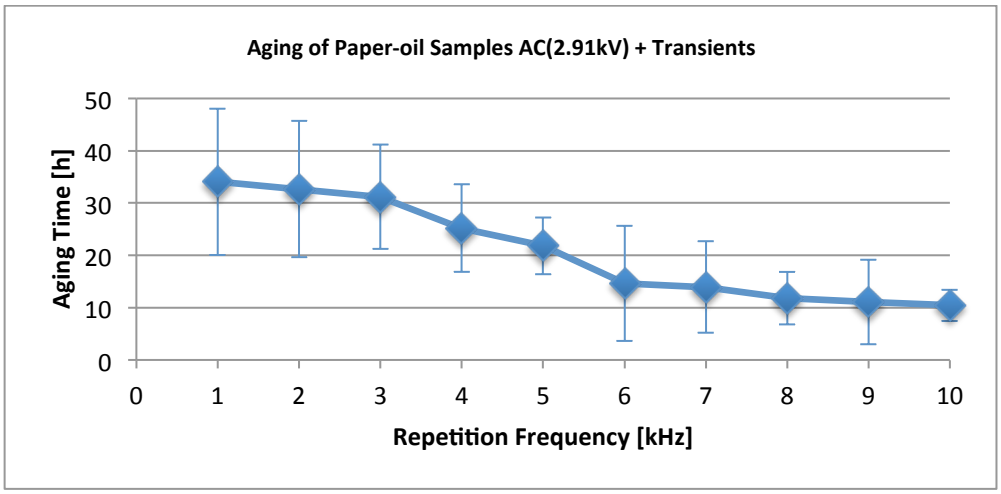


Fig. 4.19 – Mean time to breakdown as function of transients' repetition frequency with standard deviation for each repetition frequency

The results presented in Fig. 4.19 show that by increasing the repetition frequency of transients, the average time to breakdown decreases. At 1 kHz of transient frequency, the average breakdown time was 34 hours ± 13 h. This value drops to 21 hours (± 5h) at 5 kHz to reach 10 hours (± 3h) at 10 kHz.

When the magnitude of the AC waveform was lowered to 2.22 kV similar results were obtained, but on a different magnitude scale. The results are shown in Fig. 4.20.

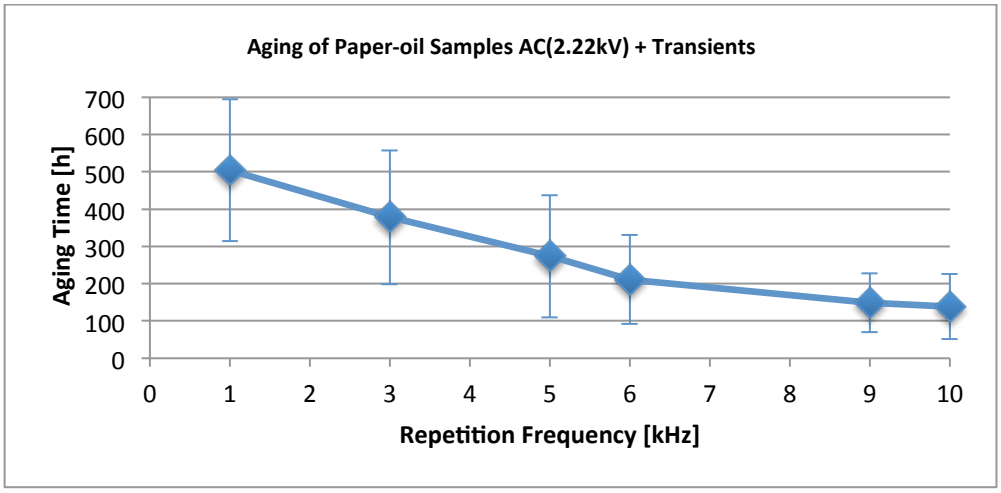


Fig. 4.20 – Mean time to breakdown as function of transients´ repetition frequency with standard deviation figures

Due to the long time needed to break down the samples at lower AC magnitude, a limited number of transient frequencies were investigated. The time to breakdown decreased with the increase of the repetition frequency of the transients. At 1 kHz, the aging time was on average 508 hours (±190 h). Once the frequency was increased to 9 kHz, this value dropped to 144 hours (±79 h). The times to breakdown are considerably higher when the AC magnitude was decreased to 2.22 kV. This indicates that the magnitude of sinusoidal waveform affects the lifetime of the samples.

To identify the aging coefficient, the average aging times of "clean" sinusoidal aging were compared to the average aging times of sinusoidal waveform superimposed with transients. The following formula was used:

$$r(V) = \frac{\overline{\tau_{AC}^{bd}(V)}}{\tau_{AC+tr}^{bd}(V)} \quad (1)$$

Where:

r(V) is the aging coefficient of the AC waveform with superimposed transients at voltage V ;

$\tau^{bd}_{ac}(v)$ *is the average aging time to breakdown of a "clean" AC waveform;*

$\tau^{bd}_{ac+tr}(v)$ *is the average aging time to breakdown of an AC waveform superimposed with 1 kV transients.*

The aging times of clean AC waveform were taken from Chapter 3. The results are presented in Fig. 4.21.

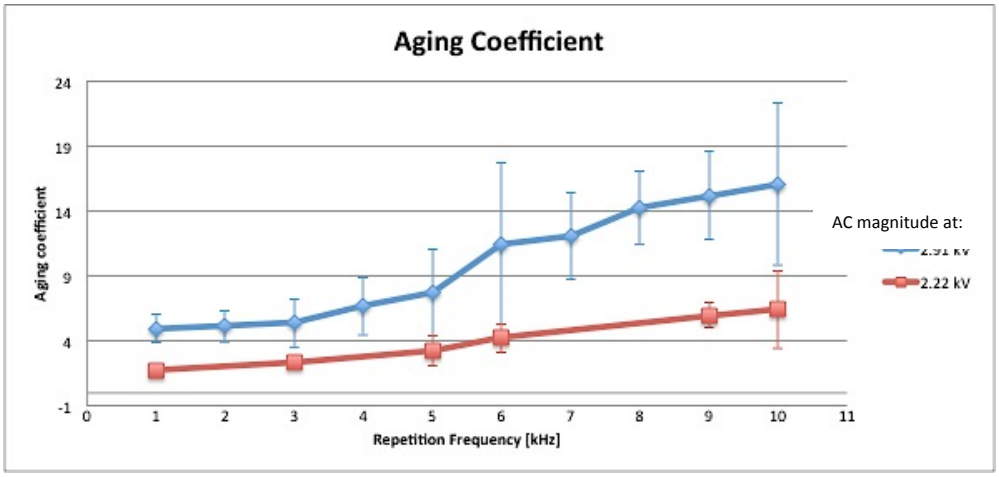


Fig. 4.21 – The aging coefficient as function of the repetition frequency of transients superimposed on 2.22 kV and 2.91 kV sinusoidal waveforms. The relative errors in standard deviation have been added.

The aging coefficient factors increase with the repetition frequency of transients and is larger when a higher magnitude AC waveform was applied. A break in proportionality at 5 kHz can also be noticed for higher AC waveforms of 2.91 kV with the aging coefficient increasing faster after this point.

The purpose of the tests, which results are presented in Fig 4.21, was to disregard the effect of aging caused by the AC waveform itself. The value of magnitude 2.22 kV was below PDIV, therefore reducing the important effects of aging, PD. It can be deducted from this figure, that transients do have an aging effect on the paper samples, when superimposed on an AC waveform. Beyond the repetition frequency of 5 kHz, the paper is more influenced by the transients causing a much faster degradation of the insulation. Further results will be presented in Chapter 4.5 where the dielectric properties of the paper will be presented.

4.4.4. Discussion

The results gathered in the previous section clearly indicate that repetitive transients accelerate the aging of paper-oil insulation. The aging rate is dependent on the repetition frequency of the transients, the higher the frequency, the faster the aging rate is.

Based on the aging test results, estimated life curves were drawn in Fig. 4.22.

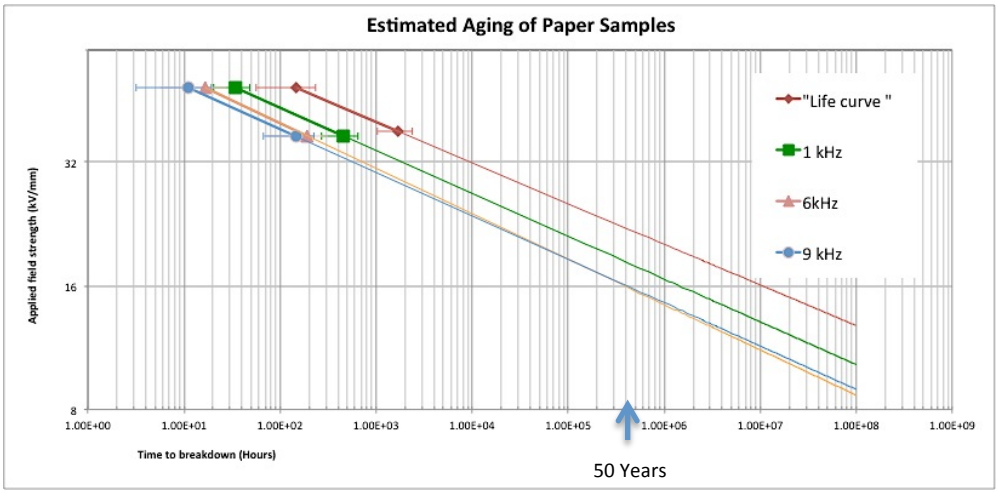


Fig. 4.22 – Estimated arithmetic mean life time curves of paper-oil samples under transient conditions and AC-only scenario

Four life curves can be seen on the graph in Fig. 4.22. The right-most upper one corresponds to the aging curve shown in Chapter 3, based only on the AC waveform-aging factor. The remaining three lines show the aging rate based on aging with AC superimposed with transients of three different repetition rates: 1 kHz, 6 kHz and 9 kHz. The top and the bottom points in the figure correspond to the results of aging with AC waveform superimposed with transients: 2.91 kV + transients and 2.22 kV + transients respectively. The electric field strength at these points was 48.5 kV/mm and 37 kV/mm respectively.

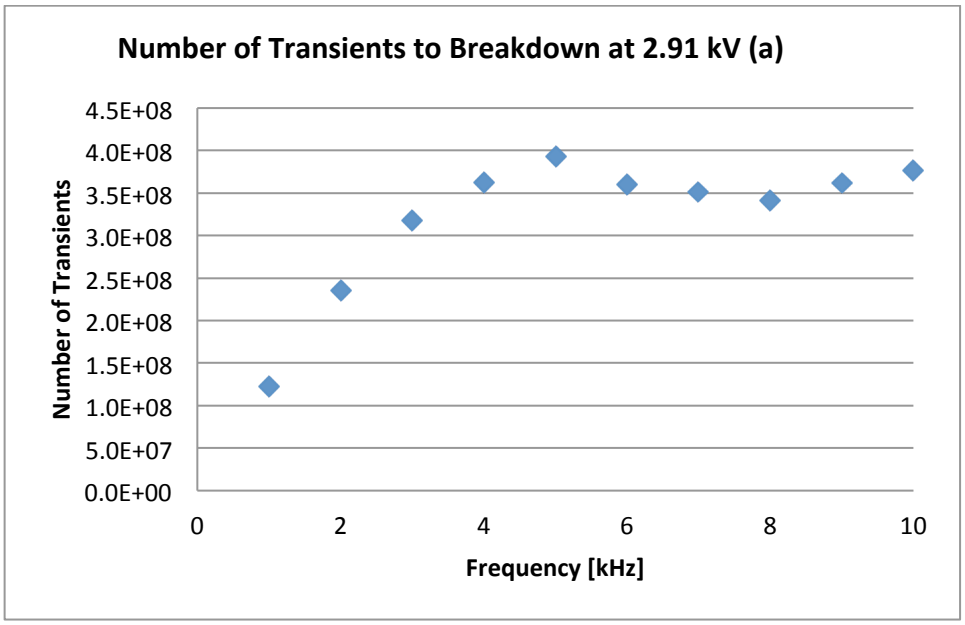
With the addition of repetitive transients, the lifetime of the tested paper-oil insulation decreased. Increasing the repetition frequency of transients decreased further the lifetime of the samples. An extrapolation of the expected lifetime has been carried out on Fig. 4.22 assuming the power law relationship of time to breakdown and voltage stress. A 50 years mark has been added to the figure, a common lifetime for HV equipment. It can be seen that to achieve this lifetime with repetitive transients, the magnitude of the carrier wave would need to be decreased from 22 kV/mm (±4kV) to 14 kV/mm (±6 kV). These values should be taken as indicative due to the relative large spread of results.

4.4.5. Influence of the number of repetitive pulses on AC dielectric strength

According to the experiments presented in Chapter 4.4.4, the number of repetitive transients applied to reach breakdown of the insulation was counted. Assuming that the time to breakdown, t *[s]*, and the rate of repetition of transients, f_t *[Hz],* are a finite number, *N*, we obtain:

$$N = t_{bd} \cdot f_{tr} \tag{2}$$

N represents the total number of pulses required to achieve breakdown. Plotting the mean number of pulses as a function of frequency, the following figures were obtained.



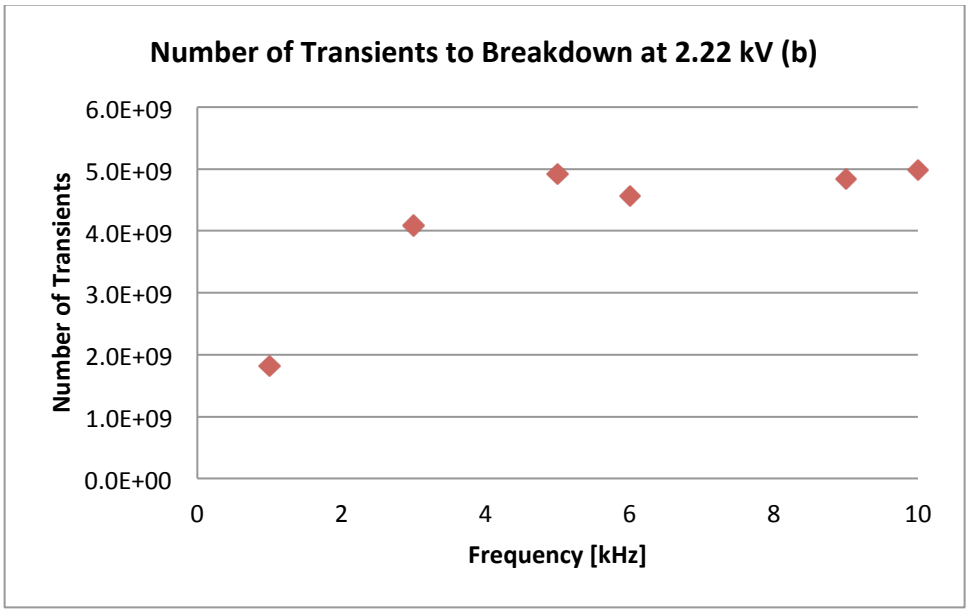


Fig 4.23 – The mean number of transients, N, required to achieve breakdown. (a) Super-imposed on a 2.91 kV waveform and (b) superimposed on a 2.22 kV waveform

From the figure above, it can be seen that a "saturation" value is achieved for the number of applied transients, *N*. This means that a finite amount of energy can be applied to the paper before breakdown occurs. This energy could be dissipated by

PD incepted, as discussed earlier. The number of pulses is also dependant on the second variable, the magnitude of the carrier voltage. The energy injected by the transients is the same in both cases, however, at 2.91 kV, more energy is applied thus reducing the number of transients required to achieve breakdown.

4.5.Tangent Delta

Tan (δ) measurements were performed on the paper-oil samples and the goal of these measurements was to investigate the degradation process of paper-oil in 50 Hz AC with and without superimposed transients. The method of analysing these changes was to observe the dielectric response of paper.

4.5.1. Test set-up and procedure

Tan (δ) measurements were performed using the dielectric spectroscopy equipment. The samples measured were Kraft paper of 0.06 mm thickness, impregnated with oil.

These samples were stressed for 20 h under AC voltage of different magnitude and of different transient repetition frequency. Afterwards, the tan (δ) measurements were performed in the frequency range from 0.01 Hz to 1 MHz. The magnitude of the voltage was 1 V.

4.5.2. Test results

Tan (δ) measurements were performed on the samples stressed with the AC waveform superimposed with transients. In particular the following combinations were applied for 20 h:

- AC waveform of 2.91 kV superimposed with transients of repetitive frequencies: 2 kHz, 6 kHz, and 9 kHz, test results in Fig. 4.24;
- AC waveform of 2.22 kV superimposed with transients of repetitive frequencies: 2 kHz, 6 kHz, and 9 kHz, test results in Fig. 4.25.

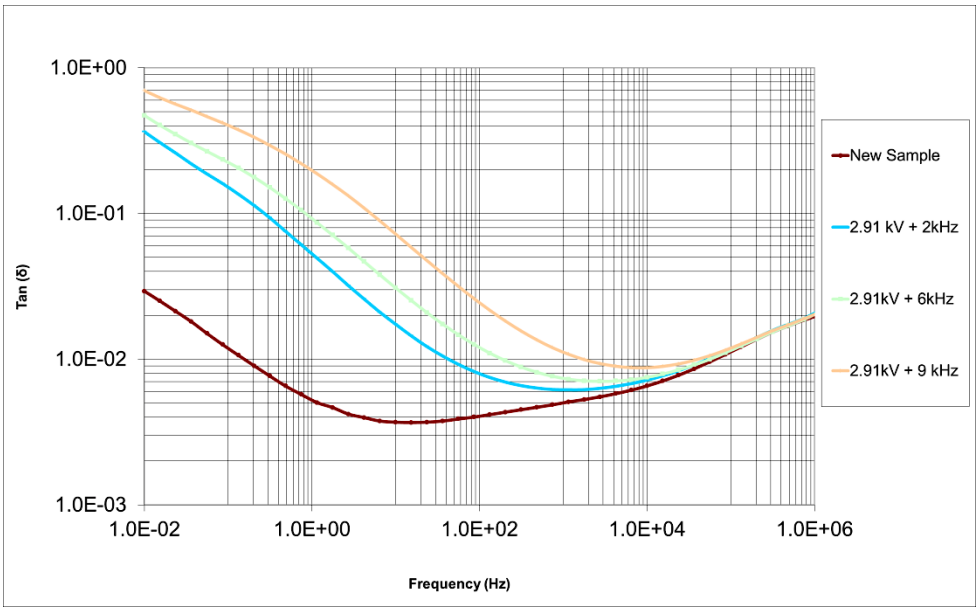


Fig. 4.24 – Tan (δ) values as a function of the measurements frequency for paper-oil samples stressed for 20 h with a carrier waveform of 2.91 kV and different transient repetition frequency

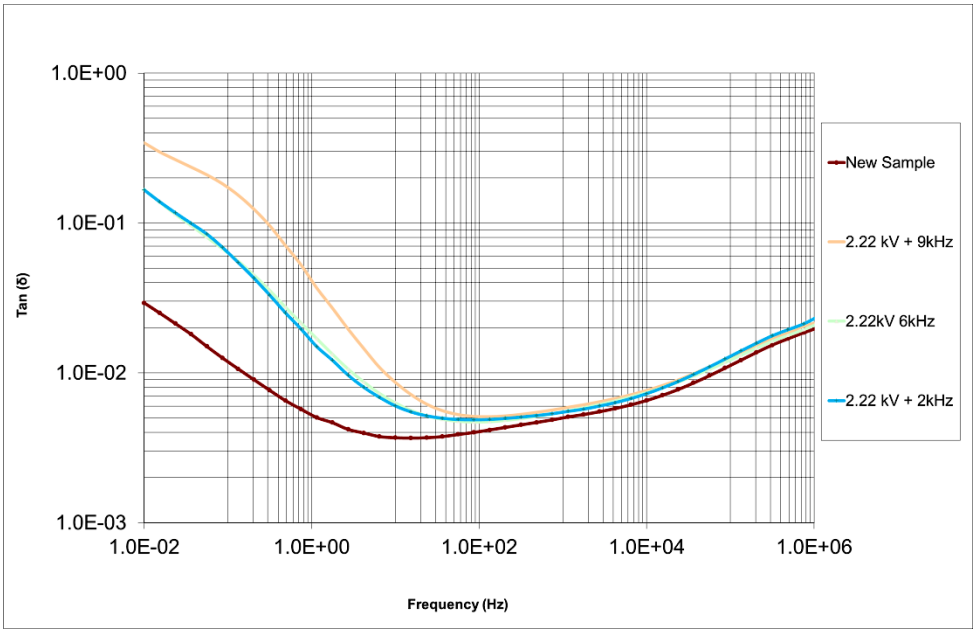


Fig. 4.25 – Tan (δ) values as a function of the measurements frequency for paper-oil samples stressed for 20 h with a carrier waveform of 2.22 kV and different transient repetition frequency

The values gathered were compared to the measurements on a new sample that was not aged. The discussion of these results is presented in the following section.

4.5.3. Discussion and Hypothesis

Similar tests, as presented in this chapter, were described in Chapter 3 where the influence of the magnitude of the AC voltage (without transients) on the tan (δ) values is shown. In that case, it was found that PD activity influences the state of the insulation and higher losses are created above PDIV (2.53 kV voltage plot, Fig. 3.9). PDs are believed to be accompanied by aging when transients are applied above a certain magnitude.

In Fig. 4.25, the loss factors are less dispersed for the 2.22kV+2kHz and 2.22kV+6kHz curves than for the 2.22kV+9kHz one. The cause is most likely attributed to the lack of PDs in these two aging procedures. In Fig. 4.5 the relation of PDIV to the applied frequency was presented. It was observed that for a square wave of 1000ns rise time and frequency 2kHz, 6kHz and 9Khz, the estimated PDIV were 5.1 kV, 4.6 kV and 4.2 kV respectively. The 1000ns rise was chosen as it is the same rise time of the transients superimposed on the carrier wave.

The wave used to stress the samples for the Tan (δ) measurements was an AC waveform with superimposed transients. In order to draw similarities with the previously used square wave, the AC part of the wave was converted from RMS values to peak one. A 2.22 kV_{RMS} can be recalculated as 3.13 kV_{pk}. The addition of the transients adds the total magnitude to 4.13 kV. This magnitude corresponds approximately to the 9 kHz frequency of the square wave at 1000 ns. This observation results that, for this kind of paper, and the aging conditions applied, no PDs occur at frequencies lower than 9 kHz, thus resulting in no apparent difference in the two curves of 2.22kV+2kHz and 2.22kV+6kHz.

Paper insulation is constituted of fibres that are comprised further polymeric chains, which carry polar groups with dipoles. In the Fluctuation Model suggested by Fothergill [78], it was stated that these structural units, identified as clusters " *move from site to site in time whilst maintaining the total free energy at a constant value. Such fluctuations in site occupancy will redistribute local mechanical strains or dipole orientations about the system and influence the relaxation currents involved in linear response theory.* "

When aged, the average length of the polymeric chains within a material decreases. The length of these chains can be observed by a higher loss factor in the

dielectric spectroscopy measurements identified in Fig. 4.24 and Fig. 4.25. Shorter chains have faster resonance frequencies, thus higher losses were observed at faster measurement frequencies in the dielectric spectroscopy test for samples stressed with higher repetition frequency of transients.

4.7. Conclusions

In this Chapter, the effect of the influence of different types of waveforms on the dielectric strength of paper-oil insulation has been analysed. The common properties of these waveforms are chosen to conform to those of power electronic inverters. These repetitive transients are characterized by high magnitudes, fast rise times and repetition frequencies over a prolonged period of time.

The square wave was the first type of waveform tested. The rise time and frequency of the square wave were changed in order to investigate their effect on the breakdown voltage and PDIV. Increasing the rise time from 300 ns to 1000 ns, it was noticed that the breakdown voltage and PDIV increase. The same observation was concluded when the repetition frequency was decreased from 10 kHz to 1 kHz.

The second type of experiment focused on understanding the behaviour of the paper-oil sample under a single impulse, similar to a repetitive transient, whilst not considering the repetition frequency factor. A similar observation was concluded as a faster rise time decrease the breakdown voltage of the samples.

During aging tests, a sinusoidal voltage waveform of carrier voltage and transient repetition frequency was applied and the time to breakdown was recorded. The AC voltage magnitude and the repetition frequency of the transients were changed during tests. As expected, the higher the magnitude of AC voltage was applied, the shorter the lifetime of the insulation samples was. For both cases of AC magnitude, the repetitive transients aged the samples further and its lifetime decreased with the increase of the rate of repetition frequency.

Partial discharges were attributed as the main source of aging of paper insulation when exposed to repetitive transients. PD causes dielectric heating within the material that leads to localised carbonisation of the paper. PD inception voltage decreased with an increase of the repetition frequency and rise time of the applied waveform.

A link between the applied transient frequency and tan (δ) value has been observed after performing dielectric spectroscopy measurements. High stresses in terms of electric field and repetition frequency of transients may lead to the scission of polymeric chains. This break is in line with higher tan (δ) values of similar samples when exposed for the same time to the mentioned variable parameters. Further investigations will be carried out in Chapter 6 when developing an aging model.

The introduction of repetitive transients is expected to increase in the near future. As already discussed in Chapter 2, the operating temperature of transformers is expected to increase with an increase of load. This would have a direct effect on the oil, which at high temperature becomes less viscous. A series of tests were carried out at elevated temperatures to investigate this phenomenon and are presented in the next Chapter.

Chapter 5
Effect of Repetitive Transients on Paper-oil Insulation at Elevated Temperatures

The short and long-term effects of repetitive transients on the dielectric properties of transformer paper-oil insulation has been analysed in ambient temperature in the previous Chapter. It was concluded that shortening the rise time and increasing the repetition frequency of repetitive transients diminish the life of paper-oil insulation.

The impact of increased temperature on the aging process of various types of insulation has been extensively studied for many years [36, 57, 59, 69]. However, the influence of temperature in combination with repetitive transients acting together on paper-oil insulation hasn't been determined. This chapter will combine some of the tests performed in the previous chapter and perform them at temperatures above room temperature.

For this purpose, three important test values will be measured and analysed in order to determine the aging rate of paper-oil insulation at elevated temperatures:

- AC breakdown voltage strength on new samples;
- Tan (δ) of samples aged with an AC waveform with superimposed repetitive transients.

The results of the investigation at ambient temperature were presented in Chapters 3 and 4 and will be taken into account for comparison.

5.1. Heat Fluctuations in Transformer

The temperature inside the transformer varies constantly during the course of a day. This variation is influenced by the electrical load i.e. related to the amount of power required. For instance, the loading conditions of transformers at wind-farms are linked to the wind speed. This makes their operation variable throughout the course of the day with random peaks in operation. The more power needs to be

processed due to strong wind, the higher the operating temperature of the transformer is expected to be.

Similar scenarios are observed in specific distribution transformers where the need for more power is observed at different times of the day. Three main daily intervals in temperature have been indicated in [59] and are shown in Fig. 5.1.

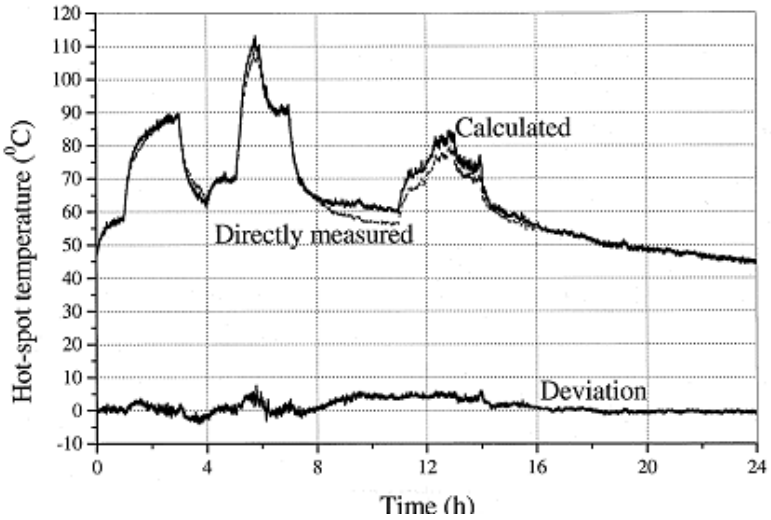


Fig. 5.1 – Hot-spot temperature variations in a distribution transformer during the course of a day [59]

The temperature measured in Fig. 5.1 corresponds to the hot-spot temperature, the hottest point in the winding of a transformer. This point is usually found in the top part of the winding where the temperature at this point can reach up to 110 °C. The average temperature of the oil, however, is much lower and should not exceed 85 ° C [60, 61].

From an analysis of the literature [5, 62, 63], several factors are attributed to thermal degradation of paper, such as bubble generation, increase of oil moisture content and viscosity. The addition of repetitive transients with temperature effect has not been addressed [3,4].

In Chapter 2.2.3, the process of bubble generation in paper-oil insulation was described indicating that cooling and heating are the main cause of moisture movement within this particular insulation system. With the application of an electric field, these bubbles can create PDs in the insulation.

During temperature changes, the moisture migrates from the paper to the oil when the temperature increases and is reabsorbed when the temperature decreases. The presence of moisture in a medium decreases its dielectric strength. In Fig. 5.2, the content of moisture in paper as function of moisture content in oil at different temperatures is shown.

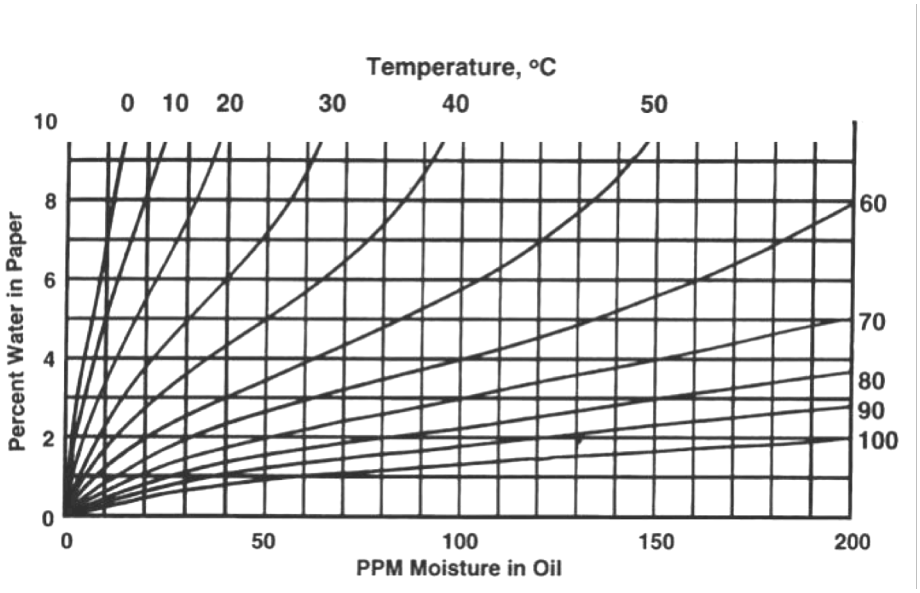


Fig. 5.2 –Relation of water percentage in paper as function of moisture in oil at different temperatures increased in 10 degree steps [6]

In the temperature up to 50 °C, a small increase in the moisture concentration in oil will result in higher water content in the paper.

Based on this information, it was estimated that the dielectric strength of oil at higher temperatures will decrease, whilst the breakdown strength of paper will increase. This relation will be verified in Chapter 5.2.

5.2. AC Dielectric Strength at Elevated Temperature

In this section, AC breakdown tests are performed at temperatures above room temperature. The results are presented and compared to room temperature breakdown tests performed in the previous chapter.

5.2.1. Test set-up and procedure

The tests were carried out according to the procedure in the standard IEC 60243-1, as described in Chapter 3.3. The impregnated paper-oil samples of 0.06 mm

thickness were used. The population of twelve samples were tested for each temperature level.

From the graph in Fig. 5.1, seven temperatures were selected for the tests: 17 °C (approx. room temperature), 40 °C, 50 °C, 60 °C, 70 °C, 80 °C and 90 °C. For safety reasons, higher temperatures were not investigated, as this was the thermal limit for connection cables in the test set-up. The device used for the heating was a vessel, with a heating element placed at the bottom. A schematic of the test set-up is shown in Fig. 5.3.

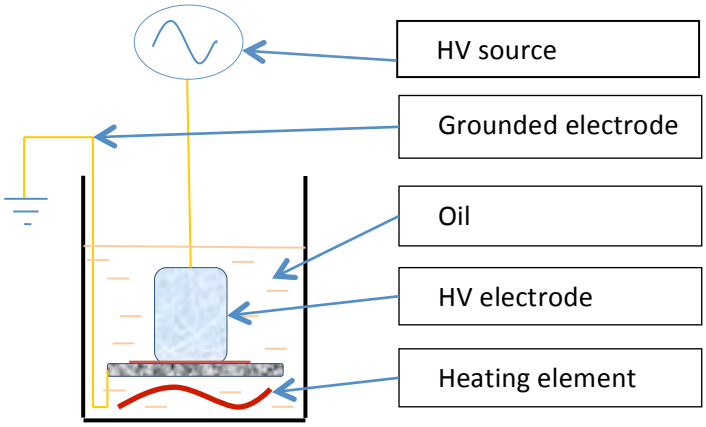


Fig. 5.3 – Experimental set-up for testing at elevated temperatures

The Rogowski shaped electrode was placed on top of the paper-oil sample immersed in mineral oil. The bottom electrode was grounded and placed above the heating element but without physical contact with it. The voltage was increased every minute in steps of 200 V until breakdown.

The temperature was measured with the precision of 1 decimal place with a probe at several locations in the container including the near vicinity to the HV electrode and the sample. When the temperature fluctuation was below 1 °C, the temperature of the oil was considered stable and tests were performed. The time required to achieve this “temperature balance” was 2 hours, at which point the samples were inserted into the test set-up in order to avoid thermal aging of the paper.

5.2.2. Test results

According to the test set-up described above, the breakdown voltages were obtained. At least 12 samples were stressed at each temperature, with the exception of the 90 °C where only 4 samples were tested. The Weibull analysis of these results is shown in Table 5.1.

Table 5.1 – 2-parameter Weibull analysis of AC breakdown voltage at different temperatures

Temperature (°C)	β	η [kV]	ρ
17	13.42	3.21	0.9885
40	18.03	3.51	0.9059
50	13.06	3.62	0.9781
60	19.91	3.67	0.9512
70	13.67	3.37	0.9463
80	36.64	3.31	0.9395
90	15.16	3.51	0.9740

The parameter ρ illustrates how well the best-fit line fits to the set of data. The number of samples influence the acceptance limits for ρ, e.g. for eight samples, ρ should be larger than 0.91 [60]. The series of tests results performed at 40 °C have the lowest ρ coefficient, but still close to the acceptance level. High β values are advisable as they indicate a small scatter of breakdown voltage values, as shown for the values at 80 °C.

The times to breakdown for 63.2% have been plotted on Fig. 5.4. The error bars have been added to illustrate the scatter of breakdown voltages.

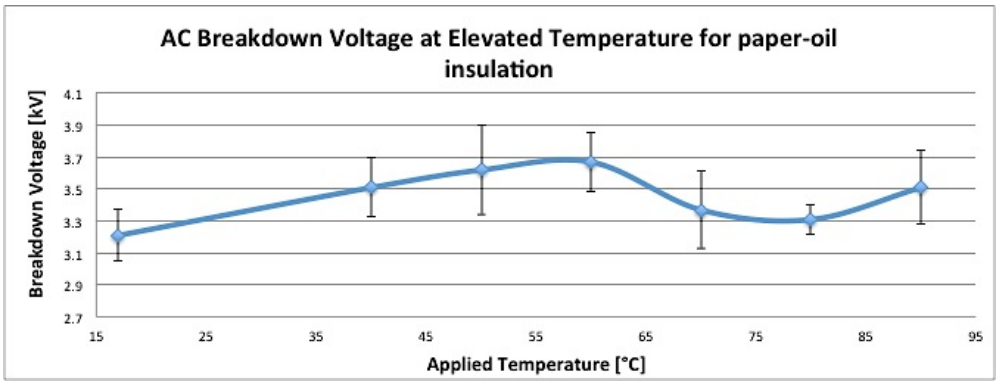


Fig. 5.4 –Dielectric breakdown voltage test results as function of temperature

In Fig. 5.4, three clear trends can be noted:

- Up to 60 °C, the breakdown voltage is increasing;
- Between 60 °C and 80 °C, the breakdown voltage drops and;
- Above 80 °C, the breakdown voltage increases again.

It should also be noted that at room temperature, the same mean V_{BD} values were obtained as in the tests performed in Chapter 3.3.2, i.e. 3.1 kV.

Only four samples were stressed at 90 °C. High levels of evaporating fumes were discharged into the air surrounding the test set-up and the coating of the leads connecting the HV source to the electrode was beginning to melt. The tests were therefore stopped for health and safety reasons and were not repeated because most transformers don't operate above 60 °C except at abnormal conditions [60]. Additionally, it should be noted that according to the oil's datasheet, an unstable behaviour occurs when the temperature of 60 °C is exceeded.

5.2.3. Discussion

According to literature, moisture at elevated temperatures exits the paper and enters into the oil. This migration of moisture influences the breakdown strength values of the two materials by improving the V_{BD} of the paper and by reducing the V_{BD} of the oil. From the data specifications of Shell Diala B, 60 °C is considered the maximum temperature at which the oil's dielectric characteristics are maintained. Any tests above this threshold degrade the oil thermally decreasing its dielectric strength.

Up to 60 °C, the breakdown voltage of the sample increases. A possible cause of this could be that the oil impregnates the samples further thus increasing their breakdown voltage. When breakdown tests were performed above 60 °C, the breakdown voltage started decreasing. According to the oil's datasheet [33], the dielectric properties of the oil decrease above this threshold temperature. This result in lower insulating capabilities, thus lower breakdown voltages

At 90 °C, the breakdown voltage of the samples increased. Though unexpected, the result was ignored as only a few samples were stressed and the testing environment became contaminated with debris from the electrical leads.

The addition of repetitive transients may have additional degrading effect on the dielectric properties of paper-oil when exposed to temperatures above room temperature. In the next section, tan (δ) measurements will be performed on the

paper-oil samples after an exposure of 20 hours to repetitive transients and three different temperatures.

5.3. Aging by Repetitive Transient at Elevated Temperature

As it was shown in Chapter 4, the continuous application of an electric field deteriorates the dielectric quality of paper-oil insulation, such as breakdown voltage and tan (δ). From literature, it was discussed that elevated temperatures above 60 °C will increase the tan (δ) values of paper [64]. It is expected that with the increase of moisture in an insulating material, the loss factor will increase due to the conductivity of water present in paper-oil (Fig. 5.5).

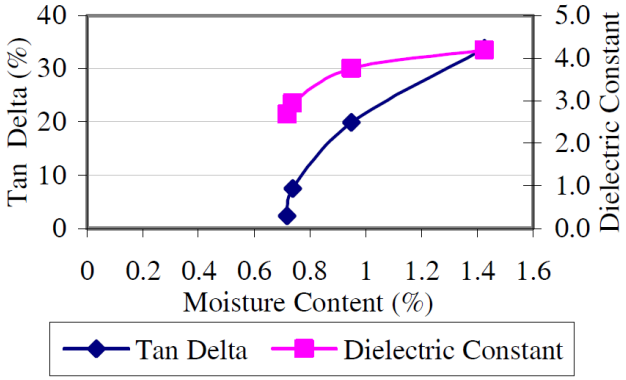


Fig. 5.5 – Tan (δ) and Dielectric Constant values due to moisture content in mineral oil [64]

In Fig. 5.5, a sharp increase in both, the tan (δ) and the dielectric constant values can be observed when the moisture content in oil increased from 0.7 % to 1 %.

The goal of the experiments is to measure the loss factor in paper-oil insulation after being exposed, in elevated temperatures, to repetitive transients superimposed on an AC wave for the defined amount of time.

5.3.1 Test set-up and procedure

The test procedure used for these tests was similar to the one described in Chapter 4.4 where tan (δ) was measured using the dielectric spectroscopy. The procedure involved three steps:

- Pre-treatment of the paper samples in an oven for 24 hours at 60 °C;
- Aging of the paper-oil sample with a 2.22 kV AC waveform with superimposed repetitive transients at elevated temperature for 22 hours;
- Measuring the tan (δ) values of the aged samples.

The aging time was set for 22 hours as it guaranteed the most convenient for a smooth aging-measuring procedure. This time frame allowed the aging test to start at the same time every day and provided two hours between the tests to perform the measurements, change of the sample and further increase of the temperature.

The tests were performed in temperatures of 17 °C, 40 °C, 60 °C and 80 °C. The same Rogowski profile electrodes were used as in the previous experiments.

For the heat application, a hot plate was chosen due to its high reliability of voltage application over long time. The hot plate's thermostat has an accuracy of ±2 °C for the temperature control. The temperature was measured in several places in the proximity of the electrode inside the beaker. When the measured temperature range was within 1 °C, the oil's temperature was considered satisfactory for the test to start. The test set-up is illustrated in Fig. 5.6.

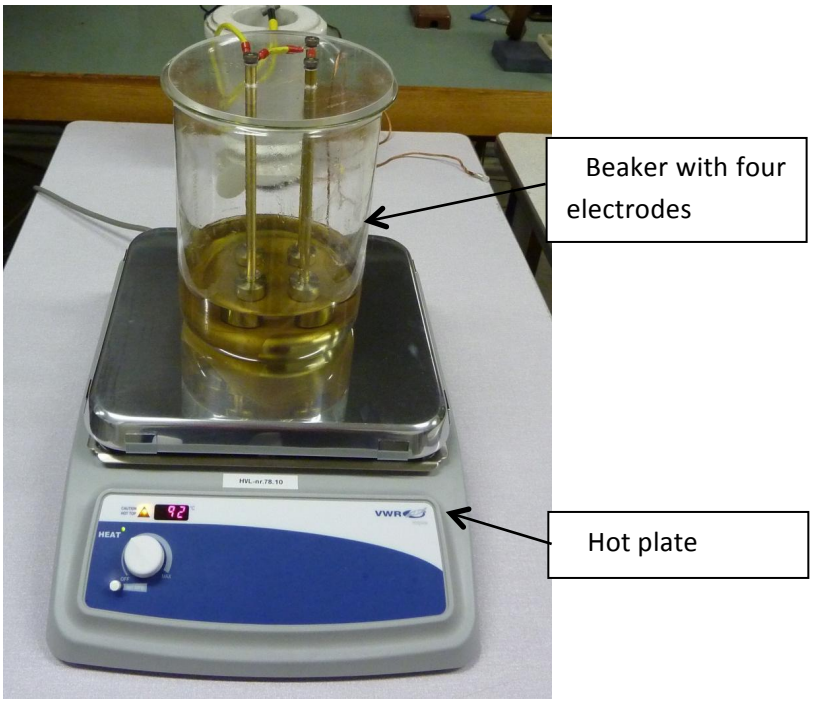


Fig. 5.6 –Test set-up used for long term tests at elevated temperature

The hot plate is shown in Fig. 5.6 with a beaker of mineral oil and four samples immersed in it. Up to four samples were stressed simultaneously and the average of their breakdown voltage values is presented. The same set-up was used for all the experiments, however, the electrodes were cleaned and the oil was changed after testing at each temperature level. After the conclusion of the aging test, the samples were removed and the tan (δ) measurements were performed immediately and measured at room temperature.

Tan (δ) measurements were performed using the Tettex 2840 device that utilised a Schering Bridge for the measurements.

5.3.2. Tan (δ) measurements results

The values presented in Fig. 5.7 (new sample) are used as a reference value for the upcoming tests. It can be seen that the tan (δ) values have the same value when measuring at voltages between 50 V and 600 V and a sharp increase is noted above 600 V of measuring voltage. Due to the paper-oil sample's small thickness, it was decided for the aged samples to limit the measuring voltage up to 350 V to protect the test equipment from the risk of any discharges.

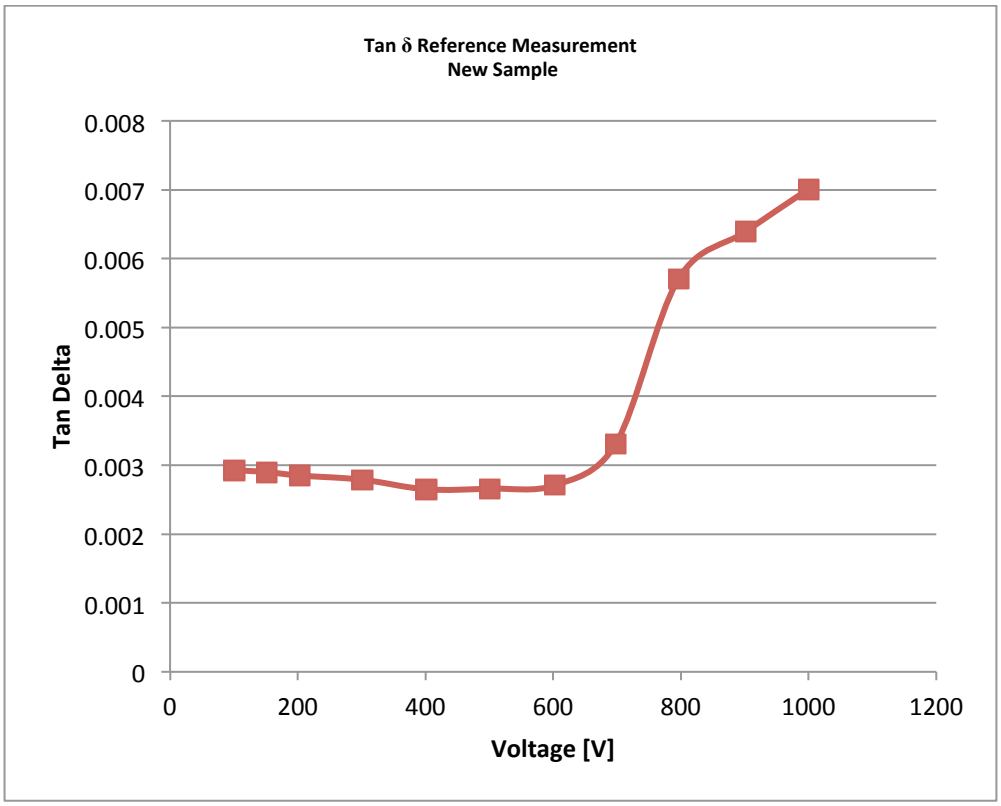


Fig. 5.7 – Tan (δ) values as function of measuring voltage for a new sample (reference data)

The results of tan (δ) measurements as a function of the measuring voltage at different temperatures are presented in Figures 5.8 to 5.11.

The results presented in Fig. 5.8 were obtained on sample stressed only with an AC waveform of 2.22 kV.

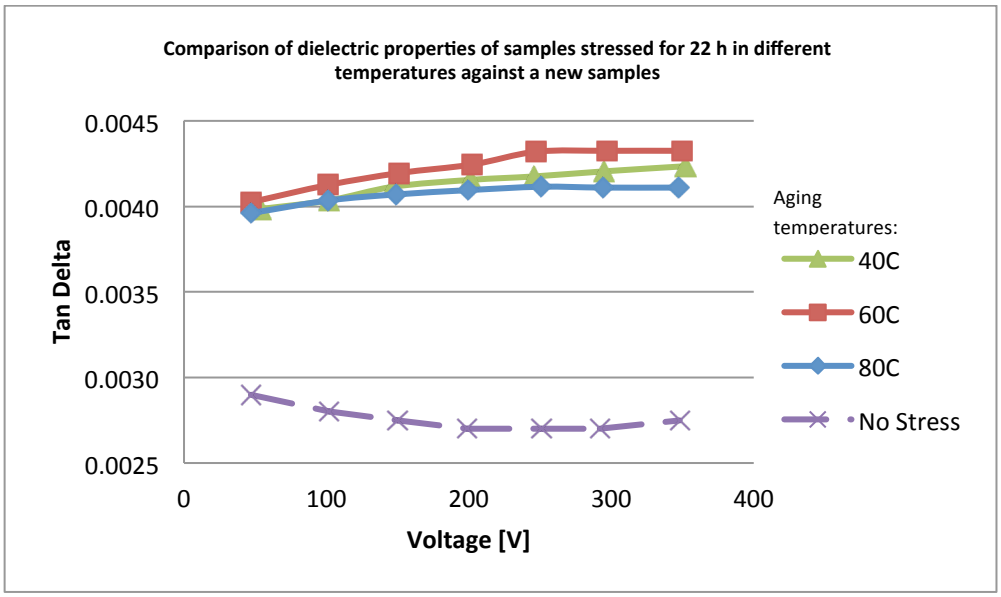


Fig. 5.8 – Tan (δ) values as function of measuring voltage for samples thermally and electrically stressed at different temperatures under an AC waveform for 22h. The data is compared to a new samples that has not been stressed

It can be seen from Fig. 5.8 that all the tan (δ) values are higher when compared to the results in Fig. 5.7. At a measuring voltage of 50 V the increase is by approx. 33 % for all temperatures whereas for 350 V this increase varies from 46 % (at 80 °C) to 55 % (at 60 °C).

The results presented in Fig. 5.9 to Fig. 5.11 illustrate the tan (δ) for samples stressed for 22 h with a 2.22 kV AC wave with superimposed transients for the same temperature selection. The repetition frequencies of transients investigated are 1 kHz, 5 kHz and 10 kHz.

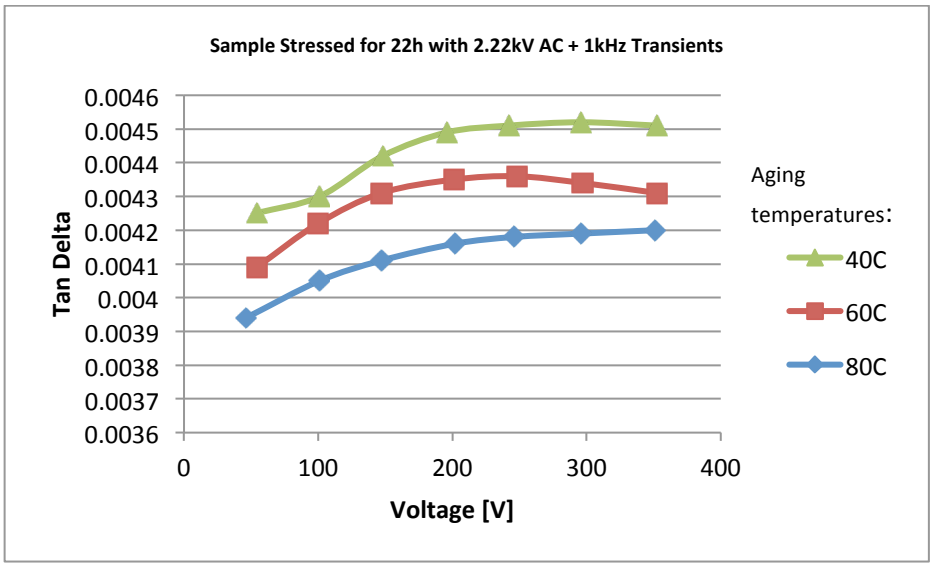


Fig. 5.9 – Tan (δ) values as a function of measuring voltage for samples thermally and electrically stressed at different temperatures under an AC waveform with superimposed 1 kHz transients for 22 h

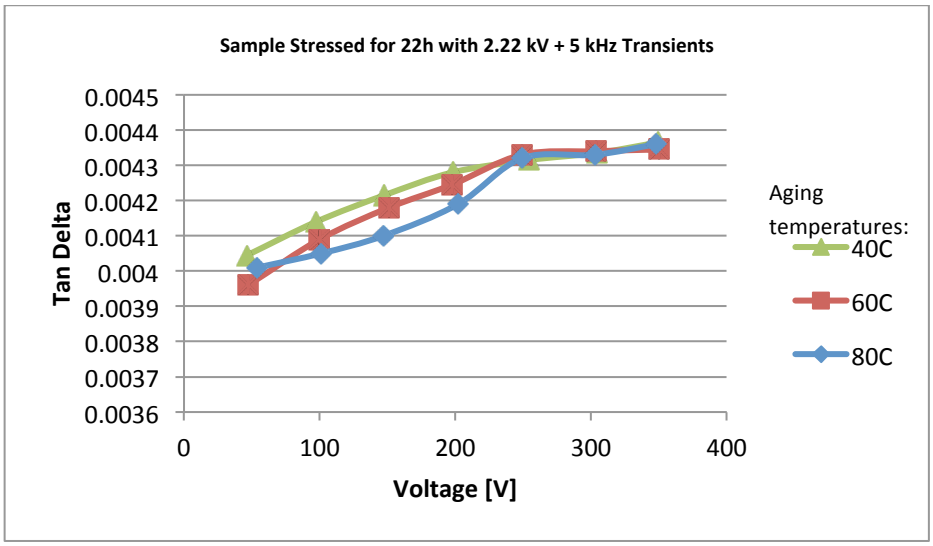


Fig. 5.10 – Tan (δ) values as a function of measuring voltage for samples thermally and electrically stressed at different temperatures under an AC waveform with superimposed 5 kHz transients for 22 h

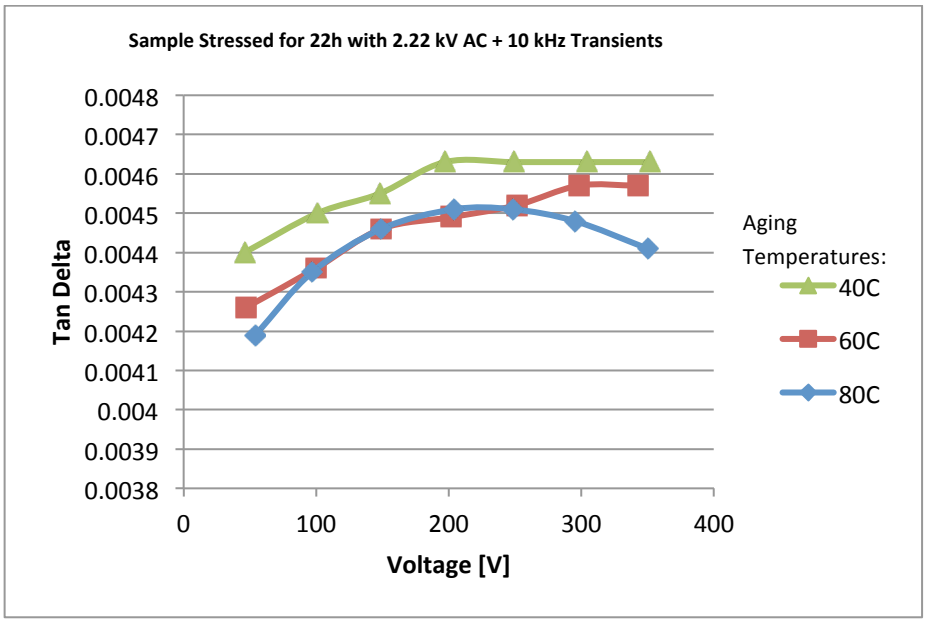


Fig. 5.11 – Tan (δ) values as a function of measuring voltage for samples thermally and electrically stressed at different temperatures under an AC waveform with superimposed 10 kHz transients for 22 h

Only very small differences can be noticed between the tan (δ) values for each test conditions. In most graphs, the increase of temperature leads to lower tan (δ) values. Contrary, the increase of the repetition frequency of transients leads to higher tan (δ) values. The biggest differences in tan (δ) values can be noticed for the measuring voltage of 350 V.

It can be noticed that the 5 kHz plot is different from the others. In Fig. 5.10, the data points are all closer to each other. This difference could be attributed to the conditioning of the samples before the aging tests.

To obtain a better overview of the results, the values of tan (δ) for the aged samples have been calculated for 50 V and 350 V, as a percentage increase relative to the reference sample, shown in Table 5.2. The tests at 5 kHz have not been considered.

Table 5.2 – Percentile change in tan (δ) value for differently aged samples at different temperature and transient frequency in comparison to the reference sample

Stress time 22 h		Tan (δ) values in % (*)	
Test Temperature	Transient Repetition Frequency	Measuring Voltage 50 V	350 V
40 °C	2.22 kV	30 %	42 %
	1 kHz	47 %	65 %
	10 kHz	52 %	66 %
80 °C	2.22 kV	33 %	38 %
	1 kHz	36 %	51 %
	10 kHz	45 %	54 %

(*) – calculated as change in tan (δ) divided by the tan (δ) of the reference sample

The interpretation of these results, in relation to the measuring technique and nature of the sample, is discussed in the next section.

5.3.3 Discussion

When observing the loss factor values at each temperature level, it can be noticed that with the increase of repetition frequency of transients, the tan (δ) values also increase. These differences are best seen when the data points are plotted for each testing temperature level. The results are shown in Fig. 5.12 - 5.14 for 40 °C, 60 °C and 80 °C.

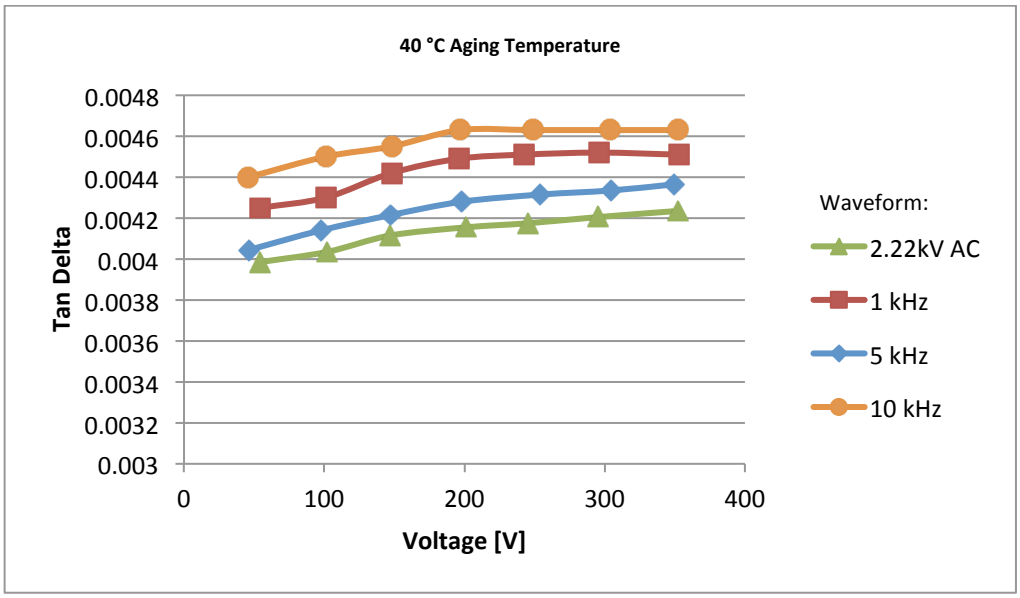


Fig. 5.12 – Tan (δ) values as function of measuring voltage for differently aged paper-oil samples at 40 °C

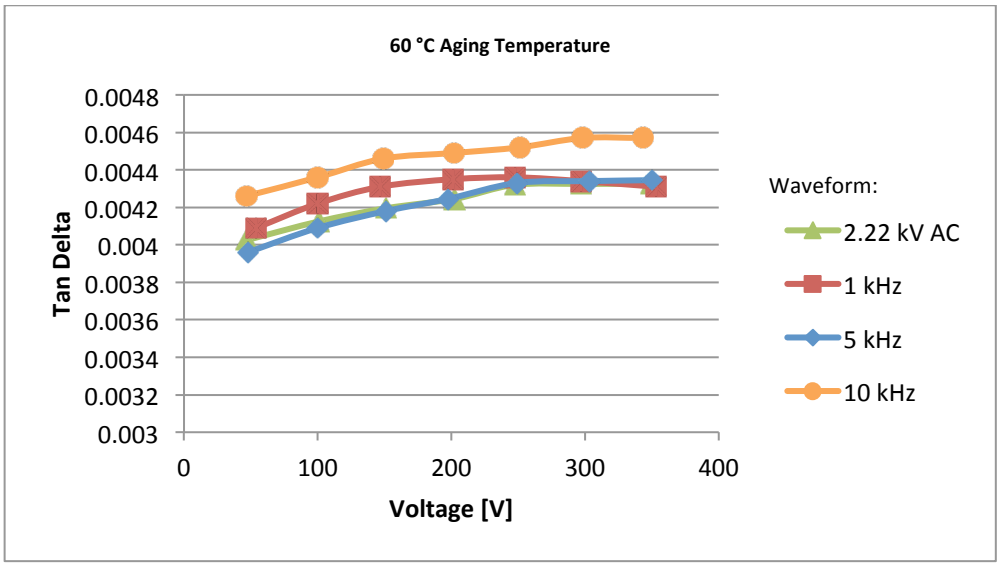


Fig. 5.13 – Tan (δ) values as function of voltage for differently aged paper-oil samples at 60 °C

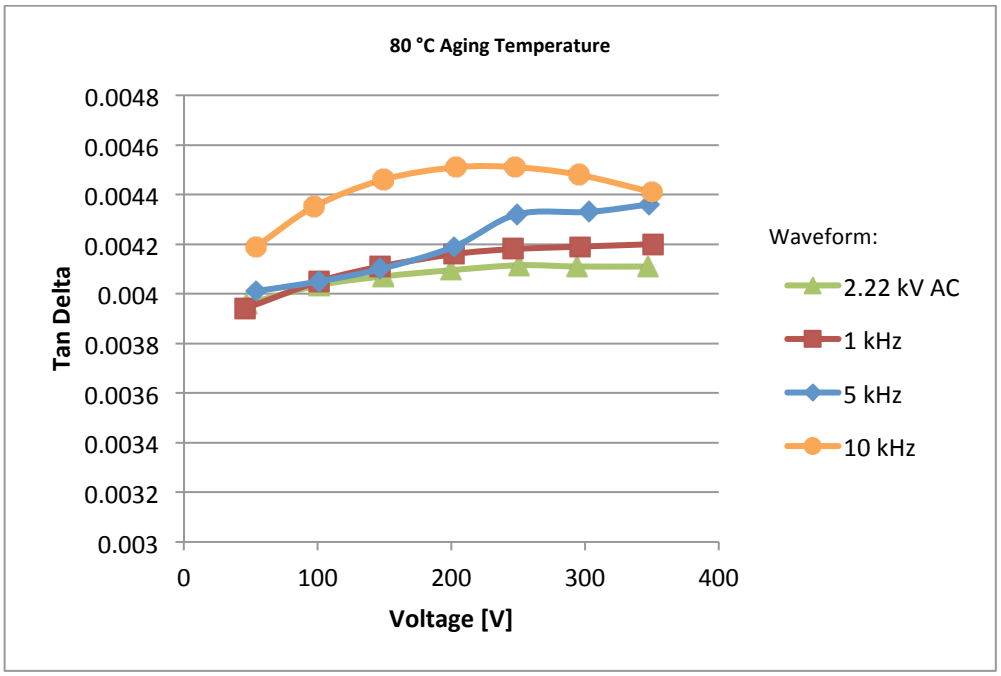


Fig. 5.14 – Tan (δ) values as function of voltage for differently aged paper-oil samples at 80 °C

Overall, the differences in tan (δ) values are very small. It should be noted that these tests were performed below the PDIV of the paper oil samples so limited aging occurred for the 22 h of aging.

The aging waveform of 2.22 kV with 10 kHz transients shows the most consistent results when observing its location relative to the other transient frequencies. Its tan (δ) values are always of the highest magnitudes on each of the various temperature graphs. As already identified in Chapter 4, 9 kHz is the threshold frequency at which PD are started. In this case, when stressing with 2.22 kV+10 kHz, PDs are present in the paper-oil sample.

5.4. Conclusion

The goal of the experiments in this Chapter was to investigate the influence of temperature on the degradation of paper-oil samples in short time and long term.

At elevated temperature a migration of moisture from the paper into the oil could become significant and the viscosity of the oil decreases. This improves the breakdown strength of the paper and reduced the one of the oil. Above 60 °C the

breakdown voltage starts to decrease as the oil's loss in dielectric properties becomes dominant.

The dielectric loss measurements of the samples aged for 22 h at an AC magnitude of 2.22 kV (below PDIV) showed that at elevated temperatures the tan (δ) values decrease. Repetitive transients increase the tan delta values at all tested temperature levels (Fig. 5.15). However, the aging time and low AC voltage magnitude were too low to see any substantial deterioration in the samples. It was noticed that the tan (δ) results for the waveform of 2.22 kV + 10 kHz transient resulted in higher values than for lower repetition frequencies at all the investigated temperatures. At this frequency and AC magnitude combination, PDs are probably present in the paper. Hence the dielectric loss measurements are more distinctive throughout the investigated range.

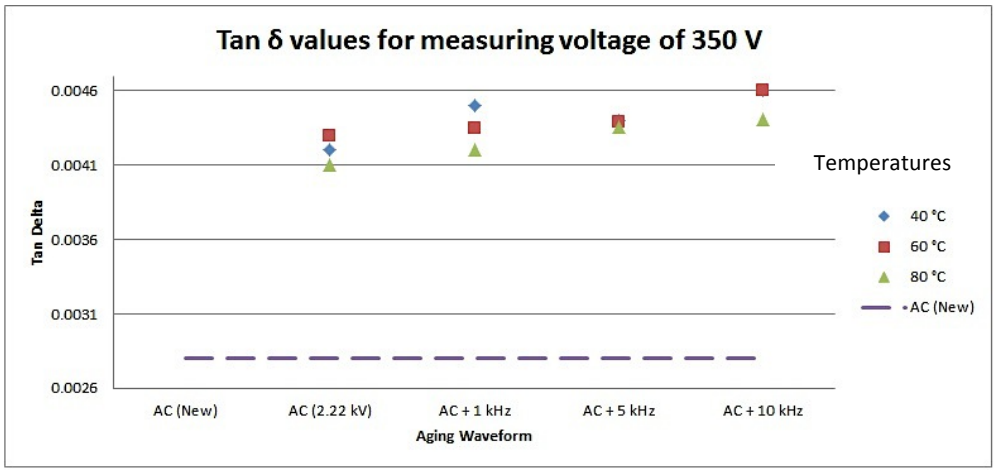


Fig. 5.15 – Tan (δ) values at 350 V measuring voltage for differently aged samples for 22 h

Chapter 6
The Aging Model for Paper-oil Insulation Considering Repetitive Transients

In the previous chapters, the aging effect of repetitive transients on paper-oil insulation has been studied. It was concluded that relatively high frequencies of repetitive transients and elevated operating temperatures decrease the lifetime of these samples. In Chapter 2, the necessity of an aging model was discussed to predict the remaining life of HV insulation, however, this can only be relevant if the aging parameters and their causes are taken into account. For example, the influence of repetitive transients is usually not considered when calculating the aging rate. Such extended models are necessary to a smart grid environment in order to maintain a reliable electricity network.

By performing Weibull statistical analysis of the times to breakdown of samples, a model will be created relating the time to failure with the carrier voltage and the applied repetition frequency of transients. Literature positions [66-71] are taken into consideration when designing the life consumption (LC) model. The final outcome allows for indicative lifetime consumption when compared to a sample not subjected to repetitive transients.

6.1.1. Dependency of Time to Breakdown on AC Voltage and Repetition Frequency of Transients

Repetitive transients are expected to be present in the future's electric grid, reducing the lifetime of devices such as transformer insulation, as discussed in Chapter 2. To understand the degree of life reduction, the influence of repetitive transient needs to be quantified into an aging model so that the consumers can rely on a steady and strong transmission and distribution network.

In Chapter 4, a waveform was designed to investigate the aging of paper-oil insulation by varying the repetition frequency between 1 kHz and 10 kHz. Based on the time to breakdown data, it was observed that the aging coefficient varied from 5 and 17 respectively to the mentioned frequencies at a carrier magnitude of 2.91

kV. On the other hand, at a carrier magnitude of 2.22 kV, the aging coefficient changed from 3 to 9 respectively for the same repetition frequency range of transients.

Despite the fact that only 2 test voltages have been investigated, the trending of the time to breakdown as a function of carrier voltage (Fig. 6.1) and repetition frequency (Fig. 6.2) is plotted for illustration. The magnitude of the carrier waveform with the appropriate frequency of the transients is plotted and a power law trend line has been plotted between the data points.

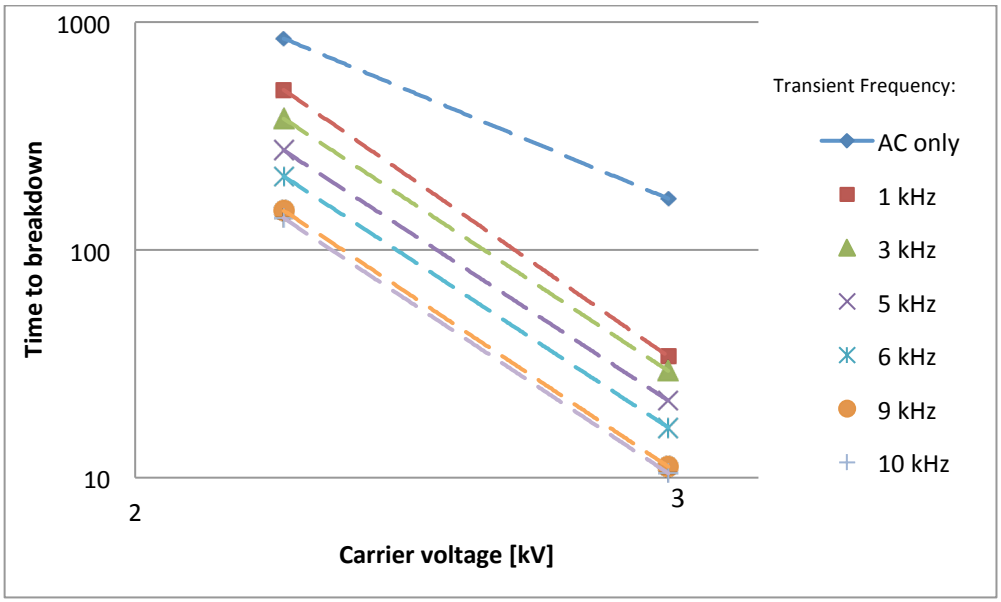


Fig. 6.1 – The effect on the time to breakdown as a function of carrier voltage magnitude. Data based on Fig. 4.19 and Fig. 4.20 where confidence bounds are indicated and Chapter 3.3.3

The inverse power law is commonly applied to the breakdown of dielectrics under an electric stress and is characterised by:

$$\tau = aV^{-k} \tag{1}$$

Where a and k are constants. τ is the time to breakdown and V is the applied voltage in kV. This relationship has been applied to the data points and the values for the " a " and " k " parameter are presented in Table 6.1.

Table 6.1 – Trend-line parameters based on the repetition frequency.

Repetition Frequency	"a" parameter [E+06]	"k" parameter
AC only, no transients	1.01	5.99
1 kHz	1.00	9.96
3 kHz	0.71	9.43
5 kHz	0.46	9.35
6 kHz	0.38	9.39
9 kHz	0.31	9.57
10 kHz	0.28	9.53

The breakdown values without transients were also plotted on the graph. As it can be seen, the exponent of this equation is different. This could indicate that additional aging mechanisms are acting on the paper samples when repetitive transients are added. The exponent of the equations is not changing with the change in frequency, suggesting that the "*k*" parameter is independent of frequency.

The constant *"a"* could be considered linked to the repetition frequency as it decreases with the application of higher repetition frequencies. The value of "a" is similar for 1 kHz and when no transients are applied. This could be coincidental and unrelated as the times to breakdown were not investigated at low magnitudes of the carrier voltage.

In Fig. 6.2, the time to breakdown has been plotted as a function of repetition frequency. The exponential relationship was applied in this case, identified as:

$$\tau = ae^{-bf} \tag{2}$$

where a and b, are constants, τ is the time to breakdown and f is the repetition frequency of transients. Additionally, the correlation coefficient (CC) is shown.

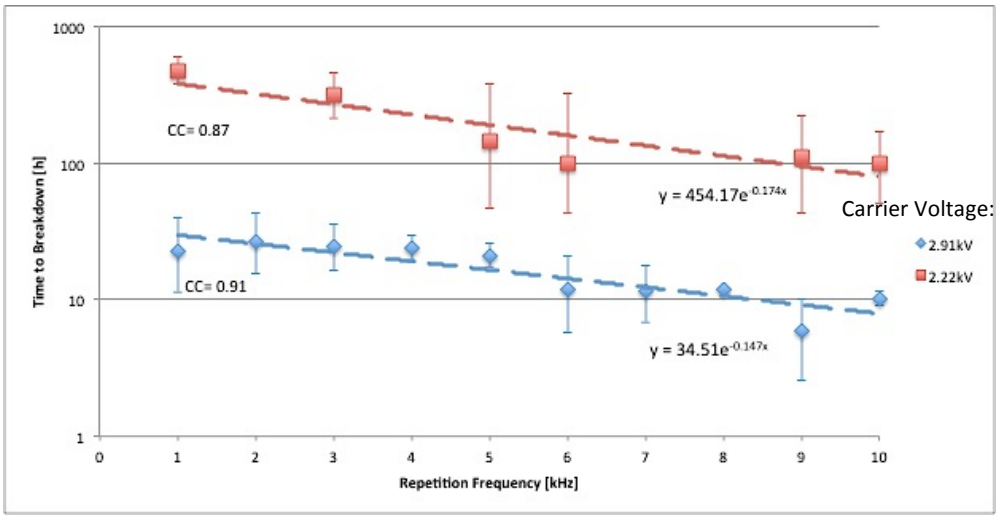


Fig. 6.2 - The effect on the time to breakdown as a function of repetition frequency of transients. The values for the time to breakdown are the geometric mean with the corresponding upper and lower 90% confidence bounds

The gradient of the two lines is similar, i.e. "*b*" is comparable, suggesting that the same aging mechanism takes place when repetitive transients are applied regardless of the carrier wave magnitude. The "*a*" parameter on the other hand is different and probably influenced by the magnitude of the carrier waveform. The correlation coefficients are 0.91 and 0.87 for 2.91 kV and 2.22 kV respectively. For the 2.22 kV carrier waveform, the stress applied on the samples is less than in the case of 2.91 kV, hence the weakest spots are less prone to breakdown, resulting in a wider spread of breakdown data. This results in a lower correlation coefficient.

6.1.2. The Fluctuation Model

Cellulose paper is a polymer consisting of structural elements such as atoms, ions and molecules termed clusters. These clusters are connected together and are susceptible to fluctuations from site to site, whilst maintaining the total free energy at a constant value in the material, when an electric field is applied. These variations redistribute the local mechanical strains and dipole orientations influencing the relaxation currents involved in dielectric linear response theory. The degree of connection between the motions of these clusters can be determined by observing the response of the material to high frequencies, identified as an index *m*. This index measures the extent of the distribution of

strain within the material. When *m* tends towards unity, a polymer is considered un-aged. When it goes towards zero, it is aged [78].

Dielectric spectroscopy was described in Chapter 4 but the loss components, ε", and real component, ε', were not investigated in detail. In Fig. 6.3 and Fig. 6.4 the dielectric response of the paper can be observed after it has been aged with different transient frequencies at a carrier waveform of 2.22 kV for 20 hours.

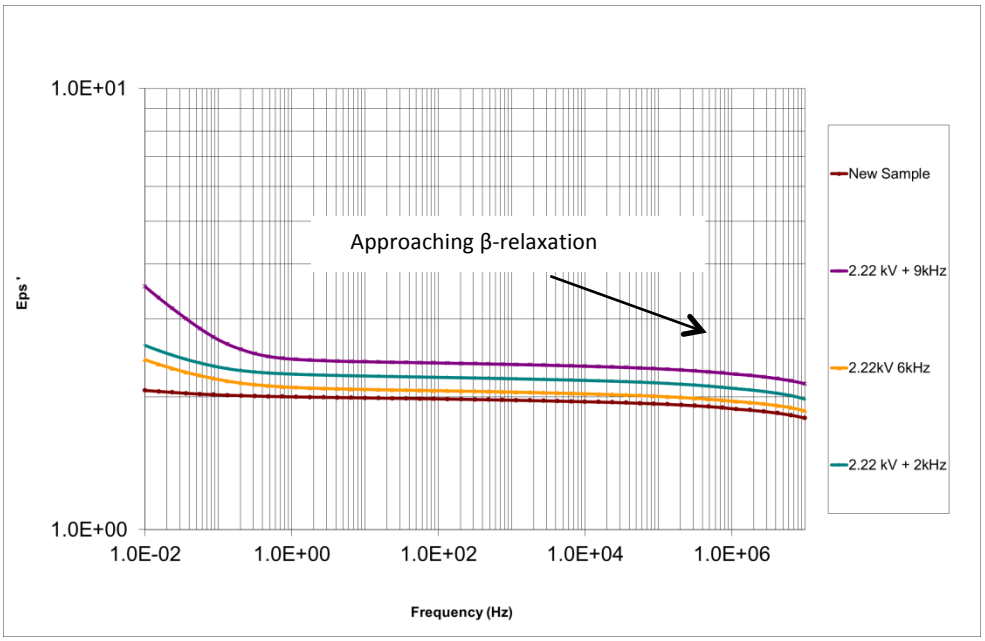


Fig. 6.3 – The real component of the complex permittivity as a function of measurement frequency after exposure for 20 h with a carrier voltage of 2.22 kV and repetition frequency of transients as indicated

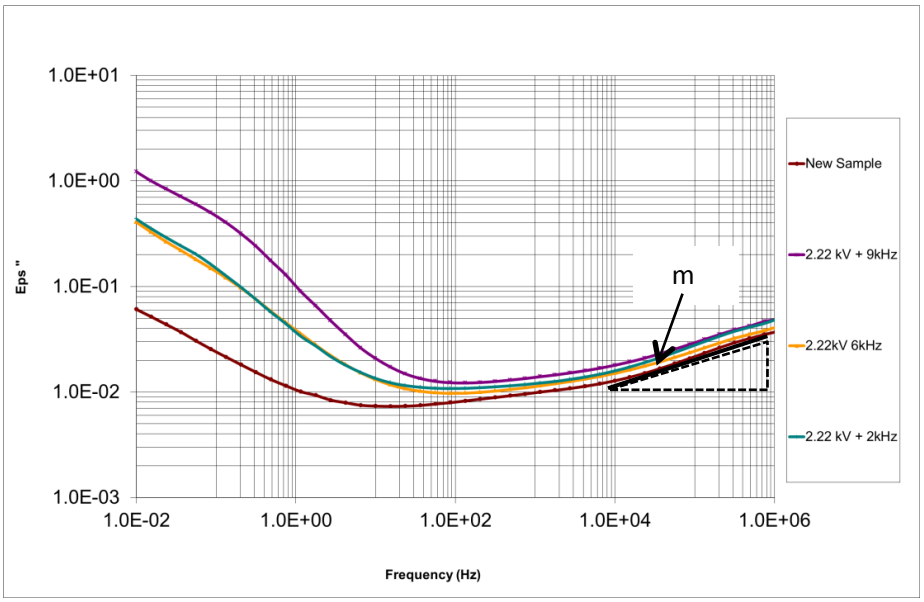


Fig. 6.4 – The imaginary component of the complex permittivity as a function of measurement frequency after exposure for 20 h with a carrier voltage of 2.22 kV and repetition frequency of transients as indicated

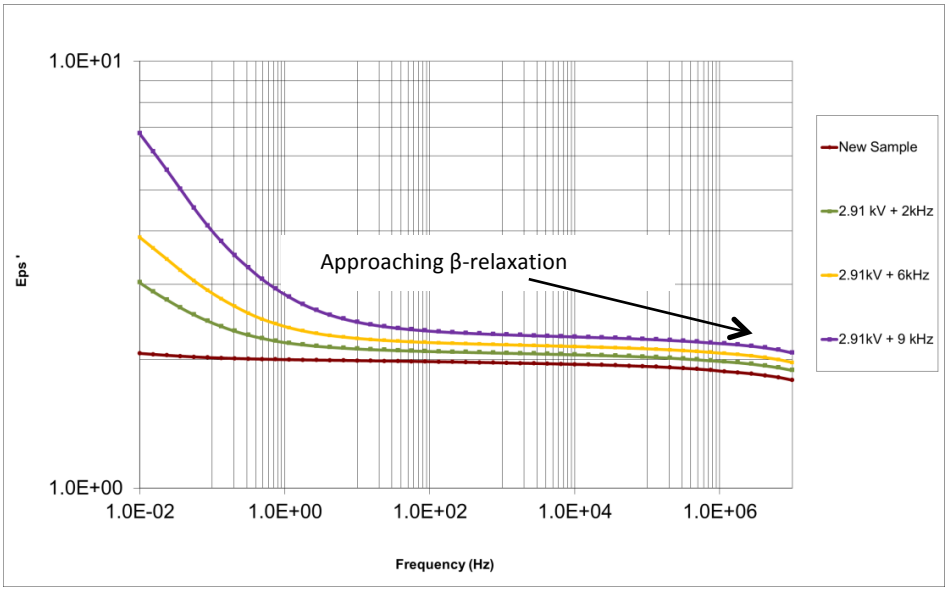


Fig. 6.5 – The real component of the complex permittivity as a function of measurement frequency after exposure for 20 h with a carrier voltage of 2.91 kV and repetition frequency of transients as indicated

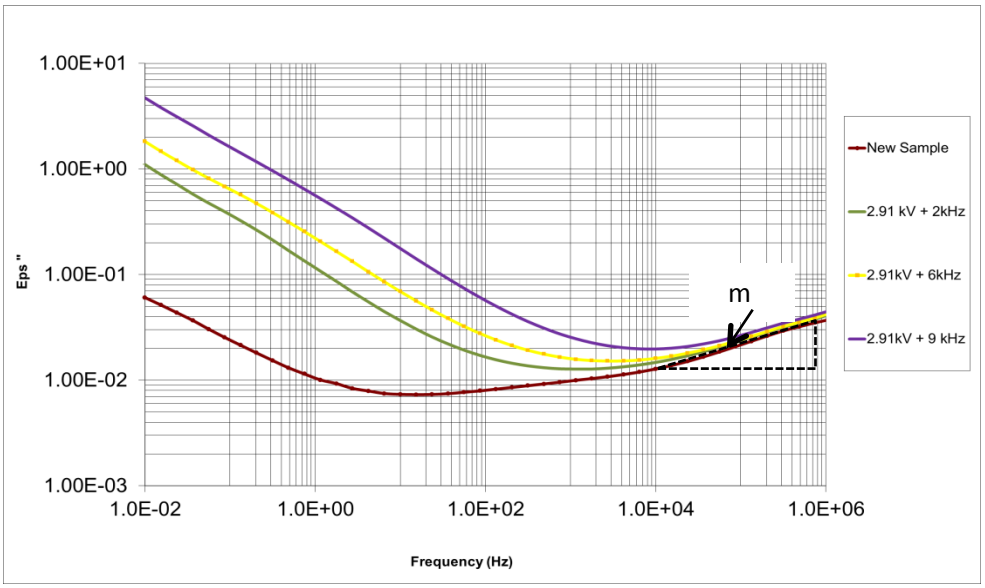


Fig. 6.6 – The imaginary component of the complex permittivity as a function of measurement frequency after exposure for 20 h with a carrier voltage of 2.91 kV and repetition frequency of transients as indicated

On a later stage, the same aging process was performed on the paper samples but the carrier waveform was increased to 2.91 kV. The results are shown in Fig. 6.5 and Fig. 6.6.

The coefficient *m* can be measured by calculating the slope of the ε" curve on the left hand side of the β-relaxation peak [78]. This peak is not visible in Fig. 6.4 and Fig. 6.6 but is considered approaching. This assumption is based on the polarisation spectrum of materials and on measurements performed on oil samples [77, 79]. From Fig. 6.3 and Fig. 6.5, the value of ε' is seen decreasing more prominently after 10^6 Hz, often an indication of approaching β-relaxation peak, see Appendix A.

A homogeneous breakdown can be assumed when the material breaks down above a certain voltage level. It was observed in Chapter 3, that the breakdown voltage of the samples was 3.2 kV. Fothergill [78] stated that the *m* coefficient is inversely proportional to the Weibull shape-parameter β in such conditions. If water trees are the source of the breakdown, β=1/m+2/3.

The results for the *m* coefficient are presented in Table 6.2. The expected corresponding β values have been added to Table 6.2

Table 6.2 – m and β coefficient calculated for various aging waveforms and transient repetition frequencies. The error in the measuring equipment was identified at 8% due to the spread in thickness of the sample.

Transient Frequency	2.91 kV			2.22 kV		
	m	β =1/*m*	β =1/*m+2/3*	*m*	β =1/*m*	β =1/*m+2/3*
9 kHz	0.18	5.62	6.28	0.21	4.76	5.43
6 kHz	0.21	4.76	5.43	0.22	4.54	5.21
2 kHz	0.22	4.54	5.21	0.24	4.17	4.83
New	0.23	4.35	5.01	0.23	4.35	5.01

From table 6.2, it can be seen that the *m* coefficient decreased when the aging due to the repetition frequency of transients was increased and a higher magnitude carrier waveform was applied. The influence of the possible error due to thickness is negligible as the average value was used. This trend indicates degradation of the polymer, as the connection between the dipole clusters is poorer than when un-aged.

Higher β values indicate that the breakdown of the polymer would be less scattered in time, hence stronger aging. In order to verify this, and to see if the values of the shape parameters match, a Weibull analysis has been performed.

6.1.3. Weibull Unreliability Plots

The statistical analysis with Weibull distribution plots can help to understand the aging processes even of a limited sample population. Additionally, it also helps to validate the fluctuation model presented preciously.

Appendix B presents the derivation of the Weibull statistical approach in locating the weakest link in a material. The probability, in this case of the time to breakdown, can be represented as:

$$F(t) = 1 - exp\left\{-\left(\frac{t}{t_0}\right)^{\beta}\right\} \quad (3)$$

Where: t_0, is the time when 63.2 % of the samples fail, also known as the scale parameter η.

The parameters β and t_0 are the shape and scale parameters of time to breakdown, respectively.

To this equation it is possible to add more variables, which were analysed, in this case the repetition frequency of the transients, f_{tr}, and the applied carrier voltage. It can be written as:

$$F(t, f_{tr}, V) = 1 - exp\left\{-\left(\frac{t}{t_0}\right)^{\beta} \cdot \left(\frac{f_{tr}}{f_{tr0}}\right)^{\alpha} \cdot \left(\frac{V}{V_0}\right)^{z}\right\} \quad (4)$$

The variables, β, α and z are the shape parameters of the individual variables. In this case, it is not postulated how repetitive transients influence paper-oil insulation. Therefore, the f_{tr} component will be replaced by a function A, obtaining:

$$F(t, f_{tr}, V) = 1 - exp\left\{-\left(\frac{t}{t_0}\right)^{\beta} \cdot \left(\frac{V}{V_0}\right)^{z} \cdot A(f_{tr})\right\} \quad (5)$$

The Maximum Likelihood Estimation model (MLE) was selected for the analysis of time to breakdown data. This method was applied to the data taking into account the un-biasing method [58]. These points, such as early failure have therefore lower impact on the shape of the fit than the points closer to the 63.2% value of time to breakdown. The paper is very thin and even small variations in thickness can have a large effect on the time to breakdown. The dependency of the time to breakdown was observed to be related to the carrier voltage and the repetition frequency of transients. This relationship can be re-written from Eq. 5 as:

$$\eta = V^{-\frac{z}{\beta}} A^{\frac{-1}{\beta}}(f_{tr}) \quad (6)$$

Where η is the time to breakdown for 63.2% of the samples. The results of the analyses of times to breakdown, for each carrier voltage and transient repetition frequency, are presented in Table 6.3. The top confidence bounds (TCB) and bottom confidence bounds (BCB) for 90% are also indicated for the η values.

Table 6.3 – β and η parameters for a two-parameter Weibull analysis of breakdown times at different voltages of carrier and transient repetition frequencies.

Repetition Frequency of transients	Weibull parameters for a Carrier Waveform with superimposed transient frequency							
	2.91 kV				2.22 kV			
	β [per unit]	η [h]	TCB [h]	BCB [h]	β [per unit]	η [h]	TCB [h]	BCB [h]
1 kHz	0.98	33.86	51.2	22.31	2.51	551	686	466
2 kHz	1.46	35.15	53.1	25.7	-	-		
3 kHz	1.68	32.32	44.6	25	1.47	410	556	312
4 kHz	3.14	27.54	34.1	23.3	-	-		
5 kHz	4.44	23.41	28.5	20.26	0.80	248	504	141
6 kHz	1.24	17.62	27.5	12.3	0.68	171	415	86
7 kHz	1.49	15.09	22.2	11.1	-	-		
8 kHz	8.69	12.35	12.9	11.8	-	-		
9 kHz	2.12	14.54	19.3	11.7	1.17	155	282	101
10 kHz	4.47	11.13	12.7	10.1	1.04	140	215	97

The following observations can be made based on Table 6.3:

- The η values are decreasing with the increase of the frequency;
- The β values are, on average, higher for 2.91 kV than for 2.22 kV;
- No correlation can be extracted between β and repetition frequency.

The analysis is graphically represented in Fig. 6.7 – 6.9. The same repetition frequency value is shown in each figure. 90% confidence bounds are indicated on each plot.

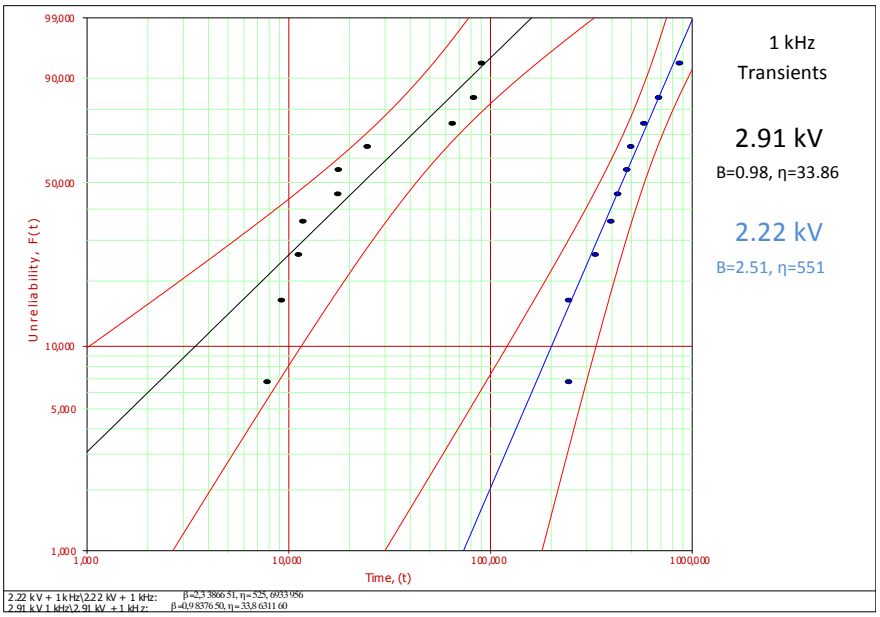


Fig. 6.7 – Weibull unreliability plot for the frequency of 1 kHz

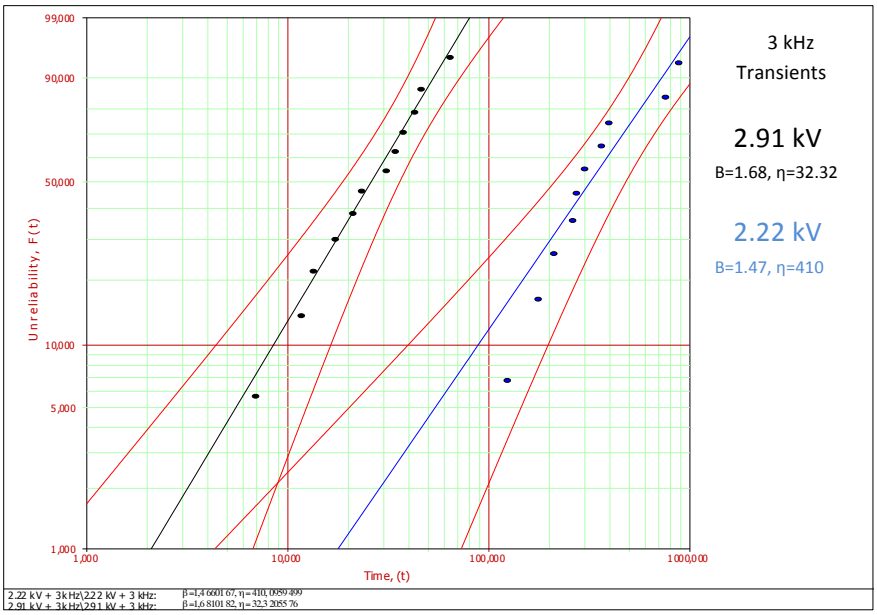


Fig. 6.8 – Weibull unreliability plot for the frequency of 3 kHz

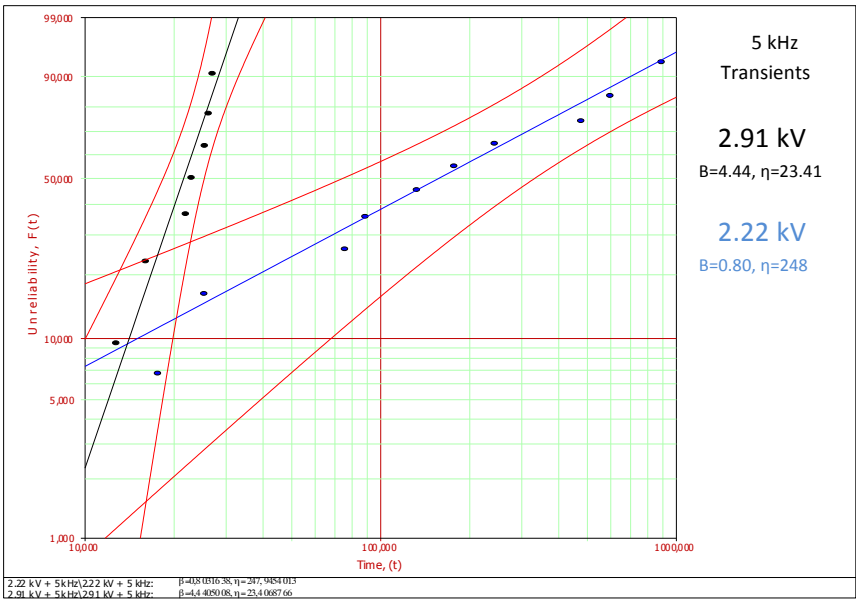


Fig. 6.9 – Weibull unreliability plot for the frequency of 5 kHz

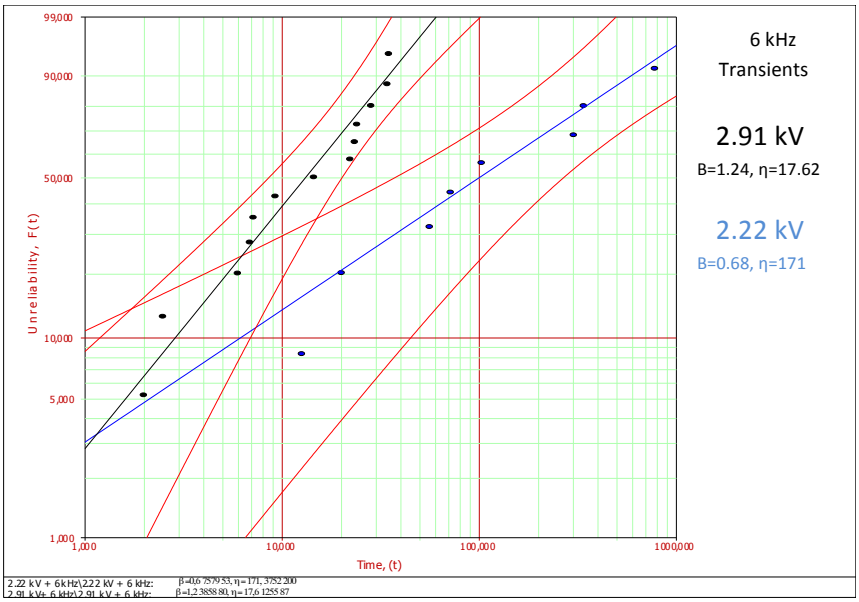


Fig. 6.10 – Weibull unreliability plot for the frequency of 6 kHz

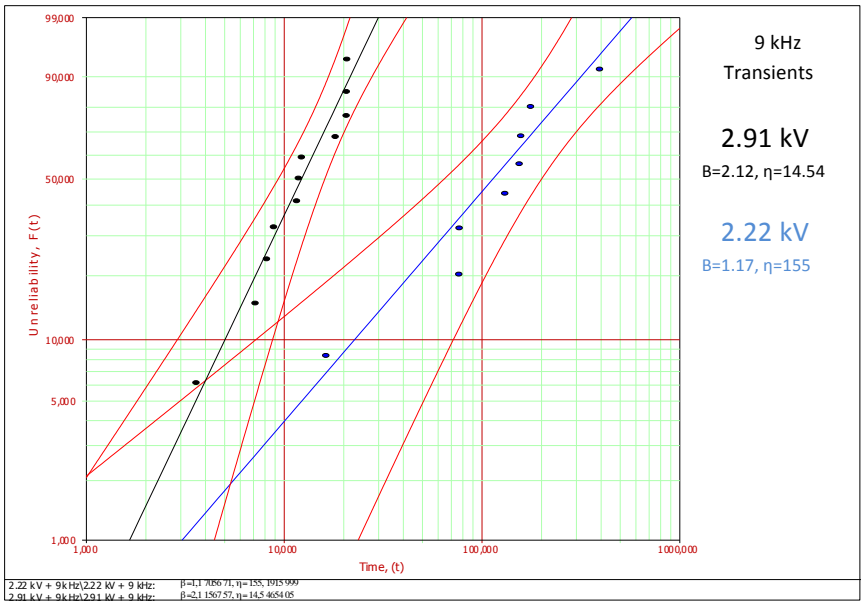


Fig. 6.11 – Weibull unreliability plot for the frequency of 9 kHz

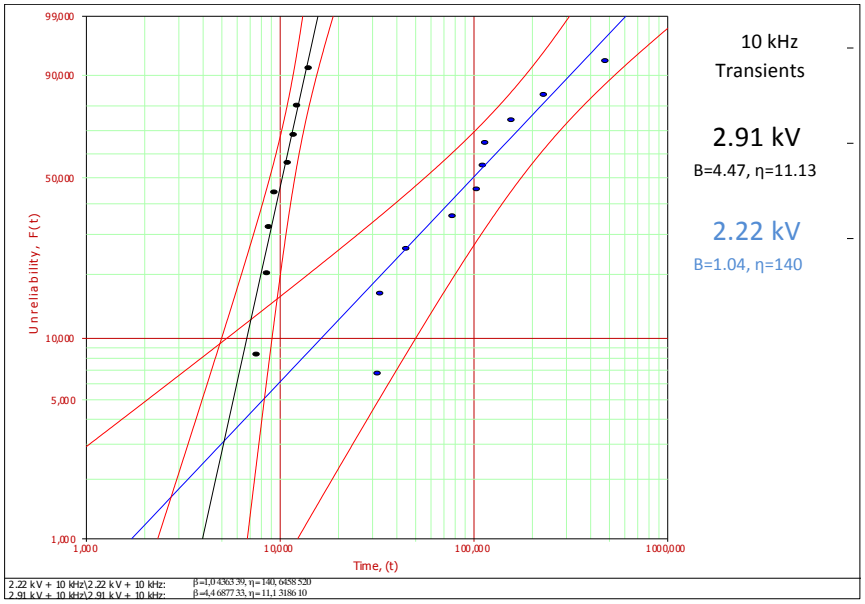


Fig. 6.12 – Weibull unreliability plot for the frequency of 10 kHz

The dependency on frequency to time can be plotted considering the η values obtained. The results are shown in Fig. 6.13 with an exponential relationship fitted through them. 90% confidence bounds are indicated.

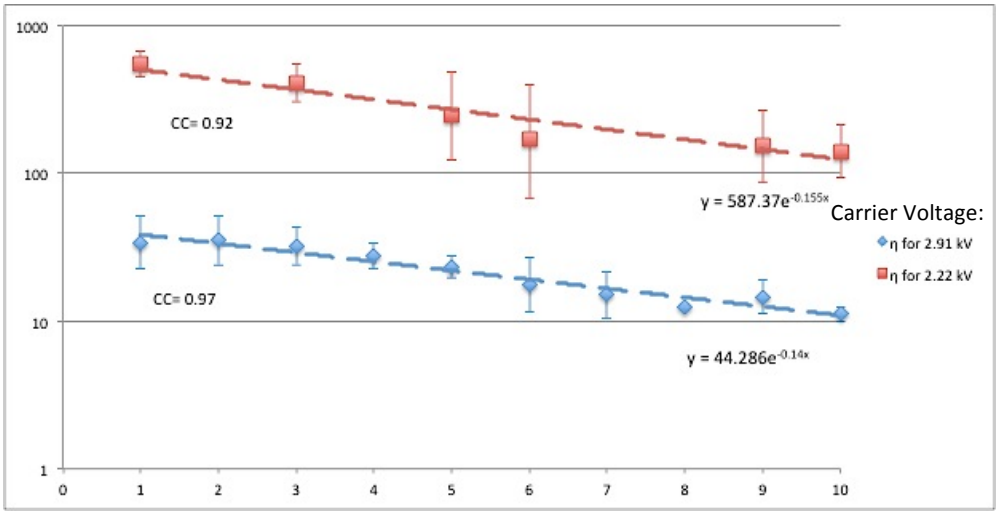


Fig. 6.13 – The effect of time to breakdown as a function of transient repetition frequency with 90% confidence bounds

In the figure above and Fig. 6.2, the following changes can be noticed:

- The exponent, i.e. the slope, for 2.91 kV has decreased from 0.147 to 0.14 and for 2.22 kV it has decreased from 0.174 to 0.155 after performing the Weibull analysis;
- The "*a*" parameter remained of the same order of magnitude;
- For both carrier voltages, the correlation coefficient has increased from 0.87 to 0.92 and 0.91 to 0.97 for 2.22 kV and 2.91 kV respectively.

In Fig. 6.14, the value of β is plotted as a function of repetition frequency for the two carrier waves. No clear trend could be extrapolated from this figure other than on average the β parameter is bigger for 2.91 kV. This could be reasonable as the aging effects of the waveform are higher at this voltage level, thus increasing the value for β.

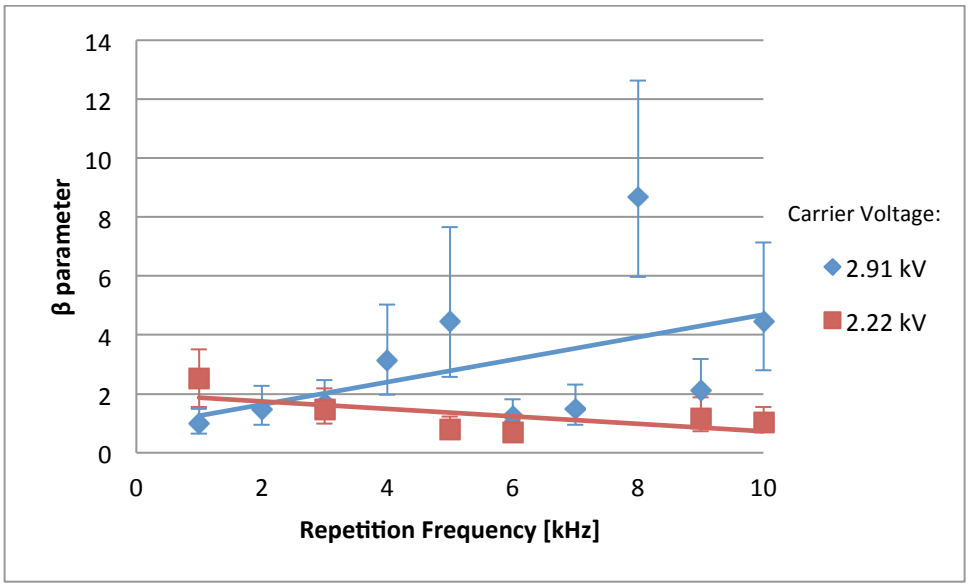


Fig. 6.14 – β parameter as a function of frequency based on a two parameter Weibull analysis with 90% confidence bounds

Various approaches were performed to extrapolate any data from Fig. 6.14. A 3-parameter Weibull showed the best improvement. The β parameter becomes unvarying for each carrier voltages, whilst its magnitude is higher for 2.91 kV. The effect on the shape parameter is shown in appendix C. This however affected the scale parameter considerably, so no clear improvements to the data were observed.

In Table 6.3, expected β values were identified from observing the degree of connection between the clusters in the material. Values between 4 and 6 were expected. The values obtained are more scattered (1-8) but can be considered of the same order of magnitude.

6.1.4. Discussion

Two factors of aging were investigated, the magnitude of the carrier voltage (V_{ac}) and the repetition frequency of added transients (f_{tr}). Plotting a V_{ac}-τ relationship, the inverse power law was identified as the most suitable. In the case of repetitive transients an exponential model seemed to be the most appropriate for the f_{tr}-τ relationship. Repetitive transients can generate local PDs and dissipate energy into the paper creating free electrons and leading to breakdown.

Fig. 6.1 showed that the slope of the lines remained almost unchanged when plotting the times to breakdown as a function of V_{ac} for the waveforms with transients. In Fig. 6.2, the slope of the lines almost didn't change as well when plotting the time to breakdown as a function of transient frequency. From these observations, it was concluded that both the AC magnitude and the transient repetition frequency have two distinct influences on the time to breakdown of the paper samples.

A Weibull analysis was performed to refine the analysis of the breakdown time data and to verify the applicability of the fluctuation model. No conclusions could be drawn from analysing the shape parameter β. The η parameter, on the other hand, was noticed to depend on the carrier voltage and repetition frequency of transients. Plotting the 63.2% breakdown time values improved the correlation coefficient of the plots.

The fluctuations model was applied to samples stressed for 20 h in different AC magnitudes and transient frequencies. Expected values for β were obtained based on these measurements in the range between 4 and 6. When analysing the times to breakdown of the samples with Weibull, it was observed that the β parameters were of the same order of magnitude as those calculated from the dielectric spectroscopy. However, exact values were not expected, as 20 h of aging is only a small fraction of the time it takes to breakdown a sample with those voltage levels.

The exponential model has been selected as the most appropriate model. However, since PDs are likely present during the application of repetitive transients, some heat dissipation could also occur. For this reason, the following section will focus on selecting the most appropriate model for representing the aging by repetitive transients.

6.2. Selecting the Appropriate Model

Three models are investigated in this section to model the time to breakdown data of the paper-oil samples. The investigated relationships are: inverse power law, Eyring relationship and the exponential relationship.

The relationship between the applied voltage magnitude and time is usually represented by the power law. As the carrier magnitude has a substantial influence on the time to breakdown, this law could be applicable. The **inverse power law** is represented by:

$$t = Cf^{-x} \tag{7}$$

Where *t* is the lifetime, *f* is the frequency of repetitive transients, *C* is parameters dependant on the experimental conditions and *x* is a characteristic of the material such as thickness of sample.

Another possible fit could be the Eyring relationship. In Chapter 4.1 it was shown that PDIV decreases as faster repetition frequencies are applied. PDs dissipate locally heat (thermal energy) in the void in which they occur, suggesting that locally temperature could have influenced the breakdown. For this reason, an **Eyring model** could be used as an alternative model:

$$t = \frac{C}{f} e^{\left(\frac{B}{f}\right)} \tag{8}$$

Where *t* is the lifetime, *f* is the repetition frequency and *C* and *B* are parameter based on the experimental data and are in function of temperature. The variation in temperature in the samples is not known in this model, it is only assumed to be present constantly the moment repetitive transients are applied.

In Chapter 6.1, an exponential model was assumed to fit best when modelling transients. The **exponential model** can be written as:

$$t = Ce^{Bf} \tag{9}$$

Where *t* is the lifetime, *f* is the repetition frequency, *C* and *B* are test results parameters to be determined.

6.2.1. Probability Lifetime Models

As discussed earlier in the chapter, Weibull analysis can be helpful to refine the data in order to find the most probable "weakest link". The Weibull function could be rewritten as [60]:

$$f(t) = \frac{\beta}{\eta}\left(\frac{t}{\eta}\right)^{\beta-1} exp\left(-\left(\frac{t}{\eta}\right)^{\beta}\right) \tag{10}$$

Where *t* is the time to breakdown, η is scale parameter and β is the shape parameter. From these values the mean time to failure (MTTF) can be calculated as:

$$MTTF = \eta \cdot \Gamma\left(\frac{1}{\beta} + 1\right) = \eta \cdot \int_0^{\infty} e^{-y} y^{\frac{1}{\beta}} dy \tag{11}$$

From the data obtained earlier, it was noticed that the shape parameter β is not related to transient frequency. This consents for the following three assumptions:

1) The lifetime data at any single voltage level satisfies a 2-parameter Weibull distribution;
2) The Weibull shape parameter, β, is a random variable independent of the frequency;
3) The MTTF obeys the selected model used for fitting.

From these assumptions we can substitute Eq. 11 into Eq. 10 and add a new parameter $K = C/\Gamma\left(1+\frac{1}{\beta}\right)$, giving:

$$\eta(V) = \frac{K}{f^x} \tag{12}$$

This allows for η to be substituted into each of the models giving:

A. By substituting η from Eq. 12 into Eq. 10, the Inverse Power Weibull model can be derived as:

$$f(t,f) = \frac{\beta f^x}{K}\left(\frac{f^x t}{K}\right)^{\beta-1} e^{-\left\{\frac{f^x t}{K}\right\}^{\beta}} \tag{13}$$

Where β, *K* and *x* need to be estimated.

B. Using the same substitution method, the Eyring-Weibull model for the probability density function is derived as:

$$f\left(t,f\right) = \frac{\beta\cdot f}{K}\cdot e^{\left(\frac{B}{f}\right)}\cdot\left(\frac{t\cdot f}{K}\cdot e^{\left(\frac{B}{f}\right)}\right)^{\beta-1}\cdot e^{-\left(\frac{t\cdot f}{K}\cdot e^{\left(\frac{B}{f}\right)}\right)^{\beta}} \tag{14}$$

Where β, *K* and *B* need to be defined.

C. Lastly the Exponential Weibull model for the probability density function is defined as:

$$f\left(t,f\right) = \frac{\beta}{Ke^{Bf}}\cdot\left(\frac{t}{Ke^{Bf}}\right)^{\beta-1}\cdot e^{-\left(\frac{t}{Ke^{Bf}}\right)^{\beta}} \tag{15}$$

Where, also in this case, β, *B* and *K* need to be defined.

The parameters that need to be estimated, are calculated based on the maximum likelihood estimation (MLE) model approach defined as:

$$\Lambda = \sum_{i=1}^{N} \ln\left[f\left(t_i, f_i\right)\right] \tag{16}$$

Where (t_i, f_i), i = 1, … , N are the i^{th} time to failure data point t_i aging with repetition frequency f_i, and $f(t, f)$ is the failure probability density function depending on the used model.

6.2.2. Results

The results shown in Table 6.4 represent the results obtained when deriving the unknown constants in equations 7 – 9. The results are divided into to the carrier voltages utilised in the experiments.

Table 6.4 – Parameter estimation and model based on the repetition frequency of transients. The unit of frequency is kHz

	2.91 kV AC	**2.22 kV AC**
A. Inverse power model		
x	0.9589	0.9806
K	107.5	1250
β	2.397	1.057
C	95.32	1223
MTTF	$95.32 \cdot f^{0.9589}$	$1223 \cdot f^{0.9806}$
B. Eyring model		
B	-1.044	-1.225
K	133.5	1769
β	2.011	1.248
C	118.3	1648
MTTF	$\frac{118.3}{f} \cdot \exp\left(-\frac{1.044}{f}\right)$	$\frac{1648}{f} \cdot \exp\left(-\frac{1.225}{f}\right)$
C. Exponential model		
B	-0.1607	-0.1414
K	52.45	596.7
β	2.012	1.255
C	46.48	555.3
MTTF	$46.48 \cdot \exp(-0.1607 \cdot f)$	$555.3 \cdot \exp(-0.1414 \cdot f)$

The value of "*x*" for the inverse power law model is very close to unity (one). This suggests that the insulation material, in this case paper-oil, will break after a certain amount of pulses, as discussed in Chapter 4.5.

The data from Table 6.4 has been plotted in Fig. 6.15 and Fig. 6.16. A representation is shown for each model relationship at each voltage level of the carrier AC waveform.

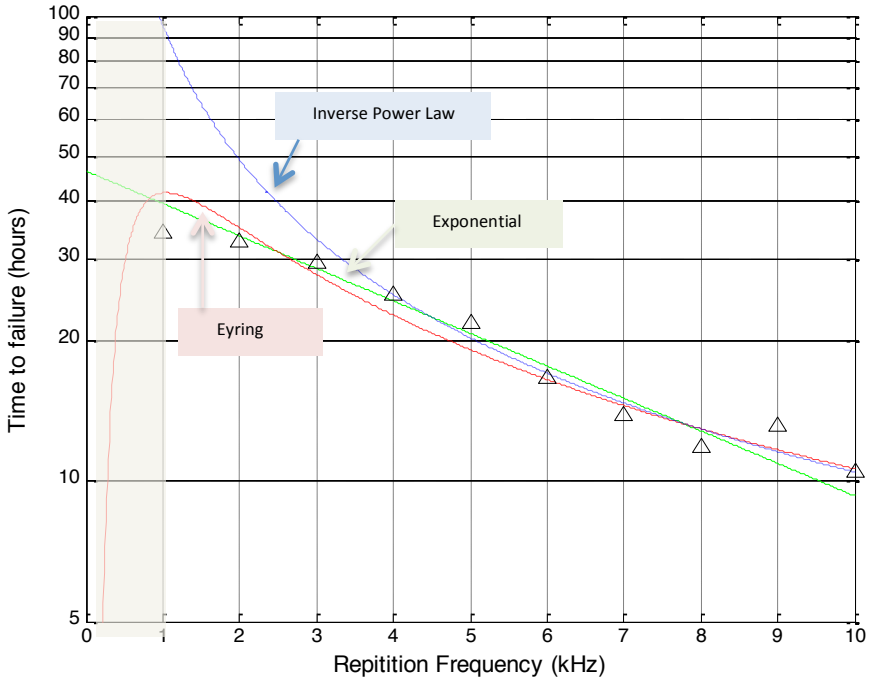


Fig. 6.15 – Modelling transients superimposed on a 2.91 kV sinusoidal waveform. The blue dotted line represents inverse power law, green straight line represents the exponential relationship and the red dashed line represents the Eyring model. The mean values are represented by the triangle

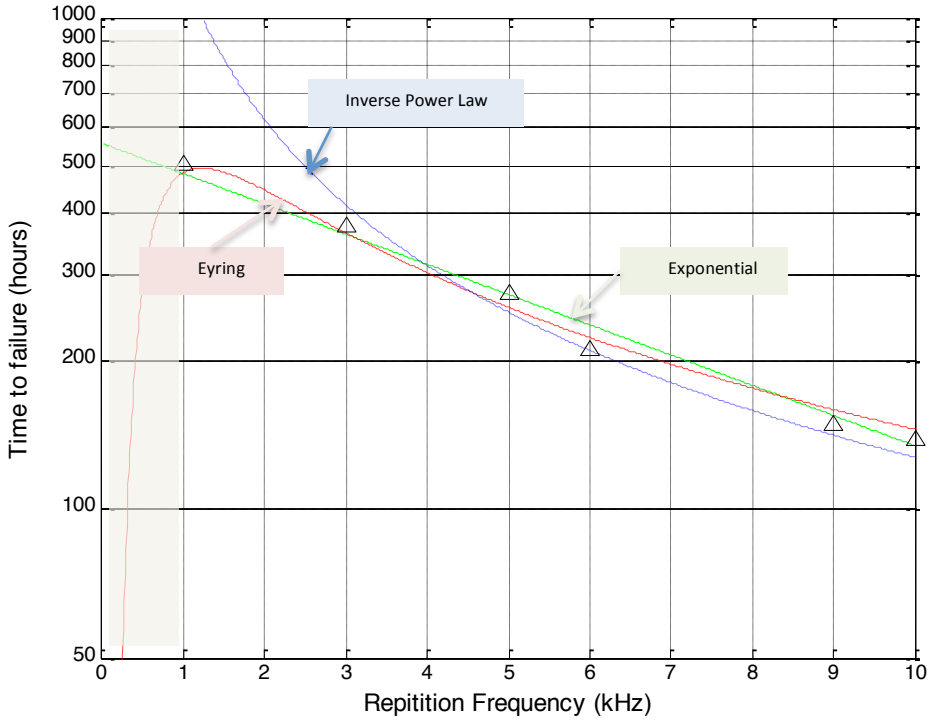


Fig. 6.16 – Modelling transients superimposed on a 2.22 kV sinusoidal waveform. The blue dotted line represents inverse power law, green straight line represents the exponential relationship and the red dashed line represents the Eyring model. The mean values are represented by the triangle

From the figures above, it can be seen that the three investigated models fit the gathered data well in the investigated range of frequencies. At the lower left end of the frequency range, the time to breakdown does not behave as expected for the Eyring and inverse power law models. The exponential model seems to offer the best fit throughout the frequency range, a straight line as identified before.

Plotting Fig 6.15 and Fig. 6.16 on a single graph, the effect of the AC voltage can be investigated. The results are shown in Fig. 6.17 where the time to failure is plotted as a function of repetition frequency between 1 kHz and 10 kHz.

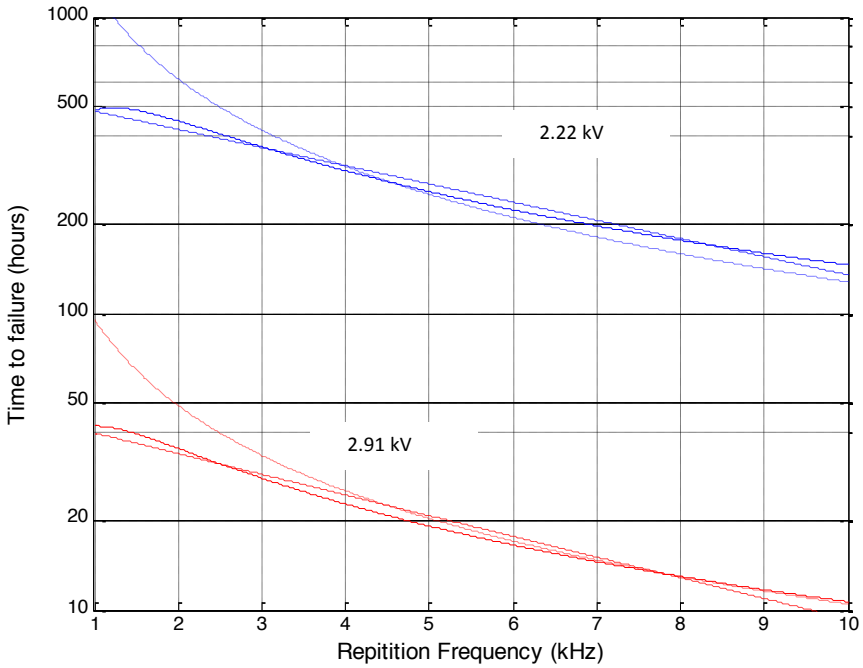


Fig. 6.17 – Comparison of the three investigated models. Time to failure is plotted as a function of repetition frequency

The three model plots for a carrier wave of 2.91 kV and 2.22 kV seem to be parallel to each other. This suggests that a certain slope in the exponential model can be expected when repetitive transients are applied. Just as in Chapter 6.2, minor variations in the slope are noticed.

6.2.3. The Transient Aging Model

It was found in this chapter that the power law is the most suitable model to represent the time to breakdown for paper-oil insulation when stressed electrically under an AC waveform. When transients are added, the exponential model was found to be more appropriate. When observing the exponential model ($\tau = ae^{-bf}$) it was concluded that the parameter a was influenced dominantly by the magnitude of the AC wave and b was influenced dominantly by the repetitive transients.

The parameter a can be represented as a power law since it is governed by the magnitude of the AC wave with an exponent of 9.57 ± 0.23 to represent the influence of repetitive transient, as shown by Table 6.1. The error is given by the standard deviation from the k parameter in Table 6.1. This gives a as:

$$a = V^{-9.565} \tag{17}$$

Where, *V* is the magnitude of the carrier waveform in kV.

The parameter b on the other hand is taken to be the slope of the exponential model, i.e. 0.15 ± 0.1. Substituting the parameter *a* into the exponential model and setting *b* to 0.15 the following equation can be obtained for the time to breakdown:

$$t_{bd} = 10^6 \cdot V^{-9.565} \cdot e^{-0.15 \cdot f} \tag{18}$$

Where, t_{bd} is the time to breakdown of paper-oil insulation in hours and *f* is the frequency of repetitive transients in kHz. A value of 10^6 has been added into the equation in order to get the time automatically in hours. This is necessary because the input to the equation is in thousands of volts and thousands of hertz.

The comparison of the calculated (from equation 18) and measured data for time to breakdown is presented in Fig. 6.18. The standard deviation error bars are indicated for the measured data.

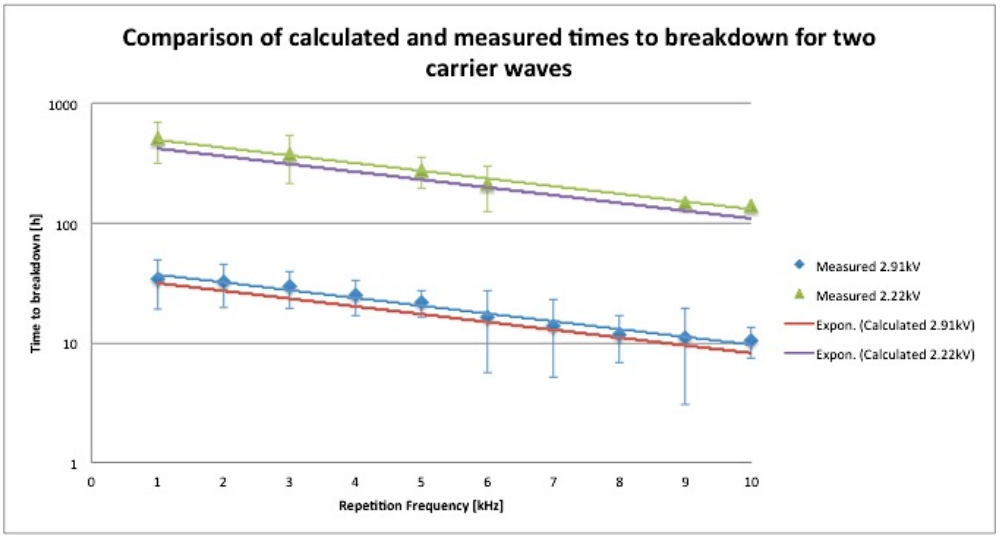


Fig. 6.18 – Comparison of measured and calculated times to breakdown as a function of transient repetition frequency superimposed on two magnitudes of carrier wave, 2.22 kV and 2.91 kV. Standard deviation is shown for the measured points

The calculated data has in general lower times to breakdown. The most likely cause is the frequent approximation of the data. Most of the calculated data points are within the error bars based on the shape parameter β.

Fig. 6.19 shows the application of the above formula, including extreme cases of repetition frequency; the data is shown in table C.4. The error bars are based on the standard deviation for each of the calculated exponents.

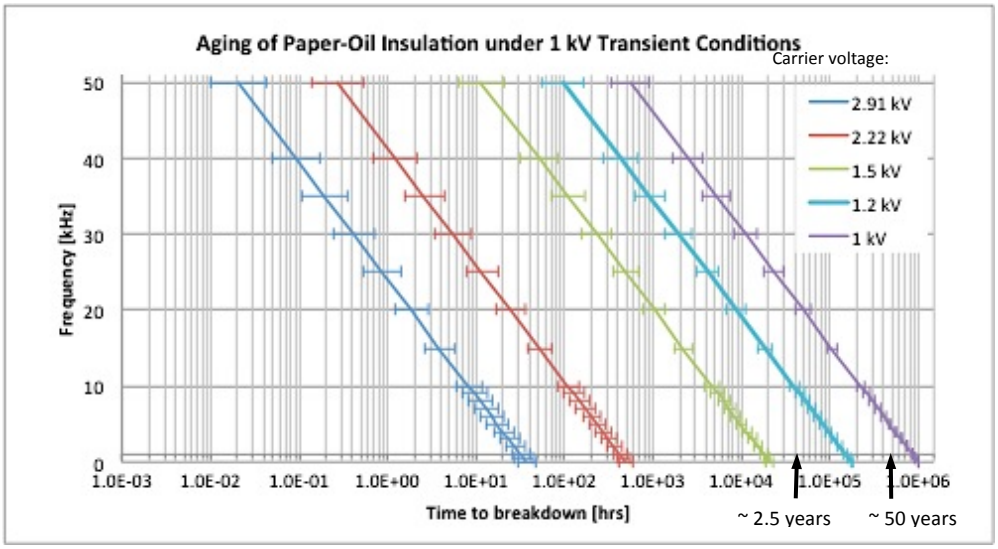


Fig. 6.19 –Equation 18 for different voltages and repetition frequencies as a function of time to breakdown. Uncertainty bars due to errors limits for the exponent within parameter a as well as for the parameter b are shown

In Fig. 6.18 it can be noticed that the application of high repetition frequencies could have a significant effect on the lifetime of insulation according to the extrapolation. In Chapter 3, it was identified that for the insulation to be functional for 50 years, a maximum voltage magnitude of 1.2 kV would need to be applied. Observing the blue line of 1.2 kV, it can be noticed that the calculated lifetime at the lowest frequency will not exceed 23 years.

The addition of transients has a significant impact on the time to breakdown. In this project, only 1 kV transients were applied with 1 μs rise time. For motor applications, the life consumption (LC) was defined as the ratio of time needed to breakdown the insulation under pulse conditions to the time needed to breakdown the insulation under normal conditions [76]. This same concept was

applied to this problem as the ratio of time to breakdown of a transient waveform of a specific frequency over the time to breakdown under pure AC conditions. This relationship is shown in Eq. 19.

$$LC = 1 - \frac{tbd_{tr}}{tbd_{AC}} \tag{19}$$

Where tbd_{tr} is the time to breakdown with superimposed transients and tbd_{AC} is the time to breakdown with AC only conditions. By using four measured frequencies, Fig. 6.20 was obtained.

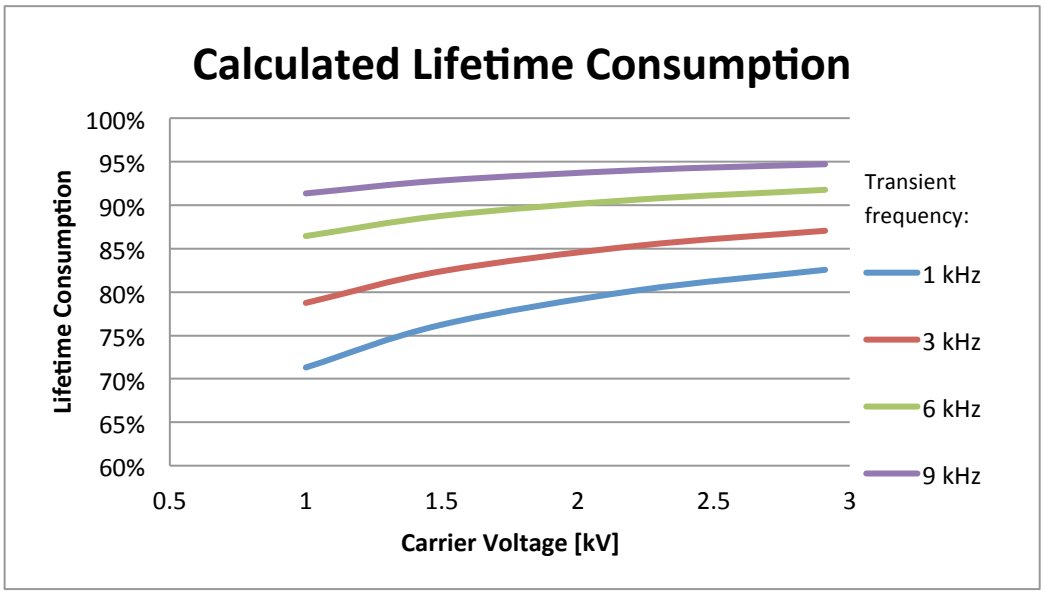


Fig. 6.20 – Life time consumption based on the ratios between transients and carrier waveform

From the figure above, the following can be extrapolated for the paper-oil samples:

- The higher the repetition frequency of transients, the more lifetime is consumed for the same carrier voltage magnitude;
- Decreasing the carrier voltage magnitude, leads to less lifetime consumption for the same repetition frequency of transients;
- At higher repetition frequencies, a smaller change in LC is noticed when decreasing the magnitude of the carrier wave. Decreasing the carrier voltage from 2.91 kV to 1 kV results in a variation of LC from 95% to 92%,

whereas performing the same change for the 1 kHz repetition frequency results in a change in LC from 83% to 72%.

6.2.4. Discussion

Eyring, inverse power law and exponential models were applied to model repetitive transients aging in terms of their repetition frequency. These three models fit well the investigated data range, 1-10 kHz; however, when extrapolating the model to higher and lower frequencies, certain weaknesses start to appear.

It was concluded that the exponential model copes best with the repetition frequency phenomenon of transients. When applying this model to the times to breakdown under transient conditions, the "b" parameter remained constant while the repetition frequency did not change.

By applying the power law to the changes due to the carrier magnitude, and the exponential model to the aging due to transients, a formula was extrapolated for the aging of paper-oil insulation under 1 kV transients, Equation 18. This formula links the magnitude of the carrier waveform with the repetition frequency of transients in order to estimate the time to failure of the insulation. Through the data gathered by applying the formula, a calculation of the consumption of lifetime was determined. Such model enables the optimal balance of transient frequencies and voltage magnitude in order to achieve longest insulation lifetimes whilst applying the required electric stresses.

6.3.Conclusion

In this chapter an attempt has been made to find the appropriate model that would calculate the time to failure of paper-oil insulation taking into account both the magnitude of the carrier voltage and the repetitive frequency of transients. The initial approach involved performing a Weibull statistical analysis on the samples' time to breakdown in order to remove any outliers that influenced the result inappropriately, such as early breakdown. The Fluctuation model was used to explain the breakdown of paper. A value for the degree of connection between the various intermolecular structural clusters was measured by dielectric spectroscopy and compared with the shape parameter in the Weibull analysis (β). A reasonable match between the expected and calculated value of β was found.

From the time to breakdown analysis, it was concluded, that the shape parameter is independent of transient frequency whereas the scale parameter (i.e. the characteristic time to breakdown) decreased with a higher application of repetition

frequency. An exponential relationship best illustrated the repetition frequency as a function of time to breakdown, whereas the inverse power law was more applicable when illustrating the magnitude of the carrier waveform as a function of time to breakdown. These two properties where combined into a life consumption model that predicted the time to breakdown of paper-oil insulation whilst exposed to a sinusoidal waveform with repetitive transients of 1 kV of frequency in the range 1 -10 kHz.

Chapter 7
Conclusions and Recommendations

7.1. Conclusions

The application of repetitive transients ages paper-oil insulation samples within the investigated parameters.

With the forecasted increase of renewable energy plants and HVDC power transmission, repetitive transients could become an important issue in the near future for HV equipment such as transformers, in particular the winding insulation. Their repetition rate influences long-term dielectric properties of paper-oil insulation, such as dielectric loss and time to breakdown. These effects, amongst others, are researched and quantified in this thesis. Based on these results, aging models are proposed to evaluate the predicted lifetime of the paper samples.

Representative, single sheets of transformer paper insulation were short and long term tested for electrical breakdown strength, times to breakdown and loss factors under various electrical and thermal conditions. The thermal conditions coincided with the transformer's typical temperature operating range.

In Chapter 3, short time breakdown tests and long term aging tests, both at AC voltage, were performed. A dielectric breakdown strength of paper-oil insulation samples equal to 51.2 kV/mm was measured. Times to breakdown were investigated for electric field strengths at 48.5 kV/mm (above PDIV) and at 37 kV/mm (below PDIV). When PD activity was present, the times to breakdown were around 170 h. Below PDIV, the average time to breakdown was 1400h.

The data collected in Chapter 3 provided the comparative results for the experiments in Chapter 4 and 5, where the influence of magnitude, rise time and repetition rate of repetitive transients were investigated. Square waves, single pulses and transients superimposed on a sinusoid were the main waveforms investigated. Additionally, dielectric loss measurements were performed at temperatures above room temperature. The time to breakdown and the

breakdown voltages were measured and a dielectric evaluation of the samples using tan (δ) measurements was performed. In particular, it was noticed that:

- Increasing the length of rise of a *square wave* from 300 ns to 1000 ns, the breakdown voltage and PDIV increased. PDs were measured and contributing to the breakdown voltage of paper. The same observation was concluded when the frequency was decreased from 10 kHz to 1 kHz;
- The behaviour of the paper-oil sample under a *single impulse* was similar as faster rise time decrease the breakdown voltage of the samples;
- In the main experiment, the insulation was stressed by *repetitive transients superimposed on a sinusoidal waveform*. As expected, the higher the magnitude of AC voltage was applied, the shorter the lifetime of the insulation samples was. The repetitive transients additionally aged the sample and the lifetime of the sample decreased from 30 h to 10 h with the increase of the rate of repetition frequency from 1 kHz to 10 kHz respectively at 2.91 kV AC magnitude;
- Breakdown voltages increased while temperatures of oil were raised to 60 °C and dropped at higher ones;
- Tan (δ) measurements showed that no conclusive information can be extrapolated from increasing temperatures, however, at all explored temperature levels, dielectric losses increased with the higher application of transient frequency.

The fluctuation model was suggested as the explanation of the breakdown process in the paper. Being a polymer, the paper's polymeric chains are susceptible to breakage when a high enough amount of energy is injected. When sufficient breakage occurs, the breakdown of the insulation takes place. Looking at the dielectric spectroscopy measurements, the index of connection between the structure units, *m*, was calculated. It was found that *m* decreased with the application of higher repetition frequency of transients. According to the fluctuations model, the connection index is inversely proportional to the shape parameter β in a Weibull analysis. Comparing the expected value of β and the actual value obtained from the analysis, a close match was identified, supporting the validity of the model.

Based on the Weibull analysis, a life consumption model was proposed. This model is built of two parts; the first takes into account the time to failure due to the AC waveform (power law), the second part takes into account the time to

failure due repetitive transients (exponential law). Comparing the theoretical values of this model to the measured ones, a close relation was obtained.

Based on this approximation, a lifetime consumption of paper oil insulation was derived. The model takes into consideration the transient repetition frequency and the carrier voltage on which they are superimposed. It was concluded, that a high repetition frequency of transients superimposed on a larger carrier voltage magnitude is necessary to obtain the highest rate of lifetime consumption.

7.2. Recommendations for Future Work

On the base of the results of the work carried out in this thesis on paper-oil insulation, the following additional experiments can be recommended to better understand the effect of repetitive transients on paper-oil insulating material:

- Perform breakdown and aging tests on multiple sheets of papers;
- Expand the investigation range of the transients in terms of magnitude and frequency to test the aging model;
- Investigate the behaviour of in-service aged paper when exposed to repetitive transients.

It would be of interest for asset managers of smart grids to investigate the influence of repetitive transients on other types of commonly used insulation, such as synthetic paper, XLPE and epoxy resin.

Appendix A – Weibull Statistics

Various parameters can give an indication whether a set of data is aging constantly in time or not. Considering that *f(t)* is the failure probability function of the insulating material at time *t*, it can be derived that [57]:

$$\int_0^\infty f(t)dt = F(t) + R(t) = 1 \tag{A.1}$$

Where *F(t)* is the cumulative failure distribution function and *R(t)* is the reliability of the material. They can be defined as:

$$F(t) = \int_0^t f(t)dt \tag{A.2}$$

$$R(t) = \int_t^\infty f(t)dt \tag{A.3}$$

Giving:

$$f(t) = \frac{dF(t)}{R(t)} = -\frac{dR(t)}{dt} \tag{A.4}$$

The instantaneous failure rate λ(t) is defined by the following equation:

$$\lambda(t) = \frac{f(t)}{R(t)} = -\frac{dR(t)/dt}{R(t)} \tag{A.5}$$

Which, integrating we obtain:

$$R(t) = exp\left\{-\int_0^t \lambda(t)dt\right\} \tag{A.6}$$

The cumulative failure distribution function can then be determined as:

$$F(t) = 1 - exp\left\{-\int_0^t \lambda(t)dt\right\} \tag{A.7}$$

Characterised by:

$$\{1 - F(t)\}^m = exp\left\{-m\int_0^t \lambda(t)dt\right\} \tag{A.8}$$

It has to be remembered that an insulating material is only as strong as its weakest spot. Therefore the reliability of the insulating material can be regarded as:

$$R_s(t) = \prod_{j=1}^{j} R_j(t) \quad \text{(A.9)}$$

The instantaneous failure rate must always be positive, therefore we can replace the integral of *λ(t)* with the condition:

$$\int_0^t \lambda(t)dt = (\frac{t}{\eta})^{\beta} \quad \text{(A.10)}$$

Obtaining:

$$F(t) = 1 - exp\left\{-\left(\frac{t}{t_0}\right)^{\beta}\right\} \quad \text{(A.11)}$$

Where: t_0, is the time when 63.2 % of the samples fail, also known as the scale parameter η.

The parameters β and t_0 are the shape and scale parameters of time to breakdown, respectively. This equation allows a higher degree of accuracy the weakest spot in the insulation system, leading to the creation of a breakdown model.

Appendix B – Dielectric Spectroscopy

In Chapter 3 and 4 paper-oil insulation was described as having fibres and molecular chains that respond to external stimulations. These stimulations can be of many sorts, electrical, mechanical or thermal amongst a few. One way to observe the state of the molecular chains within a material is to apply pulses of various frequencies and observe the dielectric response. This method named dielectric spectroscopy (DS) is capable of recording the tan (δ) of the material as a function of frequency.

The test set-up

The operating principle of DS is based on the interaction of the external field with the electric dipole moment of the sample, known as permittivity. Permittivity is the measure of the resistance encountered when forming an electric field in a medium and it is constituted of two parts: the real part and the imaginary part. It can be characterised by equation A.1:

$$\varepsilon = \varepsilon' - j\varepsilon'' \tag{B.1}$$

The real part, known as relative permittivity, is the measure of the amount of polarisation. The imaginary part is the measure of the losses involved in the polarisation process. Conductivity of the material in combination with the permittivity will result in tan (δ) values of the material at a specific frequency, characterised by equation A.2.

$$\tan(\delta) = \frac{\omega\varepsilon'' + \theta}{\omega\varepsilon'} \tag{B.2}$$

Where, θ is the conductivity of the sample.

The equipment present at Delft University of Technology from Novocontrol allows the measurement of tan (δ) continuously as a function of frequency by applying low voltage pulses at a variable frequency. The temperature of the measuring cell can also be altered. The key measurement parameters are:

- Pulse voltage between 1 V and 3 V;
- Frequency between 3 µHz and 20 MHz;
- Temperature in the measuring cell from 113 K to 673 K.

This method of evaluating the sample allows for:

- Better recognition of details about a sample. Resonant frequencies allow the identification of molecular chain lengths;
- The frequency range between 1 Hz and 100 MHz is the most susceptible to achieve polarisation. This is due to the ability of electrons to respond to changing electric fields;
- Clearer evaluation of DC conductivity at low frequencies.

The figure below shows the responsiveness of the real and imaginary parts of the permittivity of a material.

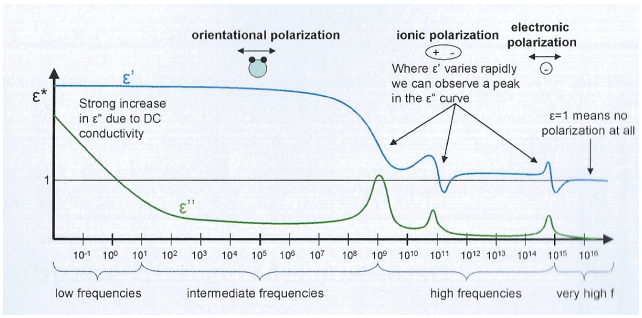


Fig. B.1 – The polarisation spectrum with different polarisation mechanisms [79]

Appendix C – Weibull Analysis

Several approaches were perused in analysing the data obtained from a 2-parameter Weibull analysis. The first one involved censoring the data points in order to achieve a constant value of the β parameter. Since the scatter of some data points was relatively large, indicated by β<1, the early failure times and the long breakdown times were attributed to sample's poor homogeneousness.

For a carrier voltage of 2.22 kV, the β values have approximated closer to unity, possibly indicating a constant failure in time. In the case of 2.91 kV, the same values are clearly above 1, strongly indicating the presence of an additional aging factor.

All the early breakdowns under 30 % of the average time to breakdown and above 200 % of the average time to breakdown were removed from the analysis. This allowed the elimination of any "extreme" breakdowns due to paper irregularities. The results for the carrier voltage of 2.91 kV are shown in Fig. C.1. The respective data is shown in Table C.1.

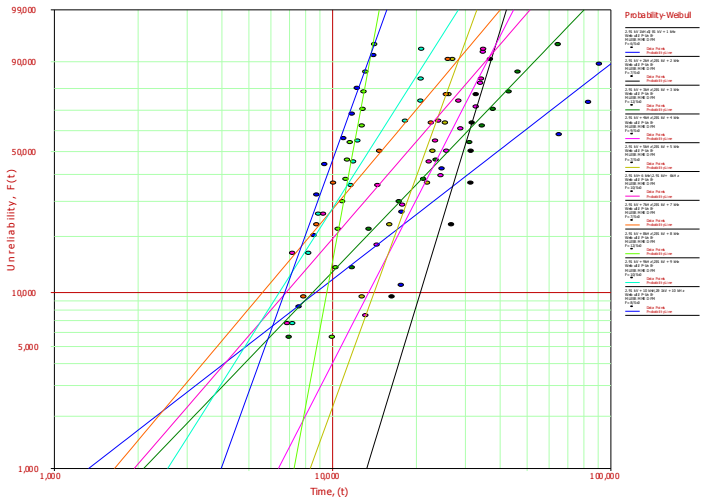


Fig. C.1 – 2 parameter Weibull unreliability plots as a function of time to breakdown for an AC waveform of 2.91 kV and transients at frequencies between 1 kHz and 10 kHz after removal of censored data

TableC.1 – 2-parameter Weibull distribution for samples aged with a 2.91 kV AC waveform with repetitive transients after removal of censored data.

Aging Waveform	β [per unit]	η [h]
2.91 kV and 1 kHz transients	1.25	52.5
2.91 kV and 2 kHz transients	5.30	31.6
2.91 kV and 3 kHz transients	1.68	32.3
2.91 kV and 4 kHz transients	3.15	27.5
2.91 kV and 5 kHz transients	4.44	23.4
2.91 kV and 6 kHz transients	1.87	22.6
2.91 kV and 7 kHz transients	1.92	18.1
2.91 kV and 8 kHz transients	8.68	12.3
2.91 kV and 9 kHz transients	2.54	15.5
2.91 kV and 10 kHz transients	4.46	11.13

The censored analysis for 2.22 kV is shown in Fig. C.2 and the corresponding data is presented in Table C.2.

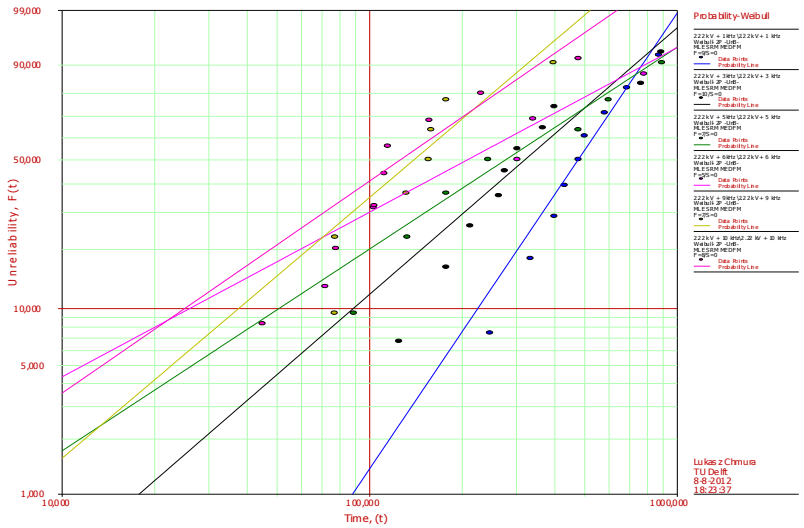


Fig. C.2 – 2 parameter Weibull unreliability plots as a function of time to breakdown for an AC waveform of 2.22 kV and transients at frequencies between 1 kHz and 10 kHz after removal of censored data

Table C.2 – 2-parameter Weibull distribution for samples aged with a 2.22 kV AC waveform with repetitive transients after removal of censored data.

Aging Waveform	β [per unit]	η [h]
2.22 kV and 1 kHz transients	2.51	550.9
2.22 kV and 3 kHz transients	1.47	410.1
2.22 kV and 5 kHz transients	1.11	384.6
2.22 kV and 6 kHz transients	0.91	311.4
2.22 kV and 9 kHz transients	1.43	179.8
2.22 kV and 10 kHz transients	1.17	172.1

This analysis minimally altered the values of the β parameter, with significant changes in the η parameter.

From tables C.1 and C.2, the average values of β can be calculated to be: 3.5 and 1.5 for 2.91 kV and 2.22 kV respectively. Since a linear trend in the aging rate could exist when varying the repetition frequency, the data could be re-analysed assuming the same β for each carrier voltage. Such analysis is possible in Weibull++ by setting the β whilst a new η value is calculated.

The error bars can be seen plotted on the figure. For 2.91 kV, the errors can be twice the value of β. In an attempt to identify a pattern from the shape parameter, a 3- parameter Weibull analysis has been performed. The addition of the third parameter allows the removal of failure data points that may have been caused by other aging factors than the ones investigated, such as infant mortality as the paper-oil samples are very thin or moisture absorption. The 3-parameter Weibull plot is characterised by the following equation:

$$f(t) = \frac{\beta}{\eta}\left(\frac{t-\gamma}{\eta}\right)^{\beta-1} e^{-\left(\frac{t-\gamma}{\eta}\right)^{\beta}} \quad \text{(C.1)}$$

Where γ is the shift factor that defines the location of the distribution in time. The analysis could not be performed for the waveform 2.91 kV + 5 kHz. The distribution of the data points was considered too random by the software and had to be left out. The results are shown in Fig. C.3.

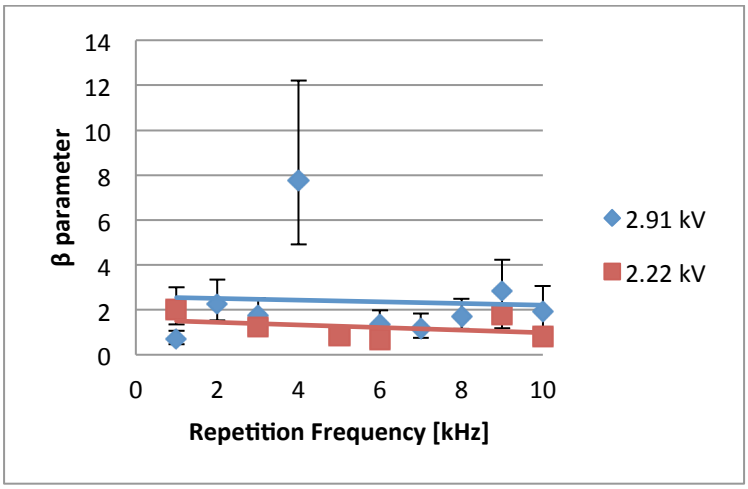


Fig. C.3 – β parameter as a function of frequency based on a three parameter Weibull analysis

The trend lines of the β parameter for the 3-parameter Weibull plots at different carrier voltages are flatter and parallel to each other. The 3-parameter analysis shows that the shape parameter is still independent of frequency. Its magnitude is however related to the magnitude of the carrier voltage. Hence, β=3 will be assumed for 2.91 kV and β=1.3 for 2.22 kV. These are the average values obtained from the 2-parameter analysis.

If the values of β are assumed constant, the Weibull η values can be re-calculated by performing a 1-parameter Weibull analysis. The new values can be seen in Table C.3.

Table C.3 – η values based on a constant shape parameter β

Repetition Frequency	η for β=3 at 2.91 kV	η for β=1.3 at 2.22 kV
1 kHz	54.8	489.5
2 kHz	43.3	-
3 kHz	37.1	398.5
4 kHz	27.4	-
5 kHz	22.9	311
6 kHz	22.6	247.8
7 kHz	18.0	-
8 kHz	12.0	-
9 kHz	15.4	159.7
10 kHz	10.85	153

Re-plotting the times to breakdown the following plots are obtained in Fig. C.4.

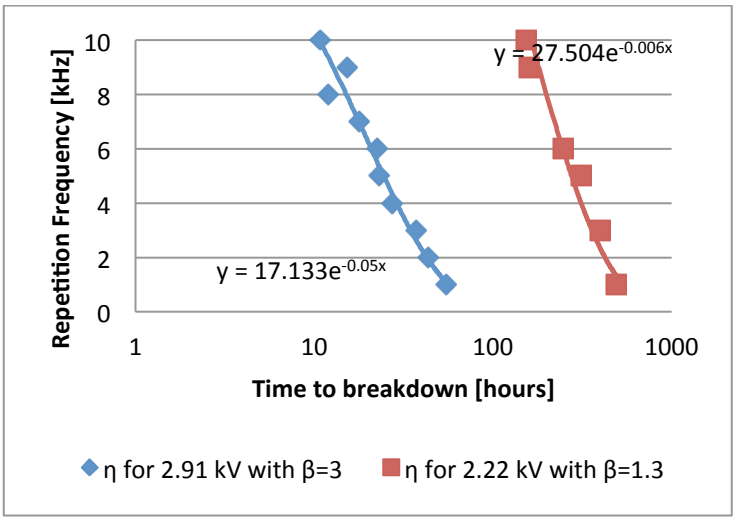


Fig. C.4 – The effect of the transient frequency as a function of time to breakdown

Appendix – D - Data Comparison

The formula in Equation 18 (chapter 6) was tested. The time to breakdown for various conditions was calculated and compared to real life data. The results are shown in Table D.1. Table D.2 shows the expected aging times, in h, when the paper-oil samples were to be stressed with a clean sinusoid (no transients).

Table D.1 – calculated times to breakdown for various conditions entered to Equation 18 (chapter 6). The green numbers represent the data values whose time to breakdown is known

Transient Frequency	Time to breakdown (h) at a carrier voltage of:			
	1 kV	1.5 kV	2.22 kV	2.91 kV
0	1000000	20686	486	36.5
0.5	927743	19191	451	33.9
1	860708	17805	418 / 505	31.5 / 34
2	740818	15324	360	27.1 / 32.7
3	637628	13190	310 / 378	23.3 / 29.4
4	548811	11352	267	20.1 / 25.2
5	472366	9771	229 / 274	17.3 / 21.8
6	406569	8410	197 / 211	14.9 / 16.6
7	349937	7238	170	12.8 / 13.9
8	301194	6230	146	11.1 / 11.8
9	259240	5362	126 / 149	9.5 / 11.2
10	223130	4615	108 / 139	8.2 / 10.5
15	105399	2180	51	3.9
20	49787	1029	24	1.8
25	23517	486	11	0.9
30	11109	229	5	0.4
35	5247	108	2.5	0.2
40	2478	51.276	1.2	0.09
50	553	11.44	0.26	0.02
100	0.3059	0.006	0.0001	1.11E-05

Table D.2 – Expected aging times of paper-oil insulation based on equation 6.30

Voltage [kV]	hours	days	years
2.91	180.1752	7.507301	0.020568
2.22	2114.994	88.12476	0.241438
1.5	74936.05	3122.335	8.554344
1.44	108648.2	4527.009	12.40276
1.3	275573.1	11482.21	31.45811
1.2	570915.6	23788.15	65.17301
1.18	665265.5	27719.39	75.94355
1	3000000	125000	342.4658

List of Figures and Tables

Fig. 1.1 – Energy generation sources in the industrialised nations in 2010 [5]. Fossil includes oil, gas and coal 3

Fig. 1.2 – Planned DESERTEC spread of renewable energy plants around Europe with HVDC interconnections [www.desertec.org] 4

Fig. 1.3 – An illustration of a repetitive transient 6

Fig. 2.1 – Concept view of the future city within the smart grid [28] 10

Fig. 2.2 – The input and output waveforms when converted using pulse width modulation (PWM) [13] 12

Fig. 2.3 – The main terms for the parameters used in describing a repetitive transient 13

Fig. 2.4 – PWM waveform generated by the power electronics in the ASD [13] 14

Fig. 2.5 - A three-phase induction motor controlled by power electronics [13] 14

Fig. 2.6 – The time to failure of a pair of twisted wires when different magnitudes and frequencies of a square waveform are applied [17] 15

Fig. 2.7 – Illustration of the effect of rise time on the life-span of insulation [18] .. 16

Fig. 2.8 – Conditions necessary for the creation of bubbles in a transformer's insulation at different pressures 18

Fig. 2.9 – Failure rates in a transformer by component [8] 20

Fig. 2.10 – Number of transformers installed in the Netherlands each year [28]. The different colours indicate the voltage class. 20

Fig. 2.11 Diagrammatic representation of the evolution of a failure in any insulation system [30] 22

Fig. 2.12 – Several stresses on a transformer's insulation [9] 23

Fig. 2.13 – Graphical aging models used to determine the state of the paper-oil insulation [6, 23] 24

Fig. 3.1 – Molecular structure of cellulose [6] 30

Fig. 3.2 – Fibres observed with an optical microscope in a cellulose specimen 32

Fig. 3.3 – Photo of a paper-oil test sample 34

Fig. 3.4 – Photo of the two types of used electrodes 36

Fig. 3.5 – The effect of sample conditioning on the AC dielectric breakdown strength of four types of samples in the test set up with different electrodes..... 37

Fig. 3.6 – Weibull unreliability plot for AC step-up breakdown values of 0.06 mm thick paper samples using a flat shaped electrode. The β and η parameters are 41.2 and 3.12 kV respectively. 90 % confidence bounds are shown in red 39

Fig. 3.7 – Weibull unreliability plot for paper-oil samples stressed at 2.91 kV and 2.22 kV. The Weibull parameter β is 0.84 and 2.14 for 2.22 kV and 2.91 kV respectively. The η parameter is 1491.8 h and 187.1 h for 2.22 kV and 2.91 kV respectively. 90% confidence bounds have been applied. 40

Fig. 3.8 – Life estimation curves for paper samples impregnated in oil as function of the applied field strength. Upper and lower 90% confidence bounds for characteristic 63.2% times to breakdown are shown 42

Fig. 3.9 – Results of tan (δ) measurements as a function of frequency of AC voltage after samples were electrically stressed for 24 hours prior to measurement 43

Fig. 4.1 – The output of a power electronic inverter seen by the transformer [14]... 48

Fig. 4.2 –Example of the square wave with location of the PD pulses on the rising positive flanks 49

Fig. 4.3 –Test set-up where the HV square wave is applied to the electrode placed on top of the paper sample and the PD pulses are measured using an antenna connected to an oscilloscope 50

Fig. 4.4 – Mean breakdown voltages of oil paper samples as function of the frequency of the square wave for different wave rise times with 90% error bounds 52

Fig. 4.5 – Mean partial discharge inception voltage as function of the frequency of the square wave for different wave rise times with 90% error bound 54

Table 4.1.1 – β parameter of Weibull distribution for V_{BD} for different rise times and frequencies of square wave [per unit]. The 90% confidence bounds are shown in the table below 55

Table 4.1.2 – η parameter of Weibull distribution for V_{BD} for different rise times and frequencies of square wave [kV]. The 90% confidence bounds are shown in the table below 55

Table 4.1.3 – ρ parameter of Weibull distribution for V_{BD} for different rise times and frequencies of square wave [per unit] 56

Fig. 4.6 – Plots with two different types of β parameter with 90 % confidence bounds: a) high β value, small scatter b) low β value, high scatter 56

Table 4.2.1 – β parameter of Weibull distribution for PDIV for different rise times and frequencies of square wave [per unit]. The 90% confidence bounds are shown in the table below 57

Table 4.2.2 – η parameters of Weibull distribution for PDIV for different rise times and frequencies of square wave [kV]. The 90% confidence bounds are shown in the table below 57

Table 4.2.3 – ρ parameters of Weibull distribution for PDIV for different rise times and frequencies of square wave [per unit] 58

Fig. 4.7a – The characteristic breakdown voltage range of a paper sample aged with a square wave 59

Fig. 4.7b – The characteristic partial discharge inception voltage range of a paper sample aged with a square wave 60

Fig. 4.8 – Schematic circuit of the impulse generator used for creating single transient-like pulses 61

Fig. 4.9 – The pulse created by the spark generator 61

Fig. 4.10 – Positive impulse breakdown voltages of paper-oil insulation as function of impulse rise time 62

Fig. 4.11 – Negative impulse breakdown voltages of paper-oil insulation as function of impulse rise time 63

Fig. 4.12 – A schematic representation in PSpice of the circuit used to generate transients. A MOSFET switch is replaced by three switches that have been timed to open and close. The sample is represented by C2 66

Fig. 4.13 – The results of simulation of the transients (circled) and their superposition on the AC waveform. The rise time is approx. 1 μs. 67

Fig. 4.14 – High Frequency transformer constructed for the purpose of amplifying high frequency impulses 68

Fig. 4.15 – Schematic diagram of the set-up used to perform the ageing tests of the paper-oil samples. The “transient box” superimposes transients on sinusoidal waveform 69

Fig. 4.16 – The transient box with the main components used to generate transients such as MOSFETs, logic circuit and HF transformer 70

Fig. 4.17 – Photograph of the equipment used 71

Fig. 4.18 – The test waveforms at the limits of performance of the set-up: 72

a) The 50 Hz waveform with superimposed transients at 10 kHz and at 1 kV and b) transient of 1 kV/µs rise time. 72

Fig. 4.19 – Mean time to breakdown as function of transients' repetition frequency with standard deviation for each repetition frequency 73

Fig. 4.20 – Mean time to breakdown as function of transients´ repetition frequency with standard deviation figures 73

Fig. 4.21 – The aging coefficient as function of the repetition frequency of transients superimposed on 2.22 kV and 2.91 kV sinusoidal waveforms. The relative errors in standard deviation have been divided by each other and displayed as error bars. 74

Fig. 4.22 – Estimated arithmetic mean life time curves of paper-oil samples under transient conditions and AC-only scenario 75

Fig. 4.23 – The mean number of transients, N, required to achieve breakdown. (a) Super-imposed on a 2.91 kV waveform and (b) superimposed on a 2.22 kV waveform 77

Fig. 4.24 – Tan (δ) values as a function of the measurements frequency for paper-oil samples stressed for 20 h with a carrier waveform of 2.91 kV and different transient repetition frequency 79

Fig. 4.25 – Tan (δ) values as a function of the measurements frequency for paper-oil samples stressed for 20 h with a carrier waveform of 2.22 kV and different transient repetition frequency 79

Fig. 5.1 – Hot-spot temperature variations in a distribution transformer during the course of a day [59] 84

Fig. 5.2 –Relation of water percentage in paper as function of moisture in oil at different temperatures increased in 10 degree steps [6]..... 85

Fig. 5.3 – Experimental set-up for testing at elevated temperatures..... 86

Table 5.1 – 2-parameter Weibull analysis of AC breakdown voltage at different temperatures..... 87

Fig. 5.4 –Dielectric breakdown voltage test results as function of temperature 87

Fig. 5.5 – Tan (δ) and Dielectric Constant values due to moisture content in mineral oil [64] 89

Fig. 5.6 –Test set-up used for long term tests at elevated temperature..... 90

Fig. 5.7 – Tan (δ) values as function of measuring voltage for a new sample (reference data)..... 92

Fig. 5.8 – Tan (δ) values as function of measuring voltage for samples thermally and electrically stressed at different temperatures under an AC waveform for 22h. The data is compared to a new samples that has not been stressed 93

Fig. 5.9 – Tan (δ) values as a function of measuring voltage for samples thermally and electrically stressed at different temperatures under an AC waveform with superimposed 1 kHz transients for 22h..... 94

Fig. 5.10 – Tan (δ) values as a function of measuring voltage for samples thermally and electrically stressed at different temperatures under an AC waveform with superimposed 5 kHz transients for 22h..... 94

Fig. 5.11 – Tan (δ) values as a function of measuring voltage for samples thermally and electrically stressed at different temperatures under an AC waveform with superimposed 10 kHz transients for 22h 95

Table 5.2 – Percentile change in tan (δ) value for differently aged samples at different temperature and transient frequency in comparison to the reference sample..... 96

Fig. 5.12 – Tan (δ) values as function of measuring voltage for differently aged paper-oil samples at 40 °C 97

Fig. 5.13 – Tan (δ) values as function of voltage for differently aged paper-oil samples at 60 °C 97

Fig. 5.14 – Tan (δ) values as function of voltage for differently aged paper-oil samples at 80 °C 98

Fig. 5.15 – Tan (δ) values at 350 V measuring voltage for differently aged samples for 22h 99

Fig. 6.1 – The effect on the time to breakdown as a function of carrier voltage magnitude. Data based on Fig. 4.19 and Fig. 4.20 where confidence bounds are indicated and Chapter 3.3.3 102

Table 6.1 – Trend-line parameters based on the repetition frequency. 103

Fig. 6.2 - The effect on the time to breakdown as a function of repetition frequency of transients. The values for the time to breakdown are the geometric mean with the corresponding upper and lower 90% confidence bounds 104

Fig. 6.3 – The real component of the complex permittivity as a function of measurement frequency after exposure for 20 h with a carrier voltage of 2.22 kV and repetition frequency of transients as indicated..... 105

Fig. 6.4 – The imaginary component of the complex permittivity as a function of measurement frequency after exposure for 20 h with a carrier voltage of 2.22 kV and repetition frequency of transients as indicated..... 106

Fig. 6.5 – The real component of the complex permittivity as a function of measurement frequency after exposure for 20 h with a carrier voltage of 2.91 kV and repetition frequency of transients as indicated..... 106

Fig. 6.6 – The imaginary component of the complex permittivity as a function of measurement frequency after exposure for 20 h with a carrier voltage of 2.91 kV and repetition frequency of transients as indicated..... 107

Table 6.2 – m and β coefficient calculated for various aging waveforms and transient repetition frequencies. The error in the measuring equipment was identified at 2%..... 108

Table 6.3 – β and η parameters for a two-parameter Weibull analysis of breakdown times at different voltages of carrier and transient repetition frequencies. 110

Fig. 6.7 – Weibull unreliability plot for the frequency of 1 kHz 111

Fig. 6.8 – Weibull unreliability plot for the frequency of 3 kHz 111

Fig. 6.9 – Weibull unreliability plot for the frequency of 5 kHz 112

Fig. 6.10 – Weibull unreliability plot for the frequency of 6 kHz 112

Fig. 6.11 – Weibull unreliability plot for the frequency of 9 kHz 113

Fig. 6.12 – Weibull unreliability plot for the frequency of 10 kHz 113

Fig. 6.13 – The effect of time to breakdown as a function of transient repetition frequency with 90% confidence bounds 114

Fig. 6.14 – β parameter as a function of frequency based on a two parameter Weibull analysis with 90% confidence bounds 115

Table 6.4 – Parameter estimation and model based on the repetition frequency of transients. The unit of frequency is kHz 120

Fig. 6.15 – Modelling transients superimposed on a 2.91 kV sinusoidal waveform. The blue dotted line represents inverse power law, green straight line represents the exponential relationship and the red dashed line represents the Eyring model. The mean values are represented by the triangle 121

Fig. 6.16 – Modelling transients superimposed on a 2.22 kV sinusoidal waveform. The blue dotted line represents inverse power law, green straight line represents the exponential relationship and the red dashed line represents the Eyring model. The mean values are represented by the triangle 122

Fig. 6.17 – Comparison of the three investigated models. Time to failure is plotted as a function of repetition frequency. 123

Fig. 6.18 – Comparison of measured and calculated times to breakdown as a function of transient repetition frequency superimposed on two magnitudes of carrier wave, 2.22 kV and 2.91 kV. Standard deviation is shown for the measured points 124

Fig. 6.19 –Equation 18 (chapter 6) for different voltages and repetition frequencies as a function of time to breakdown. Uncertainty bars due to errors limits for the exponent within parameter a as well as for the parameter b are shown 125

Fig. 6.20 – Life time consumption based on the ratios between transients and carrier waveform 126

Fig. B.1 – The polarisation spectrum with different polarisation mechanisms [79] 136

Fig. C.1 – 2 parameter Weibull unreliability plots as a function of time to breakdown for an AC waveform of 2.91 kV and transients at frequencies between 1 kHz and 10 kHz after removal of censored data..... 137

TableC.1 – 2-parameter Weibull distribution for samples aged with a 2.91 kV AC waveform with repetitive transients after removal of censored data. 138

Fig. C.2 – 2 parameter Weibull unreliability plots as a function of time to breakdown for an AC waveform of 2.22 kV and transients at frequencies between 1 kHz and 10 kHz after removal of censored data..... 138

Table C.2 – 2-parameter Weibull distribution for samples aged with a 2.22 kV AC waveform with repetitive transients after removal of censored data. 139

Fig. C.3 – β parameter as a function of frequency based on a three parameter Weibull analysis 140

Table C.3 – η values based on a constant shape parameter β 140

Fig. C.4 – The effect of the transient frequency as a function of time to breakdown..... 141

Table D.1 – calculated times to breakdown for various conditions entered to Equation 18 (chapter 6). The green numbers represent the data values whose time to breakdown is known..... 143

Table D.2 – Expected aging times of paper-oil insulation based on equation 6.30 144

Bibliography

[1] http://www.guardian.co.uk/environment/2007/apr/01/energy.theobserversuknewspages

[2] Cigre Brochure 225, Electrical Power Systems 2020", 2002.

[3] IEC 62068,Electrical Insulation Systems – Electrical stresses produced by repetitive transients. Part 1: General Method of evaluation of electrical endurance. 2013.

[4] IEC 62068,Electrical Insulation Systems – Electrical stresses produced by repetitive transients. Part 2: State of the art, 2001.

[5] World Energy Outlook 2012, International Energy Agency, 2012.

[6] Cigre Brochure 323 "Ageing of Cellulose in Mineral-Oil Insulated Transformers", Task Force D1.01.10, 2007.

[7] G. Bajracharya, "Multi-Agent Model-Based Optimization for Future Electric Grids". Ph.D. Thesis, Delft University of Technology, 2013.

[8] Cigre Brochure 248, "Guide on Economics of transformer management, 2004.

[9] Cigre Brochure 227, "Life Management techniques for power transformers", 2003.

[10] R. Bodega, "Space Charge Accumulation in Polymeric High Voltage DC Cable Systems", Ph.D. Thesis Delft University of technology, 2006.

[11] M. Claudi, S. Berliijn, P. Mohaupt, "Practical experience and performance of monitoring systems", Cigre general session, Paris, France, 2008.

[12] www.smartgrids.eu

[13] M. Madrigal and E. Acha, "Harmonic Modelling of Voltage Source Converters for HVDC Station", IEEE AC-DC Power Transmission Conference publication no. 485.

[14] T. Bengstsson, F. Dijkhuizen, L. Ming, F. Sahlen, L. Liljestrand, D. Bormann, R. Papazyan, M. Dahlgren, "Repetitive Fast Voltage Stresses– Causes and Effects"IEEE Electrical Insulation Magazine, pp. 26–39, 2009.

[15] Distributed Energy Systems, 2007. URL: http://des.coreonix4.com/data/Unsorted/Power_Converter-20640-1.pdf. Last accessed: 27 March 2009.

[16] A. Cavallini, D. Fabiani and G.C. Montanari, “Power Electronics and Electrical Insulation Systems – Part 1: Phenomenology Overview”, Electrical Insulation Magazine, May/June, Vol. 26, no.3, 2010.

[17] W. Yin, K. Bultemeier, D. Barta and D. Floryan, Critical Factors for Early Failure of Magnet Wires in Inverter Fed Motors, IEEE Electrical Insulation Magazine Vol. 13, n. 6, pp. 18-23, Nov. 1997.

[18] W. Yin, “Failure Mechanism of Winding Insulation in Inverter-Fed Motors”, IEEE Electrical Insulation Magazine, 1997.

[19] Z. Radakovic, E. Cardillo and K. Feser, “The influence of transformer loading to the ageing of the oil-paper insulation”, XIIIth International symposium on high voltage engineering, Netherlands, 2003.

[20] F. M. Clark, “Insulating Materials for Design and Engineering Practice”, p. 299, John Wiley and Sons, Inc., 1962.

[21] F. H. Kruger, “Industrial High Voltage”, Delft University Press, 1991.

[22] T. V. Oommen, S. R. Lindgren, “Bubble Evolution from Transformer Overload”, IEEE, 2001.

[23] M. Arshad, S. M. Islam and A. Khaliq, “Power Transformer Aging and Life Extension”, 8th International Conference on Probabilistic Methods Applied to Power Systems, Iowa State University, Ames, Iowa, 2004.

[24] B. Suechoey, S. Tadsuan and C. Thammarat, ”An Analysis of Temperature of Oil Immersed Transformer Under Non Linear Load”, POWERCON, Bucharest, Romania, 2009.

[25] MSA Minhas, J.P. Reynders, P.J. de Klerk, “Failures in Power System Transformers and Appropriate Monitoring Techniques”, High Voltage Engineering Symposium, 1999.

[26] J. H. Yew, A. J. Thomas, “Impact of Temperature on the Frequency Domain Dielectric Spectroscopy for the Diagnosis of Power Transformer Insulation”, 2006.

[27] S. Tenbohlen, T. Stirl, G. Bastos, J. Baldauf, P. Mayer, M. Stach, B. Breitenbauch, R. Huber, “Experienced-based Evaluation of Economic Benefits of On-line Monitoring Systems for Power Transformers”, Cigre session 2002.

[28] L. Chmura, P.H.F. Morshuis, E. Gulski, J.J. Smit and A. Janssen, “Identification and Treatment of Outliers in Failure Datasets – Practical Aspects of Statistical Analysis”. International Symposium on High Voltage Engineering, 2011.

[29] S. Bahadoorsingh and S.M. Rowland, “The Relationship between Insulation Ageing and Power Network Performance”, International Conference on Solid Dielectrics, Winchester, UK, 2007.

[30] S. Bahadoorsingh and S.M. Rowland “A Multifactor Framework Linking Insulation Ageing and Power Network Environments”, CEIDP, 2007.

[31] T. Koltunowicz, G. Bajracharya, D. Djairam, J.J. Smit, Defining a Transformer’s Aging Factors in the Future. CIRED, Jun. 2009.

[32] F.M. Clark, “Insulating Materials for Design and Engineering Practice”, p. 133, Wiley Publications, NY, 1962.

[33] Shell Diala B datasheet, available on Shell Website.

[34] V.W. Montsinger: “Loading transformers by temperature”, Trans. AIEE, pp. 776-192, 1930.

[35] F.M. Clark, “Insulating Materials For Design and Engineering Practice”, Wiley Pubblications, NY, p. 137, 1962.

[36] Frank M. Clark, “Insulating Materials for Design and Engineering Practice”, John Wiley and Sons, Inc., p. 15, 1962.

[37] F.H. Kreuger, “Industrial High Voltage”, Vol. I, Delft University Press, p. 140, , 1991.

[38] A. Bradwell, “Electrical Insulation”, Peter Peregrinus, London, UK, p.53, 1983.

[39] Life Data Analysis Reference, Reliasoft Corporation Publishing, RW7-LDAR, 2005.

[40] L.A. Dissado, J.C. Fothergill, S.V. Wolfe and R.M. Hill, “Weibull Statistics in Dielectric Breakdown; Theoretical Basis, Applications and Implications”, IEEE Transactions on Electrical Insulation, Vol. EI-19 No. 3, June 1984.

[41] “IEEE Guide for the Statistical Analysis of Electrical Insulation Voltage Endurance”, an American National Standard, 1987.

[42] L. Paulsson, B. Ekhov, S. Halen, T. Larsson, L. Palmqvist, A. A. Edris, D. Kidd, A. J. F. Keri and B. Mehraban, *High-frequency impacts in a converter-based back-to-back tie; the Eagle Pass installation,* IEEE Transactions on Power Delivery, Vol. 18, No. 4, pp. 1410-1415, 2003.

[43] M. Kaufhold, H. Aninger, M. Berth, J. Speck, M. Eberhardt, “Electrical stress and failure mechanism of the winding insulation in PWM-inverter-fed low-voltage induction motors”, IEEE transaction on industrial electronics, Volume 47, 2000.

[44] J. Pan, R. Nuqui, K. Srivastava, T. Jonsson, P. Holmberg, and Y. J. Hafner, “AC Grid with Embedded VSC-HVDC for Secure and Efficient Power Delivery”, IEEE Energy2030, Atlanta (GA), USA, 17-18 November, 2008.

[45] M. Rahimo and S. Klaka, “High voltage semiconductor technologies”, Proc. of 13th European Conference on Power Electronics and Applications (EPE '09), Sept. 2009.

[46] J. W. Palmour, J. Q. Zhang, M. K Das, R. Callanan, A. K. Agarwal, and D. E. Grider, “SiC power devices for Smart Grid systems”, Proc. of International Power Electronic Conference, pp. 1006-1009, June 2010.

[47] P. K. Steimer and M. D. Manjrekar, “Practical medium voltage converter topologies for high power applications”, Conf. records of 36th IAS Annual Meeting, Vol. 3, pp. 1723-1727, Oct. 2001.

[48] D. Fabiani, “Accelerated Degradation of AC Motor Insulation due to Voltage Waveforms Generated by Adjustable Speed Drives, Ph. D. Thesis, Gedit Edizioni, Bologna, Italy, 2003.

[49] Product datasheet : http://www.techimp.com/systems/Products/HVGenerator/HVGenerator.aspx

[50] http://www.techimp.com/systems/Products/AcqUnits/AcqUnits.aspx Product Datasheet

[51] Tektronix Oscilloscope http://www.tek.com/products/oscilloscopes/tds2000/

[52] Z. Flisowski, “Technika Wysokich Napiec”. Wydawnictwa Naukowo-Techniczne, Warsaw, Poland 1999.

[53] IEC Standard 60243-3.

[54] M. Jeroense, “Charges and Discharges in HVDC Cables”, Ph. D. Thesis, Delft University Press, Delft, the Netherlands, 1997.

[55] Behlke Switch HTS 301-03-GSM, www.behlke.com.

[56] Young and Freedman, “University Physics”, 12th Edition Pearson International Edition, ISBN-13: 978-0-321-50130-1, 2009.

[57] T. Tanaka, A. Greenwood, “Advanced Power Cable Technology, Basic Concepts and Testing”, Volume 1, CRC Press.

[58] W. Weibull, “A statistical distribution function of wide applicability”, *J. Appl. Mech.* 18, 1951.

[59] Z. Radakovic and K. Feser, "A new method for the calculation of the hot-spot temperature in power transformers with ONAN cooling," *IEEE*, October, 2003.

[60] IEEE, "Guide for the statistical analysis of electrical insulatin breakdown data," *IEEE*, 2007.

[61] ASTM International, "Standard Test Method for Dielectric Breakdown Voltage and Dielectric Strength of Solid Electrical Insulating Materials at Commercial Power Frequencies," *D 149 – 97a*, 2004.

[62] PTD T Höhlein / Heinzig Siemens AG, *IEEE Transformers Committee Meeting*. Jackson (MS): PTD T Höhlein / Heinzig, 2005.

[63] E. Peschke and E. von Olshausen, "*Cable Systems for High and Extra-High Voltage"*. Berlin: Publicis MCD, 1999.

[64] C.F. Ten, M.A.R.M. Fernando, and Z.D. Wang, "Dielectric properties measurements of transformer oil, paper and pressboard with the effect of moisture and ageing," *Annual report conference on electrical insulation and dielectric phenomena*, 2007.

[65] T. Bedford and R. Cooke, "Probabilistic Risk Analysis: Foundations and Methods", Cambridge University Press, 2001.

[66] D. Chinh, J. L. Parpal, and J. P. Crine, "Electrical aging of extruded dielectric cables: review of existing theories and data," Dielectrics and Electrical Insulation, IEEE Transactions on, vol. 3, pp. 237-247, 1996.

[67] F. H. Kreuger, "Determination of the Internal Discharge Resistance of Dielectric Materials," Electrical Insulation, IEEE Transactions on, vol. EI-3, pp. 106-114, 1968.

[68] R. J. Densley, R. Bartnikas, and B. Bernstein, "Multiple stress aging of solid-dielectric extruded dry-cured insulation systems for power transmission cables," Power Delivery, IEEE Transactions on, vol. 9, pp. 559-571, 1994.

[69] L. Simoni, "A General Approach to the Endurance of Electrical Insulation under Temperature and Voltage," Electrical Insulation, IEEE Transactions on, vol. EI-16, pp. 277-289, 1981.

[70] L. Simoni, G. Mazzanti, G. C. Montanari, and L. Lefebre, "A general multi-stress life model for insulating materials with or without evidence for thresholds," Electrical Insulation, IEEE Transactions on, vol. 28, pp. 349-364, 1993.

[71] G. C. Montanari, "Electrical life threshold models for solid insulating materials subjected to electrical and multiple stresses. I. Investigation and comparison of life models," Electrical Insulation, IEEE Transactions on, vol. 27, pp. 974-986, 1992.

[72] G. Bahder, T. Garrity, M. Sosnowski, R. Eaton, and C. Katz, "Physical Model of Electric Aging and Breakdown of Extruded Polymeric Insulated Power Cables," Power Apparatus and Systems, IEEE Transactions on, vol. PAS-101, pp. 1379-1390, 1982.

[73] J.P. Crine, "A model of solid dielectrics aging in Electrical Insulation", Conference Record of the 1990 IEEE International Symposium on electrical insulation, pp. 25-26, 1990.

[74] IEEE Guide for Loading Mineral-Oil-Immersed Transformers, ed. New York, United States of America, 1995.

[75] H.G. Tempelaar "Validity of Frequency Accelerated Aging of Generator Model Bars", Electra Publication No. 127, 1989.

[76] F. Schemmel, K. Bauer and M. Kaufhold, "Reliability and Statistical Lifetime – Prognosis of Motor Winding Insulation and Low Voltage Power Drives", IEEE Electrical Insulation Magazine, 2009.

[77] X. Chen, P.H.F. Morshuis, B. Lennon, J.J. Smit, " Experimental investigation on dielectric spectroscopy of insulating paper and oil", Annual Report Conference on Electrical Insulation and Dielectric Phenomena, 2010.

[78] L.A. Dissado and J.C. Fothergill, "Electrical Degradation and Breakdown in Polymers". The Institution of Engineering and Technology, ISBN 0863411967, 1992.

[79] T. Andritsch, "Epoxy Based Nanocomposites for High Voltage DC Applications", Ph.D. thesis, Delft University of Delft, 2010.

Samenvatting

Het elektriciteitsnet is in een tijdperk van aanzienlijke verandering. Alternatieve transmissietechnologieën zoals HVDC worden steeds vaker geïmplementeerd en kolen- en kerncentrales worden langzaam vervangen door duurzame varianten en hernieuwbare energie opwekking . Hoewel er al onderzoek is verricht naar deze duurzame technologieën, zijn de lange termijn effecten op het huidige net nog relatief onbekend. Een belangrijk punt van zorg is het effect van repeterende transiënten op de levensduur en de diëlektrische eigenschappen van de isolatie in netcomponenten.

Repeterende transiënten ontstaan bij het converteren van DC in AC als gevolg van snelschakelende processen in het bereik van 1-10 kHz in MOSFETs die zich in vermogensomzetters bevinden. Deze technieken wordt al toegepast in AC motoren en bieden economische voordelen dankzij de relatief lage kosten van de vereiste elektronica. Deze vermogensomzetters worden al gebruikt in HVDC onderstations en in windenergieparken. Gezien de trend dat energie steeds meer lokaal opgewekt wordt, is de verwachting dat deze omzetters dichter bij de consument geïnstalleerd worden.

Er was weinig bekend over de invloed van snel repeterende schakelpulsen op elektrische isolatiematerialen. Het grootste deel van de beschikbare kennis betreft de veroudering van de isolatie van elektrische motoren die blootgesteld worden aan de transiënten van “adjustable speed drives”. Het doel van dit proefschrift was om bewijs te vinden dat transiënten ook andere vormen van isolatie, zoals isolatie gebaseerd op papier en olie, kan beïnvloeden. Hierbij wordt een hypothese opgesteld voor de veroudering, die tesamen met een kwantitatief verouderingsmodel de verwachte tijd tot het falen van de isolatie geeft afhankelijk van de frequentie van de transiënten.

In dit proefschrift is een “verdeel en heers”-methode gebruikt om de effecten van de repeterende transiënten op monsters van papier-olie-isolatie te bestuderen. De invloed van individuele parameters van de transiënten zijn apart onderzocht: stijgtijd, frequentie en amplitude. Hiervoor zijn verschillende spanningsgolfvormen, representatief voor veldcondities, gebruikt: 1) blokgolf, 2) enkelvoudige pulsen en 3) AC signalen met daarop de repeterende transiënten. Tenslotte is er ook gevarieerd met de temperatuur om te onderzoeken of het

versneld verouderen door transiënten versterkt wordt door een verhoogde omgevingstemperatuur.

Een blokgolf werd aangebracht op papier-olie-isolatiemonsters en hierbij werden twee grootheden gemeten als functie van de stijgtijd en frequentie: de doorslagspanning en de ontsteekspanning voor deelontladingen. De stijgtijd varieerde van 300 tot 1000 nanoseconden en de frequentie varieerde van 1 tot 10 kHz. De verkregen meetwaarden suggereerden dat een verkorting van de stijgtijd en verhoging van de frequentie ervoor zorgden dat de doorslagspanning en de ontsteekspanning afnam. “Single voltage pulses” zijn ook toegepast op soortgelijk isolatiemateriaal met vergelijkbare resultaten wat betreft lagere doorslagspanningen bij korte stijgtijden.

Om de veldcondities na te bootsen in het laboratorium is een apparaat ontwikkeld dat in staat is om signalen te creëren bestaande uit repeterende transiënten met verschillende frequenties en amplitudes gesuperponeerd op een sinusvormige golf waarvan de amplitude gevarieerd kan worden. In deze testopstelling is de tijd tot doorslag geobserveerd bij kamertemperatuur. Voor aantal specifieke monsters is de tan (d) gemeten na 24 uur elektrische veroudering bij verschillende frequenties van de transiënten. De verzamelde meetgegevens laten zien dat de tijd tot doorslag met een factor 3 afneemt wanneer de frequentie wordt verhoogd van 1 tot 10 kHz op een AC golf van 48.5 kV/mm. De tan d metingen laten zien dat er een mogelijk sterke degradatie van de moleculaire verbindingen in het papier optreedt als er hogere transiëntenfrequenties in combinatie met hogere amplitudes van de AC golven worden toegepast.

In isolatiemonsters blootgesteld aan temperaturen van 40 °C, 60 °C en 80 °C werden gelijksoortige verouderingsverschijnselen gevonden. Tijdens het kortstondig (22 uur) aanbrengen van de transiënten werd gemeten dat de tan d waarden toenamen.

Op basis van Weibull-analyse van de verkregen gegevens is een levensduurconsumptiemodel opgesteld. Het verhogen van de frequentie van de transiënten bij een constante AC golf, blijkt de verwachte levensduur van de isolatie substantieel te verkorten.

De versnelde veroudering van isolatie door repeterende transiënten kan een invloedrijke rol spelen in de betrouwbaarheid van het toekomstige elektriciteitsnet. Gezien de verwachting dat het functie van net in de toekomst

veel complexer zal en dat netcomponenten zwaarder belast zullen worden, is de verwachting dat de levensduur van de huidige componenten aanzienlijk verkort zullen worden. Om dit te voorkomen, is het onderzoek naar de verschijnselen van repeterende transiënten een belangrijke eerste stap.

Publications

- T.L. Koltunowicz, Q. Zhuang, D. Djairam, J.J. Smit, "*A statistical aging model for paper oil insulation under repetitive transients*" High Voltage. Engineering and Application (ICHVE), Shanghai, China, September 2012.
- T. L. Koltunowicz, A. Cavallini, D. Djairam, G.C. Montanari, J.J. Smit, "*The influence of square voltage waveforms on transformer insulation break down voltage*", Electrical Insulation and Dielectric Phenomena (CEIDP), Cancun, Mexico, October 2011.
- T.L. Koltunowicz, G. Bajracharya, R. Kochetov, D. Djairam, J.J. Smit, "*Repetitive Transient Aging, the Influence of Slew Rate*", IEEE Electrical Insulation Conference, Annapolis, USA, June 2011.
- T.L. Koltunowicz, G. Bajracharya, R. Kochetov, D. Djairam, J.J. Smit, "*Repetitive Transient Aging, the Influence of Repetition Frequency*", IEEE Electrical Insulation Conference, Annapolis, USA, June 2011.
- T. Koltunowicz, G. Bajracharya, M. Al-Suhaily, D. Djairam, J.J. Smit, "*The Effects of Prolonged Exposure of Paper Insulation to Fast Repeating Transients*", International Conference on High Voltage Engineering and Application, New Orleans, USA, October 2010.
- G. Bajracharya, T. Koltunowicz, R.R. Negenborn, D. Djairam, J.J. Smit, "*Optimization of Transformer Loading Based on Hot Spot Temperature using a Predictive Health Model*", International Conference on Condition Monitoring and Diagnostics (CMD2010) , Tokyo, Japan, September 2010.
- G. Bajracharya, T. Koltunowicz, D. Djairam, J.J. Smit, "*Common Information Model (CIM) extension for Asset Management in Future Intelligent Grids*", International Conference on Condition Monitoring and Diagnostics (CMD2010), Tokyo, Japan, September 2010.
- T.L. Koltunowicz, G. Bajracharya, D. Djairam, J.J. Smit, "*Exploring the Feasibility of an Aging Model for Paper Insulation Based on the Repetition Frequency of Transients*", IEEE International Symposium on Electrical Insulation (ISEI), San Diego, USA, June 2010.
- T.L. Koltunowicz, G. Bajracharya, D. Djairam, J.J. Smit, "*Investigation of the Effects of Fast Transients on a Transformer Paper Insulation*", IEEE International Symposium on Electrical Insulation, San Diego (ISEI), USA, June 2010.

- T.L. Koltunowicz, G. Bajracharya, D. Djairam, J.J. Smit, "*Investigating the Effects of Repetitive Transients on Paper Insulation*", 10th International Conference on Developments in Power Systems Protection, Manchester, UK, March 2010.
- T.L. Koltunowicz, G. Bajracharya, D. Djairam, J.J. Smit, "*Defining a transformer's aging factors in the future*", 20th International Conference and Exhibition on Electricity Distribution, Prague, Czech Republic, June 2009.
- T.L. Koltunowicz, G. Bajracharya, D. Djairam, J.J. Smit, "*Investigation of the effects of fast rise pulses on transformer insulation*", Nordic Insulation Symposium, Gothenburg, Sweden, July 2009.
- T.L. Koltunowicz, G. Bajracharya, D. Djairam, J.J. Smit, "*Designing a Transformer's Aging Model in the Grid of the Future*", 16th International Symposium on High Voltage Engineering (ISH), Cape Town, South Africa, August 2009.
- T.L. Koltunowicz, G. Bajracharya, D. Djairam, J.J. Smit, "*Modelling of Fast Transients Using a High Frequency Transformer*", 16th International Symposium on High Voltage Engineering (ISH), Cape Town, South Africa, August 2009.
- G. Bajracharya, T.L. Koltunowicz, R. Negenborn, Z. Papp, D. Djairam, BHK. De Schutter, J.J. Smit, "*Optimization of condition-based asset management using a predictive health model*", 16th International Symposium on High Voltage Engineering (ISH), Cape Town, South Africa, August 2009.
- G. Bajracharya, T.L. Koltunowicz, D. Djairam, J.J. Smit, "*The development of an architecture of common information interface for asset management of electricity grid*", 16th International Symposium on High Voltage Engineering (ISH), Cape Town, South Africa, August 2009.
- G. Bajracharya, T.L. Koltunowicz, R.R. Negenborn, Z. Papp, D. Djairam, B. De Schutter, J.J. Smit, "*Optimization of maintenance for power system equipment using a predictive health model*", IEEE PowerTech Conference, Bucharest, Romania, August 2009.
- T.L. Koltunowicz, G. Bajracharya, S. Meijer, J.J. Smit, R.A. Jongen, "*Transformer Aging Models for Future Power System Decision support*", IEEE Young Researcher Conference, Eindhoven, the Netherlands, March 2008.

Acknowledgments

Since coming to the Netherlands, I had the pleasure of meeting many interesting people. Together with their support and that of my friends and family abroad, this thesis wouldn't have been possible.

First of all, I would like to thank my promoter Prof. Dr. Johan Smit for giving me the opportunity to work in his group. I've thoroughly enjoyed our evening conversations, not only the technical ones but also the more philosophical ones.

Secondly, I'm thankful to my daily supervisor, Dr. ir. Dhiradj Djairam for guiding me during these years and making sure I stay on track during the tough times.

My gratefulness lies also with the staff of the HV lab: Ir. Paul Van Nes, Wim Termorshuizen, Aad van der Graaf and Bertus Naagen. Your technical knowledge helped to build the most efficient experimental set-up and your personalities made the long stays in the laboratory basement bearable. Furthermore I would like to thank Dr. Sander Meijer for guiding me at the very beginning of this project.

Special thanks should also be addressed to the University of Bologna for letting me use their test set-up and for the interesting discussions afterwards.

My acknowledgements also go to AgentschapNL and their research program EOS-LT for the financial backing of the SINERGIE project.

My appreciation goes to Prof. M. Muhr, Prof. S. Gubanski, Dr. A. Cavallini, Prof. E.F. Steennis, Prof. S.J. Picken and Prof. M. Zeman for being kind enough to be part of my doctoral committee.

My fellow colleagues, Pantelis, Piotr, Roy, Mo, Ravish, Qikai, Barry, Jur and Huifei, thanks for the company and support during these years. Thomas, fellow driver and globetrotter, thanks for your help on understanding all this data and for the distractions on the weekends. On a few occasions you literally drove me out of the woods. Roma, thanks for motivating me through the tough times and for your help when I needed it. I enjoyed the fun trips together and I still believe I can beat you in drinking beer. Łukasz, I totally enjoyed sharing stories on paper-oil samples. Thanks for the help and distractions, in the office and

outside. Gautam, my fellow officemate, it was a pleasure working with you on this project.

I was also fortunate of meeting great people outside the office to which these few words can't express my full gratefulness. Joe, "Master", life in Delft wouldn't have been the same without you. Great parties but above all, thanks for the company and wisdom. Nirali, Kedar, Dana, Ana and Adolfo, I will always remember those late nights in Belvedere. Tanya, Andrey, Alina and Valentina, thank you for the nice evenings and interesting conversations. Zhenya and Pierre, we hope to see you in NL soon, after all it's our turn to pick an interesting restaurant.

Yuri and Sere, even though we live far apart I always feel like we see each other every day. Thanks for the support throughout the years, not only those in NL.

To my friends in the UK and Malaysia, thank you for the support in my move to the "continent". Paolo, thanks for the encouragement and understanding between juggling work and writing this thesis.

No words can truly describe the support of my darling wife Vera. You have given me the strength to finish this work through your love, smile, encouragement and positive approach to life. You always know how to cheer me up no matter what.

I would like to thank my entire family for their push and encouragement through the years. Dear Mom and Dad, you have given me the confidence to finish this project and to be who I am today, for this I am very grateful.

The recognition for the help in writing this thesis goes to many people. I'm sorry in advance if I forgot to mention someone.

Curriculum Vitae

Tomasz Koltunowicz was born on the 18th of December 1985 in Warsaw, Poland. After completing secondary school in Milan, Italy, in 1999 he started O-Level and A-Level secondary education at Garden International School in Kuala Lumpur, Malaysia. He received a Master of Engineering in electrical and electronic engineering with honours from the University of Nottingham in 2007. In the same year he started his Ph.D. research project at the Delft University of Technology. Since 2011 he is working in the R&D department of Prysmian Group in the Netherlands.